INFORMATION TO USERS

This material was produced from a microfilm copy of the original document. While the most advanced technological means to photograph and reproduce this document have been used, the quality is heavily dependent upon the quality of the original submitted.

The following explanation of techniques is provided to help you understand markings or patterns which may appear on this reproduction.

1. The sign or "target" for pages apparently lacking from the document photographed is "Missing Page(s)". If it was possible to obtain the missing page(s) or section, they are spliced into the film along with adjacent pages. This may have necessitated cutting thru an image and duplicating adjacent pages to insure you complete continuity.

2. When an image on the film is obliterated with a large round black mark, it is an indication that the photographer suspected that the copy may have moved during exposure and thus cause a blurred image. You will find a good image of the page in the adjacent frame.

3. When a map, drawing or chart, etc., was part of the material being photographed the photographer followed a definite method in "sectioning" the material. It is customary to begin photoing at the upper left hand corner of a large sheet and to continue photoing from left to right in equal sections with a small overlap. If necessary, sectioning is continued again — beginning below the first row and continuing on until complete.

4. The majority of users indicate that the textual content is of greatest value, however, a somewhat higher quality reproduction could be made from "photographs" if essential to the understanding of the dissertation. Silver prints of "photographs" may be ordered at additional charge by writing the Order Department, giving the catalog number, title, author and specific pages you wish reproduced.

5. PLEASE NOTE: Some pages may have indistinct print. Filmed as received.

Xerox University Microfilms
300 North Zeeb Road
Ann Arbor, Michigan 48106

74-3707

PALMERO, Horacio Fernando, 1942-
DILATION DUE TO AUSTENITE TRANSFORMATION IN STEEL AS A FUNCTION OF TEMPERATURE AND COMPOSITION.

The University of Michigan, Ph.D., 1973
Engineering, metallurgy

University Microfilms, A XEROX Company, Ann Arbor, Michigan

THIS DISSERTATION HAS BEEN MICROFILMED EXACTLY AS RECEIVED.

DILATION DUE TO AUSTENITE TRANSFORMATION IN STEEL AS A FUNCTION OF TEMPERATURE AND COMPOSITION

by

Horacio Fernando Palmero

A dissertation submitted in partial fulfillment
of the requirements for the degree of
Doctor of Philosophy
(Metallurgical Engineering)
in The University of Michigan
1973

Doctoral Committee:

Professor Richard A. Flinn, Chairman
Professor Wilbur C. Bigelow
Professor J. Donald Hanawalt
Professor William F. Hosford
Associate Professor A.S. Wineman

To my wife

ACKNOWLEDGMENTS

The author would like to express his gratitude to the many people and institutions who have generously contributed to the completion of this thesis in many different ways.

To his wife for her understanding and companionship and to his parents for their guidance.

To Professor R.A. Flinn, chairman of the doctoral committee, for his ability to direct the author's efforts to the most important aspects at each step of this thesis, for his confidence and patience both toward understanding nature and toward the author's performance and for his special assistance in writing this thesis.

To Professor W.F. Hosford, member of the doctoral committee, for his helpful suggestions and criticism and for the careful examination of the calculations of Appendix 2 and the thesis as a whole.

To the other members of the doctoral committee, Professor W.C. Bigelow, Professor J.D. Hanawalt and Associate Professor A.S. Wineman.

To the temporary members of the committee, Professor S.K. Clark and to Associate Professor O.F. Kimball who was also the author's professor in four fruitful graduate courses and papers in physical metallurgical areas closely related to this thesis.

To the institutions that assisted the author financially during the whole program:

"LASPAU, The Latin American Scholarship Program of American Universities," Cambridge, Mass., USA.

"International Center," The University of Michigan, Ann Arbor, Mich., USA.

"Universidad Nacional de Cordoba," Cordoba, Argentina.

"CIM, Centro de Investigaciones de Materiales," Universidad Nacional de Cordoba, Cordoba, Argentina.

To the institutions that supported the author financially through part of the program:

"Materials and Metallurgical Engineering Department," The University of Michigan, Ann Arbor, Mich., USA.

"International Nickel Company."

To Mr. A.J. Kiesler, General Electric Co., Research and Development Center, Schenectady, N.Y., USA, who carefully supervised the preparation of the high purity Fe-C-5% Ni steels, and to Professor W.C. Leslie, former Manager, Physical Metallurgy, Research Center, U.S. Steel Co., Monroeville, Pa., USA, who supplied other steels used and who as a newly appointed professor in the Materials and Metallurgical Engineering Department of this university helped the author with his suggestions and criticism in the later part of this program.

To Dr. N. Ridley, Department of Metallurgy, The University of Manchester, Manchester, England, who generously provided the numerical values of the lattice parameters, critical for the calculations of section IV-B, and who also arranged for high purity Fe-C samples from BISRA.

To Professor E. Abril, "Facultad de Ciencias Exactas Fisicas y Naturales," who introduced the author to metallurgy and encouraged him to undertake a formal education program in this field.

To Dr. Cias, Climax Molybdenum Co., Ann Arbor, Mich., USA, who assisted in measuring the coefficient of expansion of some alloys.

To Mrs. A.G. Crowe who patiently typed this thesis expertly.

AGRADECIMIENTO

El autor quiere exprezar su agradecimiento a personas e instituciones que directa o indirectamente han contribuido con este trabajo de tesis.

A su esposa por su comprencion y compania y a sus padres por la escala de valores que le transmitieron.

Al Profesor R.A. Flinn, presidente del comite doctoral, por su capacidad para reconocer los aspectos mas importantes en cada etapa de esta tesis, por su confianza y paciencia tanto en la naturaleza como en el trabajo del autor y por su especial asistencia en la escritura de esta tesis.

Al Profesor W.F. Hosford, miembro del comite doctoral, por su valiosas sugerencias y critica y minucioso examen del Apendice2 y de la tesis en general.

A los otros miembros del comite doctoral, Profesor W.C. Bigelow, Profesor J.D. Hanawalt y Profesor Adjunto A.S. Wineman.

A los miembros temporarios del comite doctoral, Profesor S.K. Clark y Profesor Adjunto O.F. Kimball que fue tambien profesor del autor en cuatro valiosos cursos de graduado y monografias en areas de metalurgia fisica intimamente relacionadas con este trabajo de tesis.

A las instituciones que subvencionaron al autor durante toda la duracion de su programa:

"LASPAU, The Latin American Scholarship Program of American Universities," Cambridge, Mass., USA.

"International Center," The University of Michigan, Ann Arbor, Mich., USA.

"Universidad Nacional de Cordoba," Cordoba, Argentina.

"CIM, Centro de Investigaciones de Materiales," Universidad Nacional de Cordoba, Cordoba, Argentina.

A las instituciones que subvencionaron al autor durante parte de la duracion de su programa:

"Materials and Metallurgical Engineering Department," The University of Michigan, Ann Arbor, Mich., USA.

"International Nickel Company."

Al Senor A.J. Kiesler, General Electric Co., Research and Development Center, Schenectady, N.Y., USA, que cuidadosamente superviso la preparacion de los aceros aleados de alta pureza, Fe-C-5% Ni, y al Professor W.C. Leslie, ex-Director, "Physical Metallurgy, Research Center," U.S. Steel Co., Monroeville, Pa., USA, que suministro otros aceros usados en esta tesis y que luego, como Profesor recientemente incorporado al departamento de Materiales y Metalurgia de esta universidad, ayudo al autor con sus valiosas sugerencias y criticas en la ultima parte de este programa.

Al Dr. N. Ridley, Departmento de Metalurgia, The University of Manchester, Manchester, England que

generosamente proveyo los valores numericos de los parametros de red,de tanto valor en los calculos de las seccion IV-B y que tambien suministro las muestras de aceros de alta pureza, Fe-C, provenientes de BISRA.

Al Profesor E. Abril, Facultad de Ciencias Exactas Fisicas y Naturales de la Universidad Nacional de Cordoba, Cordoba, Argentina, por introducir e interesar al autor en Metalurgia y por sugerir la realizacion de un programa de estudios formal en esta especialidad.

Al Dr. Cias, "Climax Molybdenum Co.," Ann Arbor, Mich., USA, que asistio al autor en la medicion del coeficiente de dilatacion de algunas aleaciones.

A la Senora A.G. Crowe por su experto y paciente trabajo de dactilografia.

TABLE OF CONTENTS

	Page
Dedication	ii
Acknowledgments	iii
Agradecimiento	vi
Table of Contents	ix
List of Tables	xi
List of Figures	xiii
I. Introduction, Objectives	1
II. Review of the Literature	3
A. Dilatometer construction	3
B. Previous measurements of transformation length changes	6
C. Lattice parameter measurement of austenite and its transformation products	8
D. Previous calculations of transformation length changes from lattice parameter data	17
E. Related data on bainite and martensite transformation	19
III. Experimental Procedure	24
A. Description of materials and specimen preparation	24
B. Equipment and conduct of the experiments	27
C. Explanation of dilation curves (schematic)	34
D. Experimental problems	38
E. Experimental errors	40

Page

IV. Results 43

A. Measurements of δ_ℓ using the quenching dilatometer 44

B. Calculation of δ_V and δ_ℓ from lattice parameters 80

C. Comparison of measured and calculated values of δ_ℓ 96

D. Significance of the values of δ_ℓ 115

V. Conclusion 118

Appendix 1. Regression Analysis 120

Appendix 2. Calculation of Transformation Dilation from X-ray Lattice Parameter Data 138

A. Equilibrium Transformations 141

B. Martensite Transformation 167

Bibliography 174

LIST OF TABLES

Table	Title	Page
1	Summary of dilatometer characteristics (from the literature	7
2	Summary of values of mean coefficient of expansion of α Fe	9
3	Thermal coefficient of expansion of α Fe	10
4	Summary of room temperature lattice parameters of cementite	12
5	Summary of expansion coefficients for cementite	13
6	Summary of transformation coefficient of the α-γ phase change	18
7	Summary of chemical composition and heat numbers of the alloys used	25
8	Summary of estimates of experimental errors	41
9	Summary of values of δ_ℓ obtained from dilation data	45-53
10	Lattice parameter data from Ridley and Stuart	123-134
11	Regression analysis of lattice parameter data	135-137
12	Lattice parameters of austenite, ferrite and cementite for sample calculation	162
13	Unit cell volumes and unit cell volume ratios (sample calculation)	163
14	Calculation of $(1 + C^F/Fe^F)$	163
15	Calculation of $(1 + C^A/Fe^A)$	164
16	Calculation of $\overline{V}_C/\overline{V}_A$	164

Table	Title	Page
17	Calculation of V_F/V_A	165
18	Calculation of f_F^W and f_C^W	165
19	Calculation of δ_V	166

LIST OF FIGURES

No.	Title	Page
1.	Overall view of the dilatometer A) Austenitizing position, B) Quenching position	26
2.	Details of the dilatometer equipment A) Dilatometer, B) Quenching bath	28,29
3.	Schematic illustration of dilation data. Relative length vs log time. A) Isothermal, B) Martensite	36
4.	Relative length vs time, 0.23% C-5% Ni	55
5.	Relative length vs time, 0.72% C-5% Ni	56
6.	Relative length vs time, 1.13% C-5% Ni	57
7.	Summary of transformation coefficient, δ_ℓ, for Fe-C alloys	59
8.	A) Transformation coefficient, δ_ℓ, vs temperature, 0.23% C-5% Ni	60
	B) Transformation coefficient, δ_ℓ, vs temperature, 0.44% C-5% Ni	61
	C) Transformation coefficient, δ_ℓ, vs temperature, 0.72% C-5% Ni	62
	D) Transformation coefficient, δ_ℓ, vs temperature, 1.13% C-5% Ni	63
	E) Transformation coefficient, δ_ℓ, vs temperature, all 5% Ni alloys	64
9.	Transformation coefficient, δ_ℓ, for AISI-SAE 52100 and AISI-SAE 1050 in pearlite and bainite ranges	66
10.	Transformation coefficient, δ_ℓ, vs temperature for AISI-SAE 4140 and 8640 in pearlite and bainite ranges	67
11.	Transformation coefficient, δ_ℓ, in pearlite range vs % C at 1000 (811 K) and 1200°F (922 K)	68
12.	Transformation coefficient, δ_ℓ, in bainite range showing irregular behavior	69

No.	Title	Page
13.	Relative length vs log time for lower bainite showing tempering	70
14.	Overall contraction 1650°F (1172K) to bath temperature vs quench temperature	72
15.	Relative length vs time curve showing both martensite and bainite formation (AISI-SAE 4140)	75
16.	Summary of transformation coefficient, δ_ℓ, vs temperature of transformation	77
17.	A) Transformation coefficient in pearlite range, δ_V, (calculated) vs % C	84
	B) Transformation coefficient in pearlite range, δ_V, (calculated) vs temperature	85
18.	A) Transformation coefficient in martensite range, δ_V, (calculated) vs % C	87
	B) Transformation coefficient in martensite range, δ_V, (calculated) vs temperature	88
19.	Comparison of transformation coefficients, δ_V, in pearlite and martensite ranges (both calculated) vs % C	90
20.	A) Transformation coefficient, δ_ℓ, (calculated) vs temperature in pearlite and upper bainite ranges ($\delta_\ell \cong 1/3\ \delta_V$)	93
	B) Transformation coefficient, δ_ℓ, calculated vs temperature in martensite range ($\delta_\ell \cong 1/3\ \delta_V$)	94
21.	Comparison of transformation coefficient, δ_ℓ, in pearlite and martensite ranges (both calculated) vs temperature	95
22.	Comparison of measured and calculated values of δ_ℓ for Fe-C alloys	97
23.	A) Comparison of measured and calculated values of δ_ℓ for 0.23% C-5% Ni	98
	B) Comparison of measured and calculated values of δ_ℓ for 0.44% C-5% Ni	99
	C) Comparison of measured and calculated values of δ_ℓ for 0.72% C-5% Ni	100

No.	Title	Page
	D) Comparison of measured and calculated values of δ_ℓ for 1.13% C-5% Ni	101
	E) Comparison of measured and calculated values of δ_ℓ for Fe-C-5% Ni alloys	102
24.	Comparison of measured and calculated values of δ_ℓ for AISI-SAE 52100 and 1050	103
25.	Comparison of measured and calculated values of δ_ℓ for AISI-SAE 4140 and 8640	104
26.	Comparison of measured and calculated values of δ_ℓ vs % C at 1000°F (811 K) and 1200°F (922 K)	105
27.	Comparison of measured and calculated values of δ_ℓ in bainite region showing irregular behavior	106
28.	Summary of measured and calculated values of δ_ℓ vs temperature of transformation	108
29.	Comparison of measured and calculated values of δ_ℓ with data of other investigators	109
30.	Comparison of measured and calculated values of δ_ℓ for martensite at RT with other investigators	114
31.	Lattice parameter of ferrite (1.44% C alloy) vs temperature (Ridley and Stuart, 33)	148
32.	A) "a" lattice parameter of cementite (1.44% C alloy) vs temperature (33)	148
	B) "b" lattice parameter of cementite (1.44% C alloy) vs temperature (33)	149
	C) "c" lattice parameter of cementite (1.44% C alloy) vs temperature (33)	150
33.	A) Lattice parameter of austenite of different carbon contents vs temperature (33)	151
	B) Lattice parameter of austenite of different carbon contents vs % C (33)	152
34.	Volume of unit cells of austenite, ferrite and cementite calculated from (33) and of martensite calculated from Roberts (13)	154

No.	Title	Page
35.	A) Summary of calculation procedure for δ_V (isothermal) for 0.1% C as f(T)	155
	B) Summary of calculation procedure for δ_V (isothermal) for 1.3% C as f(T)	156
	C) Summary of calculation procedure for δ_V (isothermal) for 1.9% C as f(T)	157
36.	A) Summary of calculation procedure for δ_V for 700°C as f(% C) (Isothermal)	158
	B) Summary of calculation procedure for δ_V for 500°C as f(% C) (Isothermal)	159
	C) Summary of calculation procedure for δ_V for 300°C as f (% C)(Isothermal)	160

ABSTRACT

DILATION DUE TO AUSTENITE
TRANSFORMATION IN STEEL AS A FUNCTION OF
TEMPERATURE AND COMPOSITION

by

Horacio Fernando Palmero

Chairman: Richard A. Flinn

A great deal of research effort has been devoted to measuring the rate of austenite transformation as a function of composition and temperature, while relatively little attention has been given to systematic measurement of the dimensional changes accompanying transformation at different temperatures and compositions. While the rate data are important for hardenability, the dilation data are equally important in controlling distortion, cracking, residual stresses and weldability.

In this work the length change due to transformation, "δ_ℓ", has been determined for a representative group of iron-carbon and iron-carbon-nickel alloys and AISI-SAE 1050, 8640, 4140, 52100 steels over the complete range of transformation temperatures. An improved dilatometer constructed of fused silica, employing 0.020 in. (0.5 mm) thick samples with a high velocity quenching bath was

developed for this purpose.

The limits of the wide range of dimensional changes which were encountered are:

TRANSFORMATION PRODUCT	% C	TEMPERATURE °F	TEMPERATURE K	δ_ℓ x 10^4 (in./in.) or (m/m)
Ferrite and Cementite	0.2	1300	977	35
	1.1	1300	977	12
Bainite	0.2	800	700	53
	1.1	800	700	25
Martensite	0.2	500(Mf)	533	63
	1.1	-60(Mf)	222	108

The data indicate that the carbon level was by far the most important compositional variable affecting δ_ℓ.

The significance of the magnitude of these values may be demonstrated by recalling that a strain of 30 x 10^{-4} can result in a residual stress of approximately 90,000 psi (620 MN/m^2) or would be equivalent to a temperature change of 300°F (167 K) in austenite.

Next, the theoretical values of δ_ℓ for pure iron carbon alloys were calculated from the lattice parameters of austenite and its transformation products. These data were then compared with the dilatometer data and good agreement obtained in the pearlite and martensite ranges. The dilation data show consistent deviations in the bainite range from the $\delta_\ell$values calculated for transformation to ferrite and cementite and these deviations corroborate with recent data regarding the non-equilibrium structures of bainite.

I. INTRODUCTION, OBJECTIVES

The transformation of austenite has probably received more attention from metallurgists than any other topic because it governs the hardening and annealing of steel. However, most of the research has been focused on the rate of transformation because this governs the hardenability and strengthening. Relatively little attention has been given to the dilation (usually a pronounced expansion) which accompanies the transformation. Very few designers are aware, for example, that a common transformation gives the order of 30×10^{-4} in./in., an expansion equal to a temperature change of 300°F in a typical steel. Also it should be realized that an elastic strain of this magnitude is equivalent to 90,000 psi residual stress.

The average metallurgist associates quench cracking with thermal stresses alone but a dramatic example of the importance of the stresses produced by transformation is given in commercial heat treatment. In treating austenitic manganese steel castings (12% Mn), the usual practice is to heat a container full of a variety of shapes and sections to 1900°F and then plunge into cold water. No cracking occurs because there is no phase change. The same experiment would actually be dangerous with plain carbon or low alloy steel castings. Aside from cracked parts, dangerously high levels of internal stress would be present.

The temperature at which the transformation expansion takes place is of equal importance to the magnitude. Many composite structures are being cast or fabricated by welding or powder metallurgy and,even if the part is cooled uniformly,transformation may occur at a different time in different portions of the structure leading to distortion, cracking or residual stress. There are many cases on record in which a metallurgist has devoted a good deal of effort to obtain high hardness and strength (as measured in a test bar) only to have an actual component fail catastrophically because of the level of residual stress produced by neglected dilation due to transformation.

With these factors in mind the objective of this research is to provide a quantitative knowledge of the variation of the dilation due to transformation (usually an expansion) as a function of temperature over a wide range of iron carbon alloys and steels. The simplest method is by using a quenching dilatometer but correlation of the data with calculations of expansion from basic lattice parameter measurements is also accomplished.

For general reference and to call attention of design engineers to the transformation dilation the use of the simple symbol, δ_ℓ, called the transformation coefficient (linear) and δ_v, the volumetric transformation coefficient, is proposed, with dimensionless units (in./in.) or ($in.^3/in.^3$) respectively.

II. REVIEW OF THE LITERATURE

In preparation for this investigation it was necessary to review five divisions of the literature:

A. Dilatometer construction

B. Previous measurements of transformation length changes

C. Lattice parameter measurements of austenite and its transformation products

D. Previous calculations of transformation length changes from lattice parameter data

E. Related data on bainite and martensite transformation.

A. Dilatometer construction

The dilatometric technique has been used in numerous investigations as an accurate and simple experimental apparatus to measure dimensional changes caused by a wide variety of physical phenomena in different materials. Thermal expansion or contraction, structural modifications in crystalline materials, magnetostriction, electrostriction and piezoelectric effects are some of these phenomena.

Since the dimensional changes are different in magnitude and are produced under different conditions, the dilatometers that have been developed in each case have their own characteristics, e.g. principle of design, accuracy, range of temperature, type and dimension of

specimen, etc.

The dilatometers used to study structural modifications of crystalline materials are of two types: the differential dilatometer and the non-differential or absolute dilatometer. In the former, changes in length of the sample in study are compared with those of a standard sample of known behavior under the specific treatment, and the relative dimensional change is used to compute the elongation of the sample under study. The non-differential or absolute dilatometer measures directly the length change of the sample under study, without the need of a reference sample.

With both types, quantitative length changes due to transformation can be determined over a wide range of conditions of temperature and cooling rates.

The main characteristics of the dilatometers used for the study of structural modifications and for the determination of the coefficient of thermal expansion can be classified as follows:

		CODE
A) TYPE OF DILATOMETER:	1. Non-differential or Absolute	(A)
	2. Differential	(D)
B) ELONGATION READING DEVICE		
1. Electronic or electric transducer		(E)
2. Lever: I) Optical:	a) With enlarger or microscope	(LOE)
	b) Without enlarger or microscope	(LO)

		CODE
II) Mechanical:	a) With enlarger or microscope	(LME)
	b) Without enlarger or microscope	(LM)
3. Concentric fused silica tubes and gage		(G)
4. Optical interferometer		(I)

C) ELONGATION, TEMPERATURE AND TIME RECORDING

1. Photographic or filming device		(PF)
2. Electro-mechanical recorder X-Y type		(EMR)
3. Electronic recorder X-Y-Z type		(ER)

D. SAMPLE

1. Shape:	a) Prism	(P)
	b) Cylinder	(C)
	c) Hollow cylinder	(HC)
2. Length		(given in inches)
3. Sample-dilatometer connection		
	a) Hook (specimen in tension)	(H)
	b) Compression contact (specimen in compression)	(DC)

E) ATMOSPHERE-SAMPLE INTERACTION

1. Protective atmosphere		
	a) Inert gas	(PAIG)
	b) Vacuum	(PAV)
2. Atmosphere used to incorporate some alloying elements		(AA)
3. Atmosphere used as the heating or cooling medium		(AHC)

		CODE
F)	HEATING DEVICE	
1.	Furnace	(F)
2.	Gas	(G)
3.	Molten metal	(MM)
G)	COOLING MEDIUM	
1.	Liquid quenching	(LQ)
2.	Gas	(G)
H)	SENSITIVITY OF THE ELONGATION READING INSTRUMENT (given in angstroms)	
I)	USES OF THE DILATOMETER	
1.	Study of allotropic transformations	(AT)
2.	Determination of the coefficient of thermal expansion	(TE)
3.	Other uses	(O)

The characteristics of some dilatometers found in the literature review are summarized in Table 1.

B. Previous measurements of transformation length changes

Since the mechanism, morphology and kinetics of formation of pearlite, bainite (upper and lower) and martensite are substantially different, it was expected that the transformation mode would affect the length changes accompanying their formation. Due to the fact that some transformations require too long a time to be completed or that, at the TTT diagram nose the incubation time is sometimes so short that it does not allow a complete quench of the austenite

Table 1. Summary of dilatometer characteristics in the literature search

CHARACTERISTICS	A) Type of Dilatometer	B) Elongation Reading Device	C) Elongation, Temperature and Time Recording	D1) Sample Shape	D2) Sample Length	D3) Sample-Dilatometer Connect.	E) Atmosphere-Sample Interaction	F) Heating Device	G) Cooling Medium	H) Sensitivity of the Elongation Reading Instrument Å	I) Uses of the Dilatometer
SOURCE											
(1)	D										AT
(18)	A	G	PF	P	6	DC	no	F	LQ	10^4	AT
(2)	A	G	PF	P	6-8	H	no	MM	LQ	10^4	TE
(3)	A	E	ER PF	HC	0.65	DC	PAIG	F	G		AT
(4)	A	I		HC	0.2	DC		F		25	TE
(5)	A	E	EMR	C	0.2-2	DC		F			AT
(6)	A			C	4-8	DC		F		10^3	TE
(7)	A			C	4	DC		F			TE
(8)	D	E		P	1.5	H	PAIG PAV	F			AT
(10)	A	I		C		DC				10	TE
(10)	A	LME		P	8	H	AA	F		10^4	O
Proposed dilatometer	A	G	PF	P	6-8	DC H	no	F MM	LQ	10^4	AT TE

to bath temperature, it is difficult to find complete series of measurements from the eutectoid temperature of an alloy down to its Mf. However, some series have been reported although for different purposes and in some cases not allowing complete austenite decomposition or reporting only measurements at widely separated temperatures which might lead to errors in interpolation.

Hehemann (21) in an attempt to define the temperature at which bainite formation starts reports a series of dilatometric measurements on an AISI-SAE 4340 steel at the bainite range of temperature and most of the reported measurements do not include complete austenite decomposition.

Flinn, Cook and Fellows (2) report a series of length vs. time curves for isothermal quenches on a low carbon content low alloyed steel and on a carbon tool steel of the following compositions: Low Alloyed Steel: 0.30% Carbon, 1.63% Manganese, 0.49% Silicon, 0.44% Chromium and 0.33% Molybdenum (10 measurements between 1300 and 300°F); Carbon Tool Steel: 1.04% Carbon, 0.29% Manganese, 0.17% Silicon, 0.05% Nickel and 0.04% Chromium (5 measurements between 1300 and room temperature).

C. Lattice parameter measurements of austenite and its transformation products

1. Pure Iron

Basinski, Hume-Rothery and Sutton (22) performed

x-ray diffraction measurements of the lattice parameter of pure iron at different temperatures up to delta iron temperatures. Both unfiltered Mn and Co radiations were used in the experiments and the calculations of the lattice spacings were made by standard measurement and extrapolation techniques. The results of this investigation are included in a later discussion and suggest that the forces responsible for ferromagnetism do not affect the interatomic distances by more than one part in 10000, in agreement with Esser and Müller (23) and in contradiction to Schmidt (24). The reported results are accurate to within 0.0002 Å and show that the lattice parameter of αFe at 20°C is 2.8606 Å and that its mean coefficient of thermal expansion as a function of the temperature varies from 14-14.8 x 10^{-6} ($°C^{-1}$). Table 2 shows a summary of the mean coefficient of thermal expansion of αFe as determined by Basinski et al. (22), Nix and McNair (25) and Austin and Pearce (26).

Table 2. Summary of Mean Coefficient of Expansion of α-Fe

temperature range (°C)	$\bar{\alpha}^{F} = \frac{1}{L_o} \frac{L_t - L_o}{t} \times 10^6$		
	Austin & Pearce (26)	Nix & McNair (25)	Basinski et al. (22)
0 to 300	13.1	13.3	14.0
0 to 400	13.7	14.0	14.2
0 to 500	14.4	14.5	14.4
0 to 600	14.7	14.9	14.6
0 to 700	14.9	15.0	14.7
0 to 800	14.9	-	14.8

Straumanis and Kim (27) provided measurements of the lattice parameter of pure iron to ±0.00002 Å. The reported equations for α and γFe are respectively: $a(A) = 2.8759(1 + 14.79 \cdot 10^{-6}(T-250))$ for αFe and $a(A) = 3.6566(1 + 21.5 \cdot 10^{-6}(T-900))$ for γFe, where T is the temperature in °C. A comparison between the thermal coefficient of αFe calculated from the lattice parameter and measured by dilatometry by Sounders and Hidnert (30) reveals a reasonable agreement as shown in Table 3. Finally, this work agrees with the one by Basinski et al. (22) in that there is no change of lattice parameter of αFe at the Curie temperature (768°C).

Table 3. Thermal coefficient of expansion of α-Fe (27)(28) $\times 10^{6}(°C^{-1})$

Temp. in °C	200	300	400	500	600	700	800
(X-ray (27)	14.8	14.8	14.8	14.8	14.8	14.7	14.7
(dilatom.(28)	14.5	15.5	16.2	16.1	15.8	15.8	15.4

2. Iron-carbon Alloys

So far the effect of carbon upon the lattice parameter of alpha and mainly of gamma iron has not been considered. However, for the purpose of the present work these data together with equivalent data for cementite and martensite are critical since calculations of the transformation coefficient are performed at temperature and as a function of the carbon content.

Several papers by Ridley and Stuart, 1966 (11), 1970 (31) and personal communication (33) deal with lattice parameters of ferrite, austenites and cementite. In their 1966 paper (11), the lattice parameter and thermal coefficient of expansion of cementite are specifically studied and are reported together with similar data for ferrite and 0.81% C austenite. The lattice parameter measurements were made on pure iron, on ferrite and cementite coexisting in situ in a 1.44% C alloy of high purity, and on cementite electrolytically extracted from the alloy. The equipment used was a modified Unicam S70 with a temperature control that at worst was ±2°C and in most cases considerably better. The camera was evacuated to improve temperature control and to reduce the exposure time. Cementite, pure iron, ferrite and 0.81% C austenite were exposed with Co-Kα radiation. The calculations of the lattice parameters of cubic materials were performed by the usual Nelson and Riley method (38) while the calculations for orthorhombic cementite parameters (a, b and c) were performed by the "least squares" method used by Cohen (39) and corrected with the systematic error correction of Nelson and Riley (38). The calculations in this latter case were performed by a computer using the Hoff et al.(40) method for orthorhombic materials. This technique gave a reproducibility of ±0.0002 A for pure silver (used to measure temperature), pure iron, ferrite and 0.81% C austenite. The reproducibility of cementite measurements was ±0.0005 A. These

measurements do not include refraction corrections.

For the calculations performed in the present work only the lattice parameters of ferrite and cementite in situ in a 1.44% C pure Fe-C alloy were used. The results of these measurements are transcribed in Appendix 1 from the author's personal communication (33) of the numerical results. Ferrite and cementite lattice parameters are plotted later as function of the temperature.

Table 4 shows a summary of room temperature lattice parameters of cementite (as in Table III, page 712 of 1966 Stuart and Ridley's paper) by Lipson and Petch (15), Hume-Rothery (16), Jack (41), Belikov and Savinskaya (17) and Stuart and Ridley (11).

Table 4. Summary of room temperature lattice parameters for cementite

Investigator	Lattice Parameter (Å)			Density, g/cm^3
	a	b	c	
Lipson and Petch (15)	4.5235	5.0890	6.7433	7.67*
Hume-Rothery et al. (16)	4.5246	5.0876	6.7403	7.67*
Jack (41)	4.5255	5.0885	6.7431	7.67*
Belikov and Savinskaya (17)	4.5246	5.0870	6.7428	7.67*
Stuart & Ridley (23°C) (11)	4.5246	5.0884	6.7423	7.67

*Calculated from the lattice parameters given by these workers

Table 5 is a summary of the (three directional, the volume and the mean linear) expansion coefficients for cementite as reported by Stuart and Ridley (11).

Table 5. Summary of expansion coefficients for cementite (x 10^{-6} $°C^{-1}$) from Stuart and Ridley (11)

Temp. range °C	Direction			Mean Expansion Coefficient	
	a	b	c	Volume	Linear
23-100	7.46	1.28	8.86	17.60	5.87
23-200	7.87	2.44	9.64	19.95	6.65
23-300	8.30	3.55	10.44	22.29	7.43
23-400	8.79	4.90	11.41	25.10	8.37
23-500	9.31	6.80	12.50	28.61	9.54
23-600	10.04	9.06	13.70	32.80	10.93
23-700	11.23	11.73	14.94	37.90	12.63

In another paper by Ridley and Stuart (31), austenite lattice parameter measurements were repeated and extended to five pure Fe-C alloys supplied by BISRA (0.32-0.62-0.86-1.02-1.17 and 1.44% C respectively.) Most of these measurements were performed with the Unicam S150 high-temperature x-ray camera that can work up to 1400°C but is limited to only 1200°C because of the quartz capillaries). The camera was evacuated during use and calibrated against spectrographically pure grades of silver (99.99%) and iron (99.986%) by means of the lattice parameter relationships reported by Hume-Rothery and Reynolds (42), by Basinski et al. (43) and by Goldschmidt (36).

A few measurements were performed with the modified Unicam S70 setting as reported by the same authors in their 1966 paper (11). As in the previous work, Co-Kα radiation was used to expose the 0.5 mm diameter thin-walled evacuated quartz capillaries containing stress relieved filings that passed through the 200-mesh British Standard sieve but were retained in a 350-mesh. Lattice parameter calculations were performed from the high Bragg-angle lines using the extrapolation methods of Taylor and Sinclair (37) and Nelson and Riley (38). The reproducibility attained was ±0.0002 A and the temperature control was ±2°C (K). The numerical results are summarized later in Appendix 1.

The following are linear equations reported by Ridley and Stuart for the lattice parameter of austenite as a function of the carbon content and at given temperatures:

$$a_{25°C}(A) = 3.5735 + 0.0316 \text{ wt-\%C}$$

$$a_{727°C}(A) = 3.6300 + 0.0296 \text{ wt-\%C}$$

$$a_{1200°C}(A) = 3.6681 + 0.0282 \text{ wt-\%C}$$

It should be emphasized, however, as Ridley et al. pointed out (32), that these lattice parameter equations are the result of linear extrapolation from high temperature lattice parameter measurements and should not be confused with the equation reported by Roberts (13) for the retained austenite lattice parameter:

$$a_{RT}(A) = 3.555 + 0.044 \text{ wt-\%C}$$

3. Martensite

The data presented up to this point are sufficient for the calculation of the transformation coefficient of austenite to ferrite + cementite. To perform the calculation for martensite transformation it is necessary to know the lattice parameters (a and c) of tetragonal martensite or the expanded "a" parameter of cubic martensite at the temperature and for the carbon content the transformation coefficient is to be calculated. Due to the high speed at which martensite tempers, it has not been possible to find as accurate data for martensite as for ferrite, cementite and austenite lattice parameters. This is demonstrated by the scatter presented in Roberts report (13) of the lattice parameter of tetragonal martensite at room temperature as a function of the carbon content of the alloy. Part of the scatter can be due to elastic stresses as well as to the difficulty in obtaining virgin martensite. Roberts' report summarizes the following papers: (measurements between 0.5 and 1.8% C) Hagg (44), Ohman (45), Honda and Nishiyama (46), Seljakov, Kurdjumov and Goodtzov (47), Lipson and Parker (49), Mazur (50), Arbuzov (51) and Fletcher (52). Without considering the Seljakov et al. data, because it is too low as compared to the other results, the martensite parameters at room temperature as reported by Roberts can be described by the following equations:

$$a(Kx) = 2.861 - 0.013 \text{ wt-\%C}$$

$$c(Kx) = 2.861 + 0.116 \text{ wt-\%C}$$

The maximum scatter seems to be within ±0.01 Kx. As mentioned before, this paper reports the lattice parameter of retained austenite at room temperature as a function of the carbon content of the Fe-C alloy (not necessarily the same as the carbon content of the retained austenite) as:

$$a_{RT}(Kx) = 3.548 + 0.044 \text{ wt-\%C}$$

In this case, the scatter is approximately ±0.005 Kx. Roberts' summary report on martensite also presents two graphs of the volume percent of retained austenite as a function of the carbon content after room temperature and liquid nitrogen quenches of pure Fe-C alloys as reported by Roberts, Averbach and Cohen (53), Esser and Bungardt (54) and Averbach, Castleman and Cohen (55).

Fasiska and Wagenblast (9) have measured the dilation of αFe caused by interstitial carbon as a function of the atomic percent carbon in solution. The measurements were performed by dilatometry at 719°C and by x-ray diffraction (diffractometry and Debye-Scherrer methods) measurement of the lattice parameter at room temperature. With both methods the result was the same, $(29 \pm 3)10^{-4}$/(at. % C) and is temperature independent within experimental error. The carbon contents tested ranged up to 0.11 at. % C and were obtained by carburization of thin specimens. Their equation for the lattice parameter of

BCC iron at room temperature is:

$$a_{RT}(A) = (2.8664 \pm 0.0001) + (8.4 \pm 0.8)10^{-3} \text{ at. \% C}$$

Magee and Davies (56) used this equation in their calculations to extrapolate the lattice parameter of BCC martensite up to 0.8 wt % C.

The thermal coefficient of expansion of martensite has not been reported although it is probably close to that of ferrite. The experimental difficulty in measurement is the tempering which occurs on heating even at lower temperatures of martensite formation.

D. Literature search on calculations of transformation coefficient from lattice parameter data

In previous work a few calculations of the transformation length change have been made for simple cases. Also the growth during heat treatment has been investigated. First the transformation coefficient of the α-γ Fe phase change in pure iron may be considered. The results of several investigators are summarized in Table 6. There is a reasonable agreement among the last four values.

Lement (59) presents a series of calculations using lattice parameters to determine size changes at room temperature for different carbon contents in the hardening and tempering heat treatments of tool steels. The transformation coefficients as defined in the present work could be calculated at room temperature from his summary graph of

Table 6. Summary of Transformation Coefficient ($\times 10^4$) of the α-γ Fe Phase Change at 910°C

Souders & Hidnert (1922) (28)	Sato (1925) (58)	Smith & Thompson (1952) (57)	Basinski, Hume-Rothery & Sutton (1954) (22)	Straumanis & Kim** (1969) (27)	Ridley & Stuart* (1966-70) (11) (31)
1.6	28.2	38.7	35.4	31.3	37.0

*Extrapolated to 0% C from calculations performed at carbon contents from 0.32 to 1.44% C using equations derived in present work from (33).

**Calculated from the lattice parameter equations reported for α and γ Fe extrapolated to 910°C.

the specific volume of austenite, ferrite + cementite aggregate, ferrite and epsilon carbide aggregate, low carbon martensite and epsilon carbide aggregate and martensite. However, since the accurate high temperature austenite lattice parameter measurements performed by Ridley and Stuart (11,31) were not available to Lement in 1959, he uses Roberts (13) lattice parameter summary equation for retained austenite. Because of this the transformation coefficient of low carbon content alloys would have a positive error both for pearlite and martensite transformation coefficients. This error would give a slight decrease of the martensite transformation coefficient with increased carbon content as calculated from the specific volumes in contradiction with Magee and Davies (56). It should be emphasized, however, that Lement calculations of dimensional changes (not transformation coefficients) are not affected because the lattice

parameter of retained austenite is used correctly.

Magee and Davies (56) have reported transformation coefficient calculations for tetragonal martensite from Ridley and Stuart and Roberts and for cubic martensites from Fasiska and Wagenblast (9) data for Fe-C alloys. As is shown later these calculations have been performed at room temperature presumably assuming 100% transformation from austenite to martensite, not taking into account the rather large amounts of retained austenite that would result even with very low temperature quenches. It is reported that the major factor in establishing the magnitude of the martensite transformation coefficient is whether or not the austenite phase of the given alloy exhibits Invar behavior. However, only highly alloyed steels exhibit Invar behavior. Magee and Davies' calculations for alloys containing up to 5% Cr, 5% Mn or 10% Ni do not show any appreciable difference from pure iron alloys, while alloys with Invar behavior (with up to 25% Ni-30% Co) do not exhibit the large volume changes calculated for non-Invar alloys of the same carbon content.

E. Related topics

Other data regarding austenite transformation which are used in the analysis of the results are as follows:

Flinn, Cook and Fellows, in the previously reported paper (2), also describe a simple technique to determine the Ms temperature from dilatometric data. Since it is

going to be discussed further later, it is not described here. It is only to mention that the same principle for determining Ms temperature has been extended in the present work to determine Mf.

Hehemann (21) also reports a dilatometric contraction curve that describes the transition from epsilon carbide to Fe_3C. This is of interest mainly for the tempering of martensite, but it can be of significance in understanding the transformation mechanism of lower and perhaps upper bainite. It is also reported that Si delays this transformation. It is also stated that incomplete transformation can occur in bainite formation and that in hypo-eutectoid steels the carbon content of the untransformed austenite tends to increase, whilein hyper-eutectoid steels the carbon content of the remaining austenite tends to decrease.

Fletcher and Cohen (60-62) present data on dimensional stability of tool steels. In the first part (60), dilatometric measurements were made of the length changes occurring during subatmospheric treatments after oil or water quenching to room temperature as a function of the tempering time at room temperature. In other words, the degree of austenite stabilization is measured quantitatively both by dilatometry and x-ray diffraction. The second part of the work (61) shows that when martensite is

produced in a quench to room temperature and then tempered, this treatment stabilizes the retained austenite so that it does not transform with refrigeration later. The third part of the work (62) deals with austenite and martensite decomposition at room temperature as a function of the tempering temperature and time after either RT or sub-atmospheric quenching. From this research, it can be concluded that the faster the quench to the desired martensite transformation temperature, the smaller the degree of austenite stabilization. In other words, if a stepped quench is performed in a total period of a few minutes, there is no danger of large amounts of austenite stabilization. Therefore any untransformed austenite resulting from a fast quench to a given temperature can be considered as normal retained austenite.

As mentioned earlier, the carbon content of the metastable retained austenite may not be the same as the carbon content of the alloy and this fact would vary its lattice parameter. However, even if the carbon content does not vary, the lattice parameter of austenite can be altered by elastic stresses from what would be expected from extrapolation of high temperature measurements. This fact is clearly illustrated by Yershov and Olson's paper (14). The lattice parameter of austenite of alloyed steels of relatively high hardenability was measured every 20 or 30°C at the upper and lower bainite and in the

martensite temperature ranges. When the quenching speed was high enough to avoid high temperature transformation, the plot of the lattice parameter of austenite vs. temperature was a straight line from the austenitizing temperature down to the Ms temperature. Below Ms, coherency between martensite and austenite expanded the austenite unit cell with respect to the mentioned straight line. Later, at about 30 to 50% martensite formation, coherency between the network of martensite and retained austenite was disrupted with further cooling as evidenced by the return of the lattice parameter contraction to the extrapolated line. Coherency can also be destroyed by a tempering of a structure with 30 or 50% martensite plus the stressed austenite, at some higher temperature, as shown by another series of lattice parameter measurements. The lattice parameter of untransformed austenite than follows the original "free" austenite line on a subsequent quench. However, if the original quench from austenitizing temperature is not fast enough to avoid high temperature transformation, the austenite lattice parameter line of hypoeutectoid steels is shifted upwards (lattice parameter expansion) and parallel to the original line revealing an increase in the carbon content of the untransformed austenite.

Therefore, Yershov and Olson's paper is in contradiction to Roberts equation of the lattice parameter of retained austenite. The former have measured even positive

or at most no deviations from a linear extrapolation while the latter has summarized the data of other authors and predicted a negative deviation for carbon contents up to 1.45% C. As suggested by Ridley et al. this is a matter of controversy and there is further work in progress to test whether fast quenches can avoid the negative deviation observed especially in low carbon alloys, by avoiding possible carbon segregation or even precipitation as epsilon or Fe_3C in the high density network of lattice defects generated in retained austenite as martensite forms. This would lower the retained austenite carbon content with respect to the overall carbon content of the alloy and explain the lower lattice parameter measured at low carbon contents (refer to Ridley, Stuart and Zwell (32), Fig. 1).

In conjunction with this matter, it is interesting to compare the previous discussion regarding carbon content in retained austenite during martensite transformation with the carbon content of untransformed austenite in bainite transformation. According to Hehemann as stated before, in hypo-eutectic steels untransformed austenite would have a tendency to increase in carbon content with respect to the overall carbon concentration and vice versa for hyper-eutectoid steels. This could be due to a) a lower density of lattice defects in bainite than in martensite, b) a longer transformation time, therefore allowing more time for the carbon concentration of austenite to go to the $\alpha+\gamma-\gamma$ line and c) the higher temperature that would favor carbon diffusion.

III. EXPERIMENTAL PROCEDURE

This section is divided into five parts:

(1) Description of materials and specimen preparation.

(2) Equipment and conduct of the experiments.

(3) Explanation of dilation curves(schematic).

(4) Experimental problems.

(5) Experimental errors.

A) Description of materials and specimen preparation

The materials listed in Table 7 fall into three groups. High purity Fe-C alloys were investigated first and specimens were obtained from BISRA and the U.S. Steel Research Laboratory materials. These were vacuum melted, carbon deoxidized materials.

When it became evident that some transformation was encountered during quenching with the lower carbon alloys, a new series was planned with nominally 5% Ni. These alloys were melted under argon and cast at the General Electric Research and Development Center. The ingots were homogenized at 1000°C in dry argon for 24 hr, the hot rolled in an argon atmosphere from a 0.56 x 2 in. (14 x 51 mm) cross section to 0.100 in. (2.5 mm). The samples were then cold rolled to 0.080 in. (2.0 mm), annealed at 1832°F (1273°K) for 30 minutes in dry argon and mechanically straightened.

Table 7. Summary of chemical composition and heat numbers of the alloys used

Heat No.	Chemical Composition in wt %						Source
	Pure "Fe-C" Alloy Series						
1	0.16% C						USS Co.
2	0.31% C						USS Co.
3	0.36% C						BISRA
4	0.42% C	All heats were vacuum					USS Co.
5	0.55% C	melted and carbon de-					BISRA
6	0.61% C	oxidized. All other					USS Co.
7	0.76% C	elements concentration					BISRA
8	0.64% C	is <0.01.					BISRA
9	1.10% C						BISRA
10	1.28% C						GE
	Pure "Fe-C-5% Ni" Alloy Series						
11	0.23% C-4.55% Ni	All other					GE
12	0.44% C-4.58% Ni	elements concen-					GE
13	0.72% C-4.63% Ni	tration is					GE
14	1.13% C-4.70% Ni	<0.01.					GE
	AISI-SAE Steel Series						
	No.	C	Mn	Cr	Ni	Mo	Si	
15	4140	0.38	0.93	0.93	-	0.16	-	M&M Dept.
16	4140	0.39	0.86	0.99	-	0.22	0.28	USS Co.
17	8640	0.40	0.84	0.49	0.54	0.22	-	M&M Dept.
18	8640	0.38	0.89	0.61	0.62	0.21	0.31	USS Co.
19	52100	0.99	0.36	1.47	0.11	0.02	0.27	0.07 Cu
20	1050	0.49	0.40	<.01	<.01	<.01	<.01	M&M Dept.

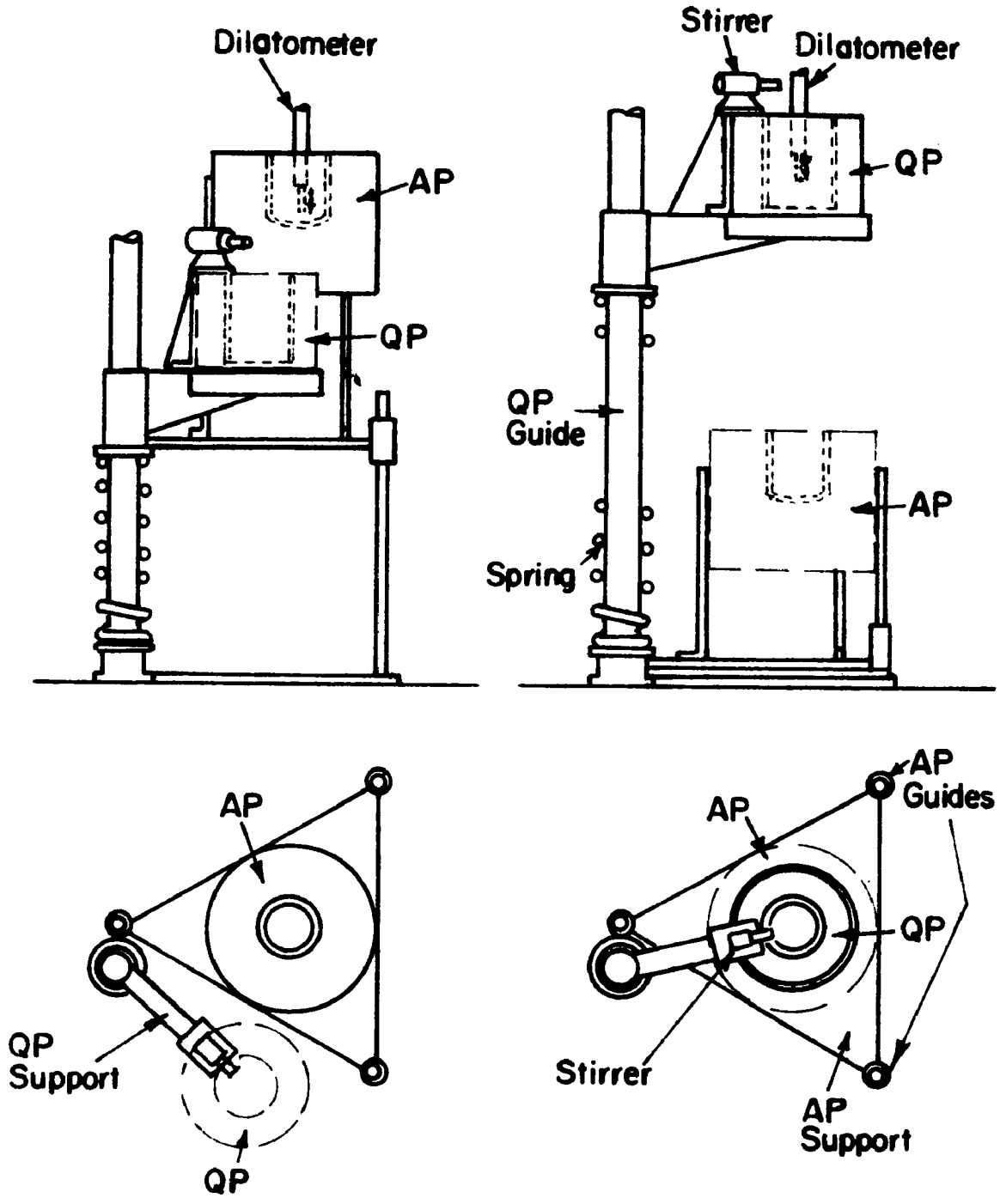


Fig. 1. Overall view of the dilatometer

The third group of samples was composed of representative AISI-SAE steels.

In all cases the samples were machined to 0.060 in. (1.5 mm) with a shaper and then carefully surface ground (wet) to 0.030 x 1/2 x 4-1/2 in. (0.76 x 12.7 x 114 mm). The distance between the furthest edges of the holes (contact points) was 4 in. (102 mm).

B) Equipment and conduct of the experiments

Basically the apparatus used in the present work consists of four parts, Fig. 1:

(1) Dilatometer

(2) Austenitizing furnace

(3) Quenching pot

(4) Recording device.

Before describing the details of the equipment, the conduct of a typical run may be discussed. The sample is first placed in the dilatometer at room temperature. The austenitizing pot, at 1650°F (1172 K) , for example, is raised to cover the specimen, Fig. 1A. After the sample is fully austenized, the austenitizing pot is lowered quickly and the quenching pot is swung over and up around the specimen, Fig. 1B. The movement of the dial gage is recorded with a movie camera at 16-64 f.p.s. The critical portion of the quench, that is, the immersion of the specimen in the quenching pot, takes less than 1 sec.

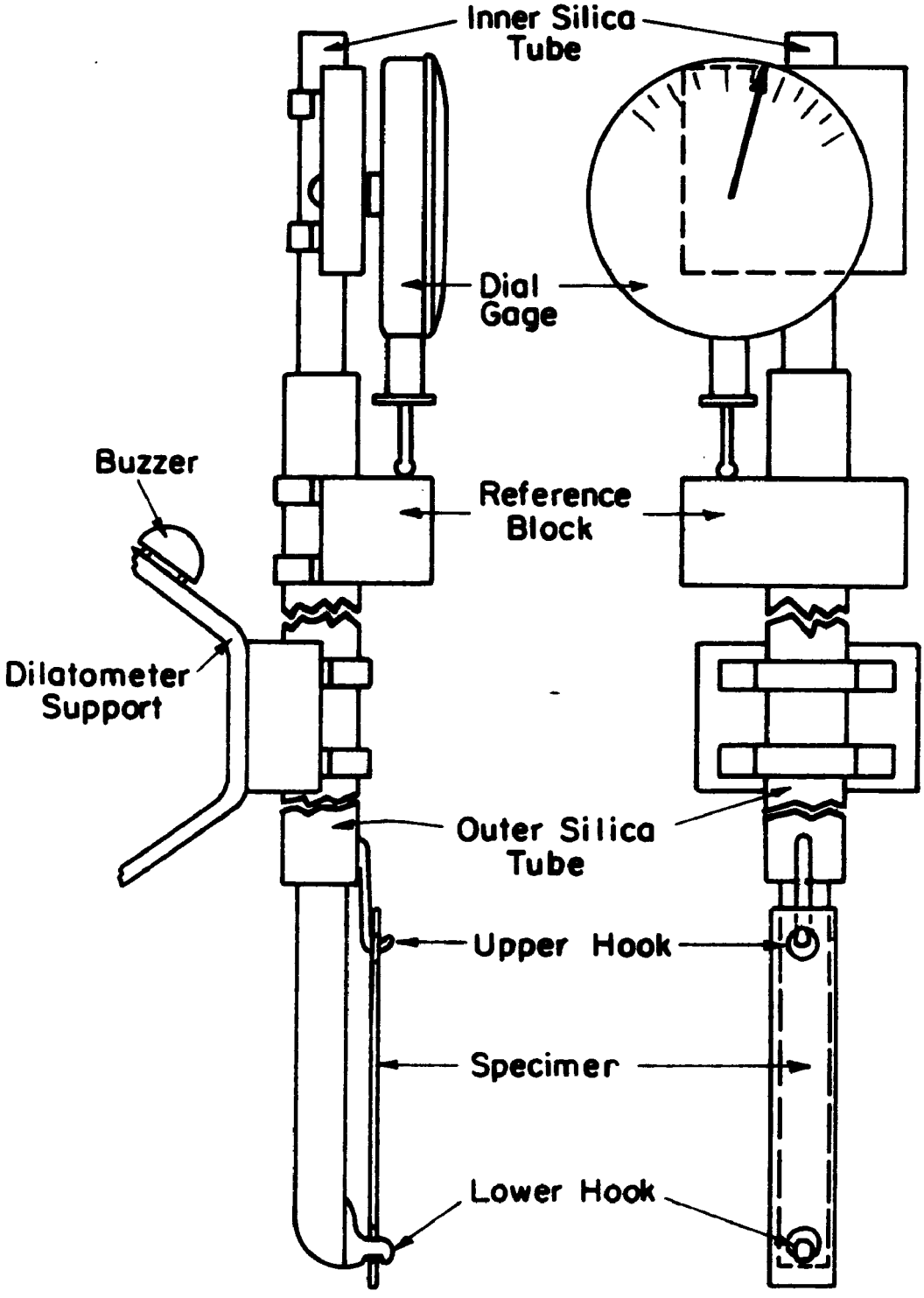
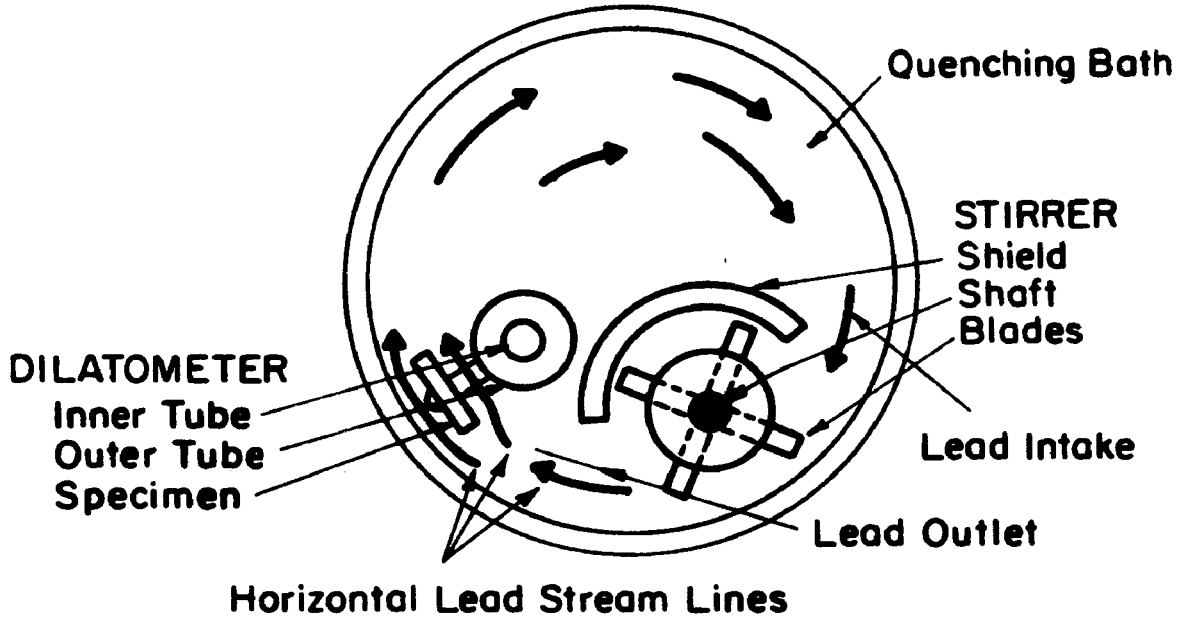


Fig. 2. Details of the dilatometer equipment
(A) Dilatometer



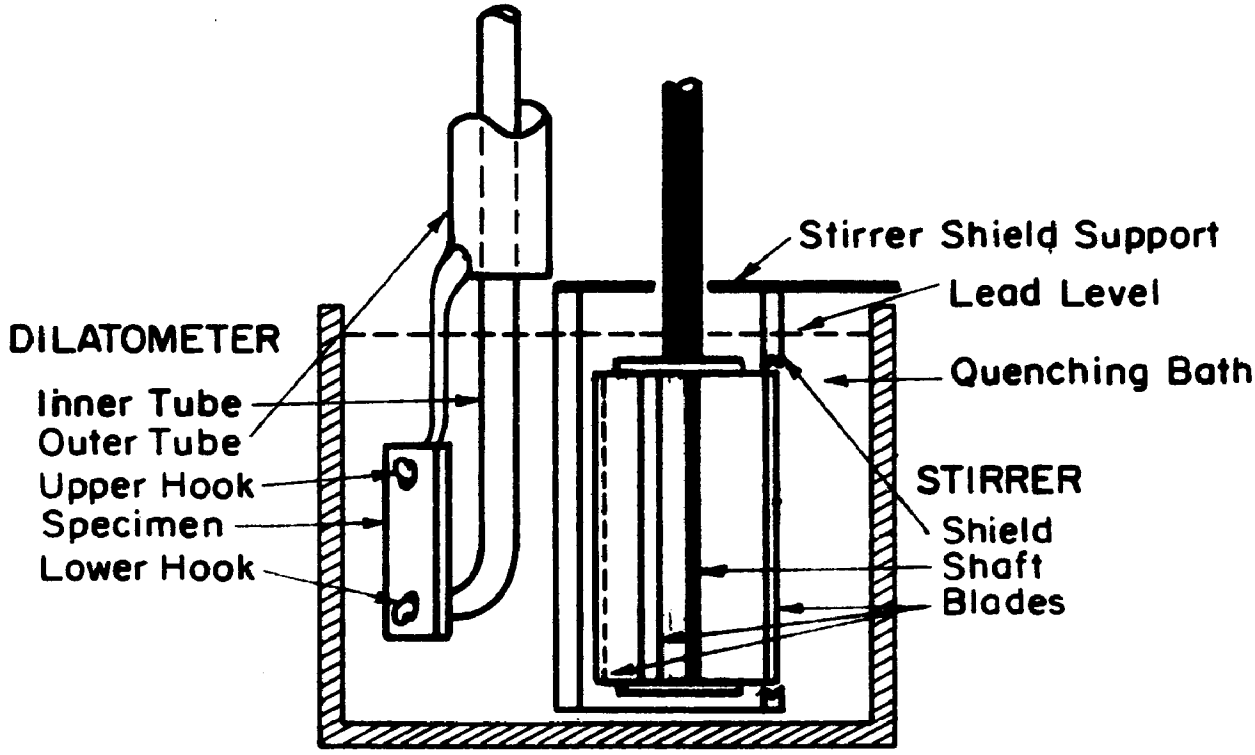


Fig. 2. Details of the dilatometer equipment
(B) Quenching bath

Once the specimen attains the quench bath temperature, recording of specimen length and time are taken by single frame exposures.

As one indication of the completeness of isothermal transformation, especially in the ferrite-pearlite range of hypoeutectoid steels, the quenching pot is lowered and the sample (in place at the dilatometer) is cooled to room temperature and then reheated by raising the quenching pot. If this causes an increase in length, the isothermal transformation was incomplete and the run is rejected.

(1) Dilatometer. The quenching dilatometer was designed to provide a very rapid quenching rate and is a modification of an earlier design (1). The outer fused silica tube, Fig. 1,2A, is anchored to the supporting fixture. The specimen is hung from a fused silica hook at the bottom of the outer tube and then the inner tube is hooked into the lower hole of the specimen, placing the sample in tension. This is a key feature because in this way thin samples can be used which would buckle if loaded in compression. The dial gage is then fastened to the top of the inner tube and the spring loaded tip of the gage contacts a platform attached to the outer tube. The dial gage and timer are photographed at 16 frames/second for the initial stages of a run. The tubes are separated by the three beads of silica fused to the inner tube.

Another important feature is that the dilatometer is stationary and the moving units to perform the heat

treatment are both the austenizing and quenching furnaces. This allows more stable dilation readings to be obtained.

The dial gage sensitivity is 0.0001 in. (2.5 μm) and the range or maximum displacement is 0.400 in. (10.2 mm). The same dilatometer support is used to hold the timer close to the dial gage. The smallest scale reading of the timer is 0.1 seconds.

(2) Austenitizing pot. The austenitizing furnace is a 15% chromium, 12% nickel steel crucible, 3 in. (76.2 mm) diameter and 8 in. (203.2 mm) height containing commercially pure lead. It is heated with a chromel (grade A) wire winding (90 volts - 15 amps for the maximum power output). The maximum operating temperature, 1750 to 1800°F (1227-1255 K) is set by the danger of generating excessive lead vapors. The oxidation of lead is reduced with a layer of cocoanut charcoal.* Lead oxides react with the fused silica tube forming a low melting point yellow glass which interferes with the proper operation of the dilatometer. The charcoal layer also prevents, at least partially, the escape of lead vapors. The whole furnace is supported by a triangular platform that allows the furnace to move up and down as illustrated in Fig. 1.

The advantage of using lead as the heating medium is that lead does not dissolve carbon and iron does not dissolve lead. Therefore neither decarburization nor lead contamination of the specimen can occur. Specimens used

*An oxidized bath would decarburize the specimen surface.

for a number of long time, high temperature runs were examined for decarburization metallographically and no signs could be found even in hypereutectoid alloys.

(3) Quenching pot. This furnace is very similar to the austenitizing furnace but it is of larger size [diameter: 3.5 in. (89 mm) and height: 10 in. (254 mm)] to minimize the rise in bath temperature when the hot sample and lower portion of the dilatometer enter the bath, Fig. 2-B.

The minimum temperature of operation was 630°F (605 K) when operating with pure Pb or 400°F (477 K) when operating with the Pb-Sn eutectic alloy. The upper temperature of operation was the eutectoid temperature of the alloy tested when operating with lead and about 630°F (605 K) when the Pb-Sn alloy was used.

To maximize the quenching speed, a stirrer has been developed to generate a circular horizontal flow on a cross section of the furnace as is portrayed in Fig. 2-A. Originally the quench was performed without stirring but the quenching speed proved to be too slow. A second try was made with stirring using a regular helicoidal propeller that generated a vertical current. Although some improvement was obtained, faster quenches were required. The problem of helicoidal propellers was that the stirring action was effecient only at a short distance. If the propeller was at the bottom of the quenching pot no appreciable stirring action was obtained at the top and vice versa. In addition, in order to increase the heat transfer

between the specimen and lead, a faster relative speed was desired.

Four design modifications were performed in order to increase relative speed and increase its uniformity. 1) The fastest speed of rotation was used (500 rpm); 2) a horizontal circular flow was created by a propeller with vertical blades; 3) the length of the blades [6.5 in. (165 mm)] was made longer than the specimen itself; and 4) a shield was used to concentrate the stream toward the specimen. The maximum quenching speed* obtained with this arrangement is 2800(°F/sec)[1556(K/sec)].

The quenching pot and the stirrer are both supported by a horizontal platform held in position by a vertical case hardened shaft with a concentric helicoidal spring. Two ball bearings facilitate either rotation or translation of the platform, furnace and stirrer with respect to the shaft. A groove and pin mechanism allows rotation of the quenching pot only when it is in the down position, to one side and below the dilatometer, Fig. 1-A. The same groove pin mechanism allows upward translation of the quenching pot only when it is directly below the sample ready for the quench. At this time the compression spring is released and raises the pot, Fig. 1-B.

---

*This is the maximum recorded speed. The actual speed for any volume of the specimen is higher because of the time for immersion of about 0.5 sec.

(4) Recording. Dilation and time readings are recorded during each run by means of a 16 mm movie camera. Continuous recording is done during quenching with the camera set at 16-64 frames per second, which provides adequate accuracy considering that the smallest scale division of the timer is 0.1 seconds. Frame by frame recording is performed during austenitization and transformation.

C) Explanation of dilation curves (schematic)

In order to explain other details of procedure such as problems in quenching and estimation of errors it is necessary to discuss briefly the type of data obtained.

First the method of reporting specimen length should be considered. As mentioned earlier the distance between dilatometer contacts is 4 in. (102 mm). Also the original dial reading is merely a starting point and the important data are the changes in dial reading. For easy comparison of data from different runs and to show differences in dimensionless terms, all the data are considered as though the specimen was exactly 1.0000 in. (25.4 mm) long at austenitizing temperature, to give a "relative length." In other words, consider the following experimental data:

Temperature	Dial reading	Measured difference	Measured difference/4	Relative length
1650°F	.3207	-	-	1.0000
1250°F	.2019	.0198	0.0049	0.9951

Therefore the "relative length curve" is a graph of the relative length changes observed after austenitization as a function of the logarithm of the time.

Next the two types of experimental conditions should be considered, Figs. 3-A,B. 1) No transformation occurs during the quench and then isothermal transformation takes place at temperature. 2) Some (unavoidable) transformation to martensite takes place during the quench. In some cases the balance of the austenite is allowed to transform isothermally to bainite and in others the specimen is subjected to further cooling to transform additional austenite to martensite.

A schematic graph of relative length vs. time in the first case is shown in Fig. 3-A. The specimen begins with a relative length of 1.0000 (25.4 mm) at point A in the austenitizing furnace. The following periods can be recognized in each isothermal transformation run:

Period A-B. Austenitizing Period

The sample is at the austenitizing temperature, in the γ-Fe field of the equilibrium phase diagram, to allow complete solution of carbides.

Period B-C. Air Cooling Period

The austenitizing furnace is removed at point B and the sample starts to cool slowly in the air as revealed by a slight contraction in the relative length curve.

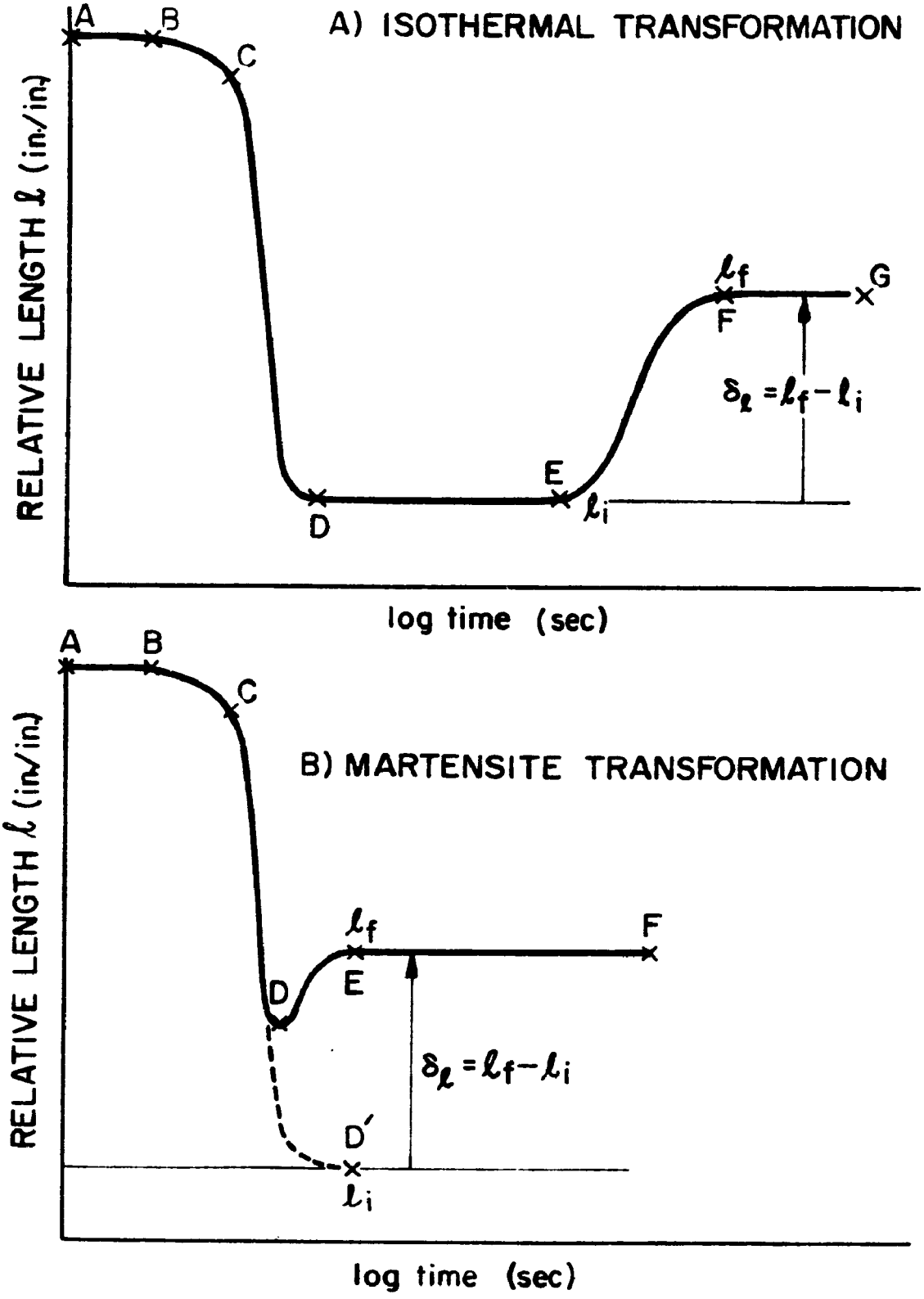


Fig. 3. Schematic illustration of dilation data.. Relative length vs log time

Period C-D. Lead Quench Period

The sample is now quenched to the desired transformation temperature.

Period D-E. Incubation Period

No length changes can be seen in the dilation curve during this period because the sample is still austenite. The length of this period depends mainly on the transformation temperature and analysis of the alloy and is of great importance since it should be long enough to allow the measurement of the relative length, "ℓ_i", before transformation.

Period E-F. Transformation Period

At point E transformation begins. During this period the fraction of austenite decreases and the fraction of the product phases increases as the transformation goes to completion. Although the temperature is constant, the reference length curve shows an expansion due to the transformation. In some cases, contraction due to transformation can also occur as discussed later. Point F defines the end of the transformation period and the final relative length reading, "ℓ_f". The linear transformation coefficient can be calculated now by

$$\delta_\ell = \ell_f - \ell_i \quad \text{(in./in.)} \tag{1}$$

When martensite is formed during quenching, Fig. 3-B, the minimum reading "D" is not characteristic of 100% austenite but of an austenite martensite mixture. It is

possible, however, to calculate the value D' which would have been obtained if no transformation took place. From the quenches to temperatures above Ms an accurate relation between contraction and quench bath temperature is developed. This curve is then extrapolated to give the expected contraction of 100% austenite, establishing point D' giving ℓ_i (calculated). The transformation coefficient is calculated as: $\delta_\ell = \ell_f - \ell_i$.

It should be recognized that at point E, when quenching between Ms and Mf, the sample will contain a mixture of martensite and retained austenite. The transformation coefficient in this case is therefore not the result of isothermal transformation, but still has practical engineering value in estimating distortion. These points are discussed further in considering the results.

D) Experimental problems

To obtain accurate data for the transformation coefficient two types of potential errors have to be overcome. 1) Spurious dilation at high temperatures, 2) stabilization of retained austenite at low temperatures.

Spurious dilation at high temperatures can be caused by four effects: a) transformation to high temperature products during the quench, b) creep, c) tempering of bainite, d) sluggishness of the reaction towards the end of some transformations.

(1) If the incubation time at the nose of the TTT curve is less than one second, it is difficult to avoid transforamtion during a quench into the bainite range. In pure low carbon alloys this difficulty was encountered and necessitated the production and use of the 5% Ni series. It is easy to determine if this effect is occurring because the first reading, ℓ_i, at bath temperature will be higher than the reading calculated from the normal graph of contraction vs. bath temperature. In other words, if the coefficient of expansion calculated from the quench data is less than $11 \times 10^{-6}/°F$ ($19.8 \times 10^{-6}/K$) the run is suspect and repeated or rejected if the problem persists.

Creep is encountered at high transformation temperatures especially with specimens thinner than standard used only when faster quenches were desired. The effect was minimized by counterweighting the inner member of the dilatometer.

The "tempering" of bainite is not really a spurious effect but must be recognized. In some cases* after the specimen transformed to bainite a small contraction took place due to structural changes. This point is discussed further under Results. Some temperatures, especially those close to the eutectoid temperature of the alloy and at pronounced bays of the TTT diagram lead to incomplete transformations, which makes it difficult to assess when the transformation finished. However, it has been observed

*Usually at the lower bainite range, Fig. 13.

from the experiments that in transformations shorter than 10,000 seconds the end reading, "ℓ_f", is sharp and easily obtained.

(2) Stabilization of austenite at low temperatures. In runs in which it was necessary to cool below the original quench temperature the amount of transformation during cooling is reduced if the cooling is not done promptly. To avoid this well known effect it was necessary to quench to the lower temperatures rapidly with prepared baths. In some cases it is not possible to obtain complete transformation even with liquid nitrogen and this point is discussed further under Results.

E) Experimental errors

In addition to the problems discussed in (4), the errors associated with the instrumentation are summarized in Table 8. To determine these values the dial gage was checked against standard gage blocks. The standard cell of the potentiometer was checked against a precision standard and the Chromel-Alumel thermocouples were calibrated against a Bureau of Standards Pt-10% Pt Rh thermocouple.

The correction for fused silica contraction requires separate discussion. The dilation which is transmitted to the dial gage when the temperature is decreased is made up of specimen contraction plus the contraction of the 4 in. (102 mm) length of fused silica which is immersed in the

Table 8. Summary of estimates of experimental error

Source of Error			Precision	Accuracy
Dilatometer	Specimen	Gauge	±0.00005 in.	±0.0025% of full scale
		Misallignment and vibrations	< -0.4% + 0.0% for max.	< -0.4% + 0.0% (max. misallignment angle: 5°)
		Bowing	< -0.08% + 0.0% for bowing radius of 15 in.	< -0.08% + 0.0% for a bowing radius of 15 in.
Temperature		Potentiometer	± 0.02 mv ± 0.5°F	+ 0.08 mv - 0.00 mv + 2°F - 0°F
		T.C.	± 0.02 mv ± 0.5°F	± 0.10 mv ± 3°F

bath. To obtain the true contraction of the specimen it is necessary to subtract the silica contraction. This correction has been made and is of the order of 2.5×10^{-4} for a quench into the bainite range.

IV. RESULTS

In this portion of the thesis the data are reviewed and discussed in the following sections:

A) Measurements of δ_ℓ using the quenching dilatometer.

B) Calculation of δ_V and δ_ℓ from lattice parameter measurements of Ridley and Roberts.

C) Comparison of measured and calculated values of δ_ℓ.

D) Significance of the values of δ_ℓ and the effects of composition and temperature.

(A) Dilatometric measurement of δ_ℓ

From the experimental data it is possible to describe the effects of both composition and temperature upon the transformation coefficient, δ_ℓ. The discussion begins with samples of typical data showing these effects. Next the data are grouped into three divisions for discussion according to the transformation mode:

The ferrite-pearlite-carbide range

The upper and lower bainite ranges

The martensite range.

Finally the overall behavior of δ_ℓ as a function of composition and transformation temperature is summarized.

It should be realized at the outset that it is theoretically possible to obtain data for δ_ℓ at all temperatures for all the alloys. However, due to experimental difficulties such as rapid transformation near 1000°F, all transformation modes have not been studied for all three groups of alloys. For example, the Fe-C-5% Ni group of alloys is useful to show the effect of carbon content upon the pearlitic, upper bainitic and martensitic transformations. However, due to the high Ni concentration, the lower bainite and the pearlite transformations close to the eutectoid temperature have not been studied in this group of alloys because of the extremely long transformation times required. On the other hand, pure Fe-C alloys

Table 9. Summary of values of δ_ℓ obtained from dilation data

Run No.	%C	Quenching Temperature °F	Austenite Coefficient of Expansion α_A (in./in. °F)	Linear Transformation Coefficient δ_ℓ (in./in.)·10^4	Aust. Temp. °F	Remarks
			Fe-C Alloys			
60	0.55	1258	12.0	27.7	1592	
59	0.76	1266	12.7	23.4	1510	
52	0.94	1286	11.8	14.1	1571	
48	0.94	1271	12.5	17.8	1568	
51	0.94	1253	11.5	13.5	1574	
47	0.94	1233	12.3	16.0	1563	
44	0.94	829	11.2	17.1	1568	
86	0.94	723	12.2	25.4	1630	
87	0.94	635	12.5	29.1	1613	
99	0.94	646	-	28.6	1626	
90	0.94	614	12.3	27.2	1649	
89	0.94	598	12.2	26.1	1637	
88	0.94	574	12.3	27.4	1628	
94	0.94	533	12.0	38.3	1630	
93	0.94	517	12.1	39.4	1612	
91	0.94	480	11.8	40.7	1612	
92	0.94	394	11.1	38.6	1630	

Table 9 (continued)

Run No.	%C	Quenching Temperature °F	Austenite Coefficient of Expansion α_A (in./in. °F)	Linear Transformation Coefficient δ_ℓ (in./in.)·10^4	Aust. Temp. °F	Remarks
			Fe-C Alloys (cont.)			
75	1.10	1306	11.2	13.8	1661	
74	1.10	1288	12.3	11.5	1664	
77	1.10	1281	11.9	13.6	1665	
55	1.10	1251	11.6	12.9	1663	
56	1.10	1250	11.8	12.8	1669	
85	1.10	749	12.1	21.0	1667	
71	1.10	720	11.6	18.2	1680	
82	1.10	672	12.3	25.4	1673	
83	1.10	621	12.9	34.4	1680	
73	1.10	528	12.6	40.5 (34.4*)	1672	
84	1.10	504	12.7	38.1 (35.6*)	1665	
			Fe-C-5% Ni Alloys			
145	0.23	1169	12.6	25.7	1691	
166	0.23	1125	12.3	41.3	1705	

Table 9 (continued)

Run No.	%C	Quenching Temperature °F	Austenite Coefficient of Expansion α_A (in./in. °F)	Linear Transformation Coefficient $\delta_{4\ell}$ (in./in.)·10^4	Aust. Temp. °F	Remarks
			Fe-C-5% Ni Alloys (cont.)			
144	0.23	1069	12.1	33.6	1715	
167	0.23	1025	11.2	35.1	1684	
159	0.23	979	12.1	44.0	1706	
143	0.23	958	12.0	41.1	1709	
162	0.23	913	11.7	43.6	1686	
142	0.23	851	12.3	50.1	1700	
169	0.23	813	12.2	47.2	1693	
141	0.23	765	12.1	52.5	1718	
174	0.23	723	12.1	51.3	1685	
140	0.23	689	12.0	43.9	1701	
180	0.23	443	12.4	66.6		
		204#		84.7		
		146#		88.3		
		89#		91.9		
		58#		93.8		
		30#		95.6		
		-58#		102.9		
		-319#		125.8		
158	0.44	1092	12.0	26.0	1703	
146	0.44	967	12.2	39.4	1690	

Table 9 (continued)

Run No.	%C	Quenching Temperature °F	Austenite Coefficient of Expansion α_A (in./in. °F)	Linear Transformation Coefficient $\delta_{4\ell}$ (in./in.)·10^4	Aust. Temp. °F	Remarks
			Fe-C-5% Ni Alloys (cont.)			
147	0.44	901	12.7	42.7	1652	
163	0.44	899	12.1	39.6	1700	
164	0.44	856	12.3	45.8	1691	
148	0.44	813	12.2	45.1	1688	
149	0.44	756	12.1	43.8	1660	
175	0.44	703	12.0	39.7	1710	
151	0.44	685	12.6	51.6	1691	
181	0.44	444	12.4**	44.7	1625	
		192#		81.6		
		145#		85.8		
		100#		88.9		
		62#		92.0		
		41#		96.7		
		-7#		101.3		
		-60#		107.9		
		-319#		128.6		
156	0.72	1020	11.8	21.2	1707	
160	0.72	948	12.4	28.4	1695	
161	0.72	903	11.8	27.9	1683	
154	0.72	841	12.6	37.6	1695	
170	0.72	788	12.2	33.9	1707	

Table 9 (continued)

Run No.	%C	Quenching Temperature °F	Austenite Coefficient of Expansion α_A (in./in. °F)	Linear Transformation Coefficient $\delta_{4\ell}$ (in./in.)·10^4	Aust. Temp. °F	Remarks
			Fe-C-5% Ni Alloys (cont.)			
173	0.72	736	12.8	37.5	1690	
152	0.72	702	12.7	42.9	1670	
182	0.72	394	12.4**	0.0	1592	
		256#		38.1		
		208#		59.7		
		164#		74.2		
		120#		78.9		
		66#		91.3		
		-49#		111.9		
		-319#		134.0		
165	1.12	936	-	21.4	1680	
155	1.12	905	12.2	16.8	1698	
153	1.12	751	11.8	21.4	1700	
171	1.12	734	12.6	27.6	1708	
172	1.12	680	12.3	27.8	1697	
179	1.12	442	12.4**	0.0	1619	
		200#		3.1		
		161#		26.5		
		84#		49.3		
		-76#		104.2		
		-319#		124.6		
	tempering	64		97.4		after 1 hr at 76°F
		75		89.2		after 20 min at 185°F
		82		75.5		after 30 min at 460°F
		80		60.0		after 1 hr at 1080°F

Table 9 (continued)

Run No.	%C	Quenching Temperature °F	Austenite Coefficient of Expansion α_A (in./in. °F)	Linear Transformation Coefficient $\delta_{4\ell}$ (in./in.)·10^4	Aust. Temp. °F	Remarks
			AISI-SAE Steels			AISI-SAE No.
136	0.99	1245	-	21.1	1562	52100
137	0.99	1166	11.6	19.1	1560	52100
134	0.99	1110	12.2	21.9	1563	52100
133	0.99	1041	12.0	23.9	1561	52100
128	0.99	1008	12.1	25.9	1558	52100
129	0.99	944	12.2	26.0	1564	52100
130	0.99	823	12.5	34.7	1560	52100
132	0.99	796	12.4	35.5	1557	52100
120	0.99	752	12.3	44.3	1550	52100
121	0.99	725	12.5	44.2	1560	52100
123	0.99	673	12.4	52.3	1556	52100
124	0.99	641	-	51.5	1511	52100
122	0.99	572	12.6	56.6	1556	52100
66	0.38	1197	12.3	26.4	1550	4140
65	0.39	1165	12.7	25.0	1548	4140

Table 9 (continued)

Run No.	%C	Quenching Temperature °F	Austenite Coefficient of Expansion α_A (in./in. °F)	Linear Transformation Coefficient $\delta_{4\ell}$ (in./in.)·10^4	Aust. Temp. °F	Remarks
			AISI-SAE Steels			AISI-SAE No.
119	0.39	956	12.3	29.8	1569	4140
70	0.39	913	12.5	32.5	1567	4140
118	0.39	878	12.5	33.7	1563	4140
117	0.39	843	12.4	34.1	1559	4140
113	0.39	809	12.2	33.0	1563	4140
114	0.39	799	12.5	34.5	1551	4140
115	0.39	787	12.4	33.8	1548	4140
116	0.39	745	12.2	35.6	1561	4140
101	0.39	722	12.5	36.3	1567	4140
104	0.39	699	12.5	31.9	1570	4140
112	0.39	672	12.3	33.4	1567	4140
103	0.39	670	12.2	32.6	1559	4140
110	0.39	629	12.2	35.0	1572	4140
111	0.39	617	12.3	41.4	1553	4140
109	0.39	597	11.6	49.8	1561	4140
105	0.39	543	12.4**	53.2	1560	4140***

Table 9 (continued)

Run No.	%C	Quenching Temperature °F	Austenite Coefficient of Expansion α_A (in./in. °F)	Linear Transformation Coefficient δ_{ℓ} (in./in.)·10^4	Aust. Temp. °F	Remarks
			AISI-SAE Steels			AISI-SAE No.
106	0.39	504	12.4**	56.7	1564	4140
125	0.39	432	12.4**	57.8	1560	4140
177	0.39	406 140#	12.4**	55.7 66.3	1576	4140
79	0.49	1298	12.3	32.0	1671	1050
78	0.49	1262	12.1	31.2	1673	1050
E24	0.40	1191	12.0	30.1	1570	8640
E25	0.40	1147	12.2	30.5	1569	8640
E26	0.40	1099	12.2	30.5	1573	8640
E18	0.40	1006	11.7	32.5	1587	8640
E21	0.40	967	11.3	32.2	1562	8640
E16	0.40	931	11.4	35.4	1587	8640
E15	0.40	900	11.5	35.0	1576	8640
E14	0.40	859	11.3	37.5	1570	8640
43	0.40	762	12.0	40.0	1581	8640
E 3	0.40	744	12.1	46.2	1583	8640

Table 9 (continued)

Run No.	%C	Quenching Temperature °F	Austenite Coefficient of Expansion α_A (in./in. °F)	Linear Transformation Coefficient $\delta_{4\ell}$ (in./in.)·10^4	Aust. Temp. °F	Remarks
			AISI-SAE Steels			AISI-SAE No.
E 2	0.40	732	11.7	48.0	1566	8640
E10	0.40	710	12.4	48.6	1510	8640

* This value was obtained after holding at temperature about 20 hours.

In this case the same specimen was quenched in bath at successively lower temperatures.

**Assumed coefficient because quench temperature below Ms.

***Martensite and bainite.

can be used to determine the effect of carbon at the upper range of pearlite transformation temperatures but not at the lower range because of the rapid transformation. Fe-C alloys can also provide data for the irregular behavior observed in the upper to lower bainite transition. The selected group of AISI-SAE steels permits complete measurements at both pearlite and bainite temperature ranges (AISI-SAE 52100 steel) and shows the effect of carbon in high temperature pearlite transformations (by comparing AISI-SAE 52100 with 1050). Finally, by the comparison of AISI-SAE 52100 steel, Fe-1.12% C-5% Ni and Fe-1.12% C alloys together with AISI-SAE 4140, 8640 and 1050 steels, Fe-0.44% C-5% Ni and Fe-0.55% C alloys, it is possible to indicate the effect of alloying elements at different carbon levels. The data are summarized in Table 9.

1) Samples of experimental data showing overall effects of temperature and composition.

The most comprehensive data, Figs. 4, 5 and 6 were obtained for the 5% Ni alloys with carbon varying from 0.23% and 1.12% C because it was possible to measure the dilation at practically all temperatures. The actual data are shown for the 0.23, 0.72, 1.12% C levels.

Beginning with the 0.23% C material, Fig. 4, it is seen that δ_{ℓ} for bainite is greater than for the reaction to ferrite and pearlite.

The 0.76 and 1.12% C alloys, Fig. 5 and 6, show

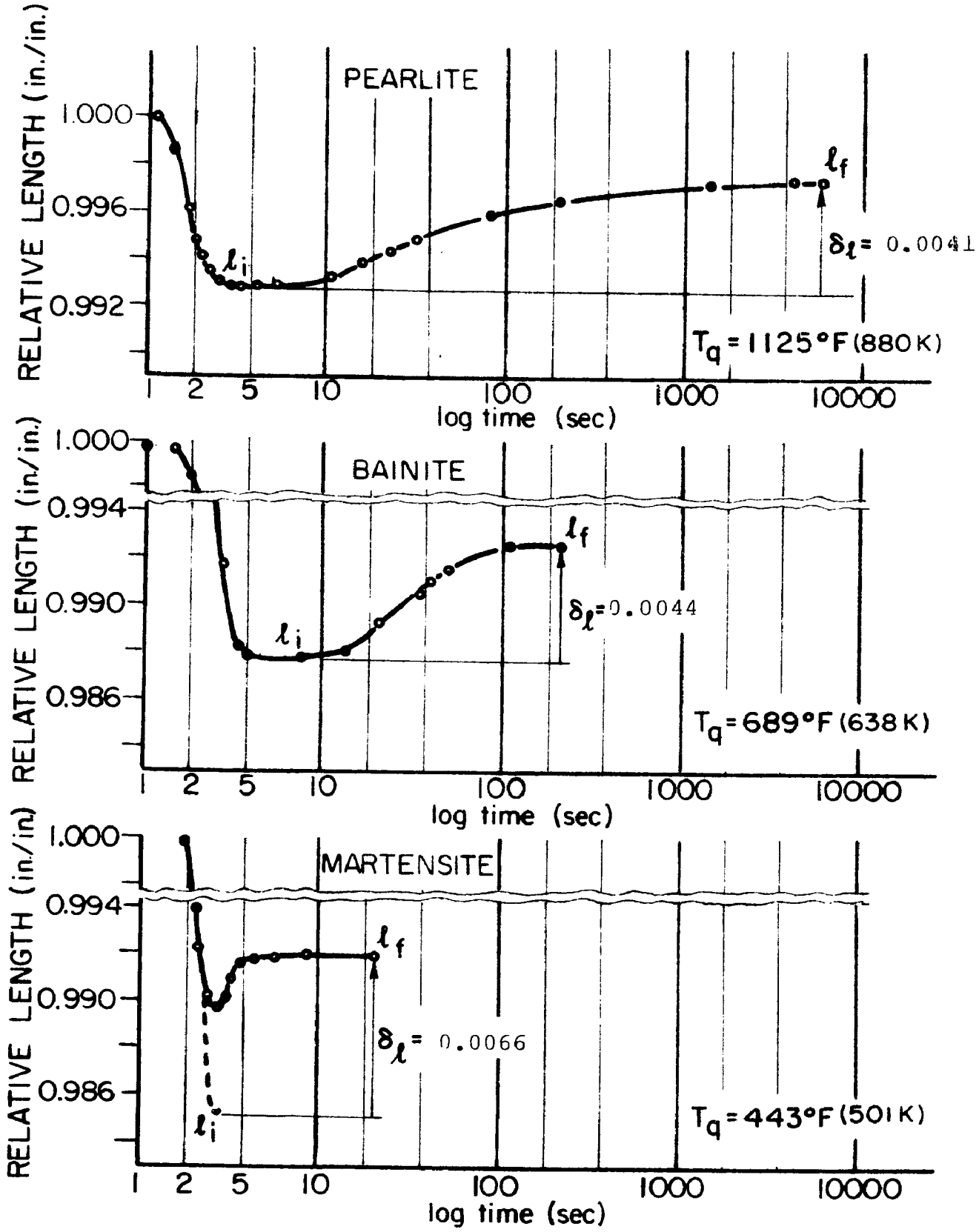


Fig. 4. Relative length vs time, 0.23% C-5% Ni. Note the increase in δ_l as the quench temperature is lowered.

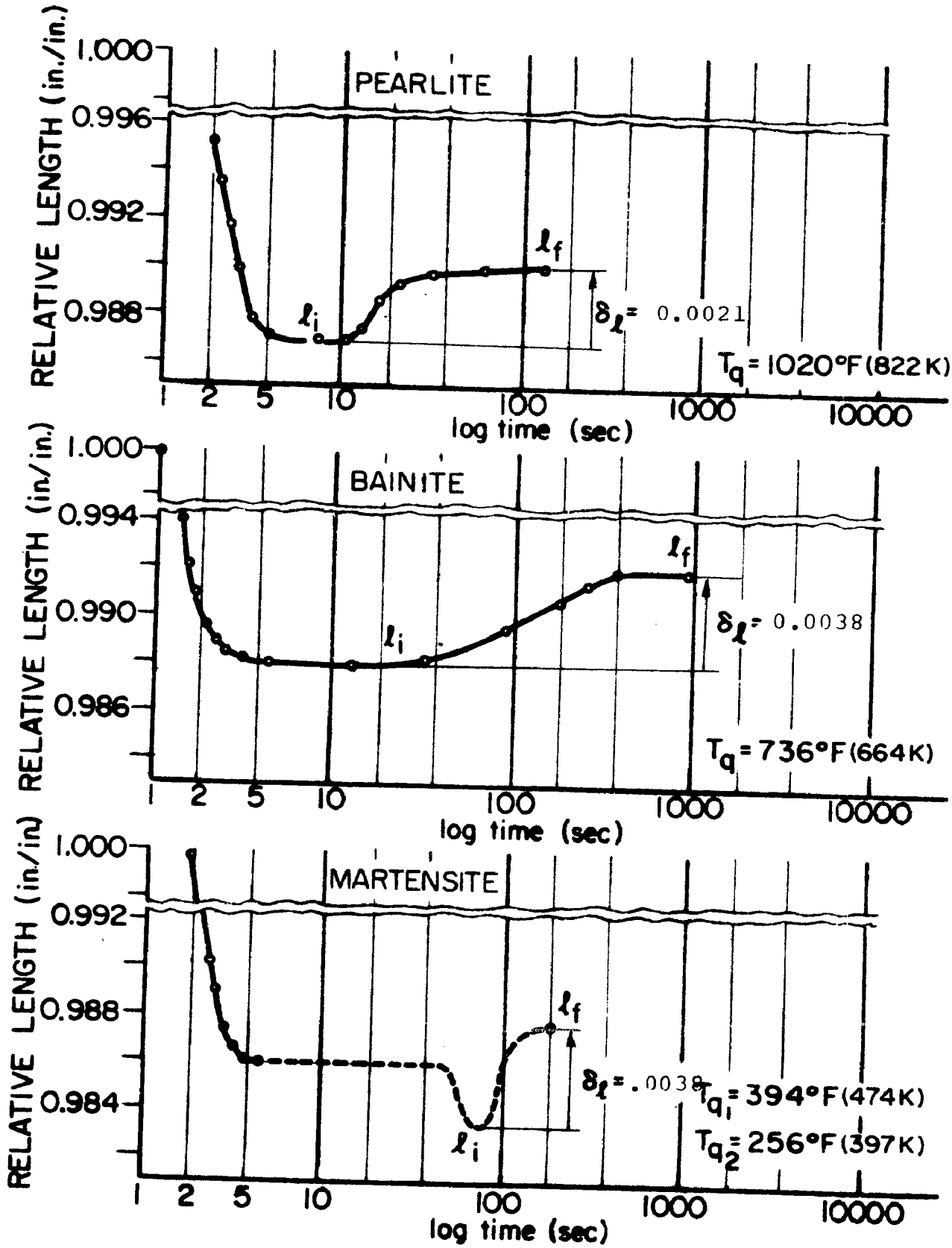


Fig. 5. Relative length vs time, 0.72% C-5% Ni. In the case of martensite the specimen was first quenched in a bath above Ms(394°F), then in a bath at 256°F producing some martensite.

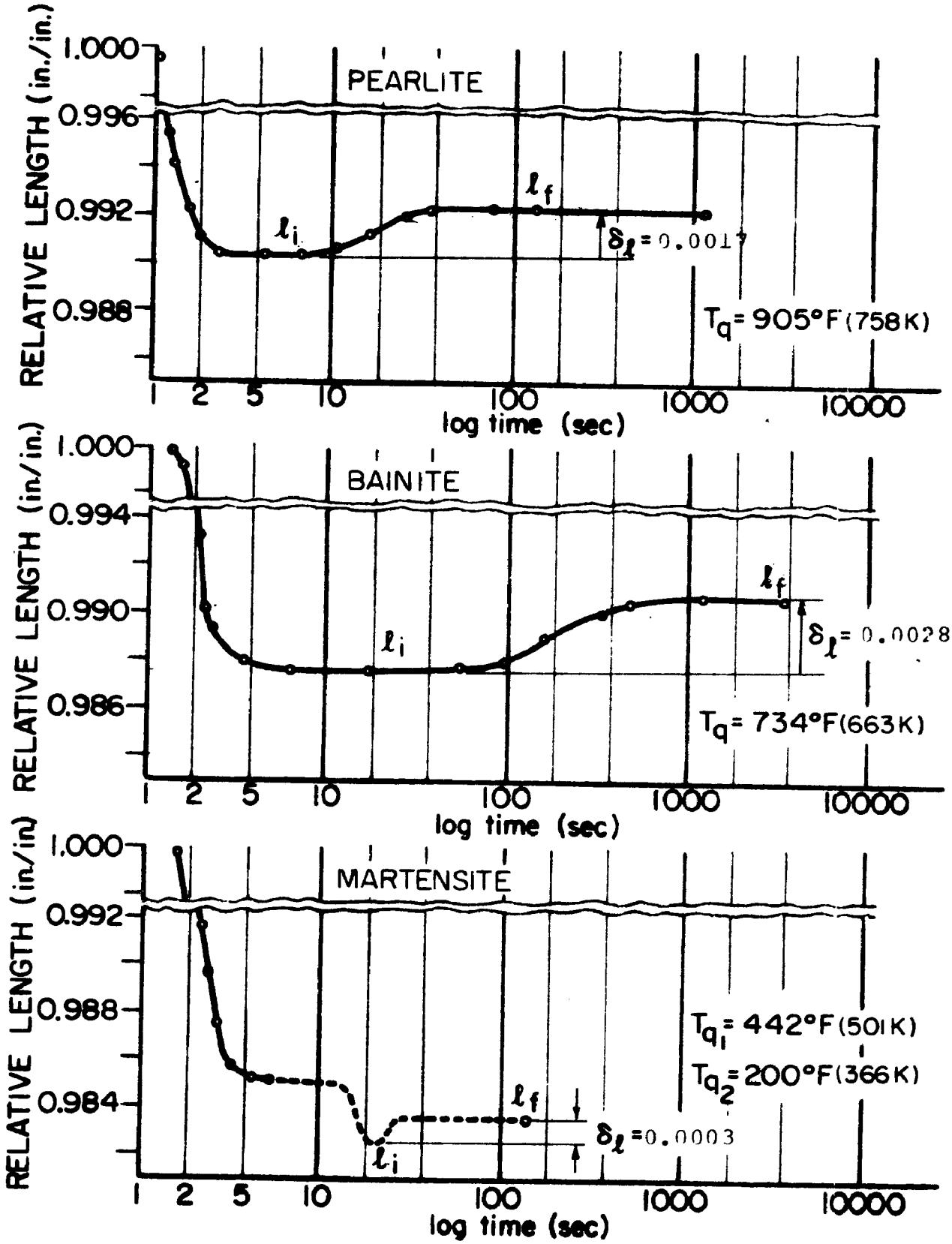


Fig. 6. Relative length vs time, 1.13% C-5% Ni. In the case of martensite, specimen quenched first to above Ms, then to 200°F.

progressively lower values of δ_ℓ for the pearlite and upper bainite regions. The martensite region requires special discussion later because of retained austenite. From basic data of this type transformation coefficients for a variety of analyses and temperatures of transformation were calculated as shown in Table 9. These data may now be compared.

2) The ferrite-pearlite-cementite range

In discussing these higher temperature transformation data, first the pure Fe-C alloys, then the Fe-C-5% Ni alloys and finally the AISI-SAE steels may be considered in the range of 1300-1000°F (977-811 K).

In the pure Fe-C alloys satisfactory data were obtained over a wide range of temperatures with the 0.95% and 1.1% C materials, Fig. 7. At lower carbon contents the coefficient could only be obtained for a few runs above the nose temperature. Even with the best quenching procedures some austenite transformed during the quench in runs attempted at lower temperatures. However, the satisfactory data show a trend toward higher transformation coefficients at lower carbon contents, Fig. 11.

The Fe-C-5% Ni data are practically complete over a wide range of carbon contents, Figs. 8-A,B,C,D, and consistent with the findings for Fe-C alloys. The martensite range in these figures is discussed later in part 4). In this

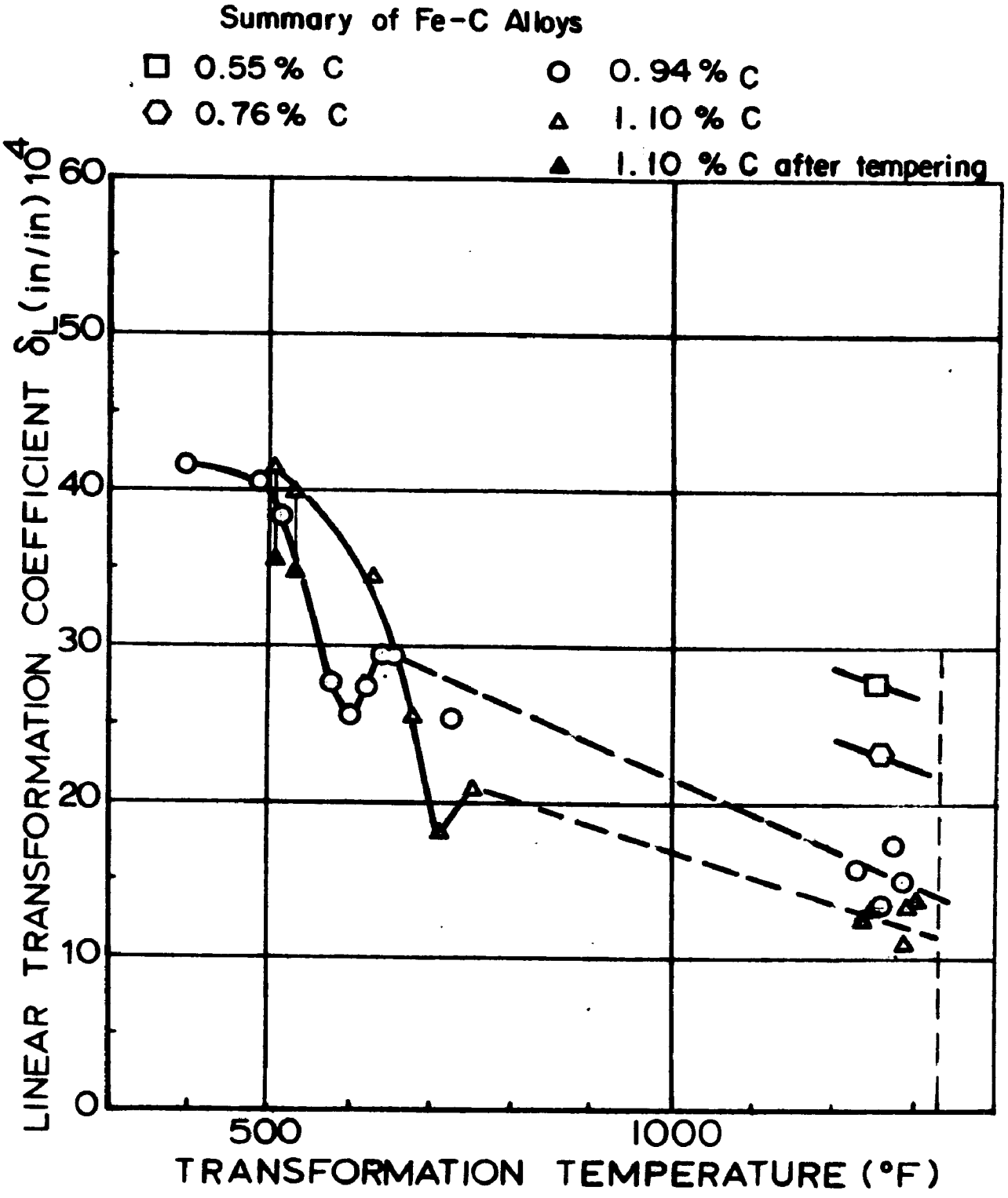


Fig. 7. Summary of transformation coefficient, δ_ℓ, for Fe-C alloys.
Note decrease in δ_ℓ as %C increases in pearlite range. Dashed line indicates region where data were not obtainable due to fast transformation rate. Bainite reaction discussed later in part 3).

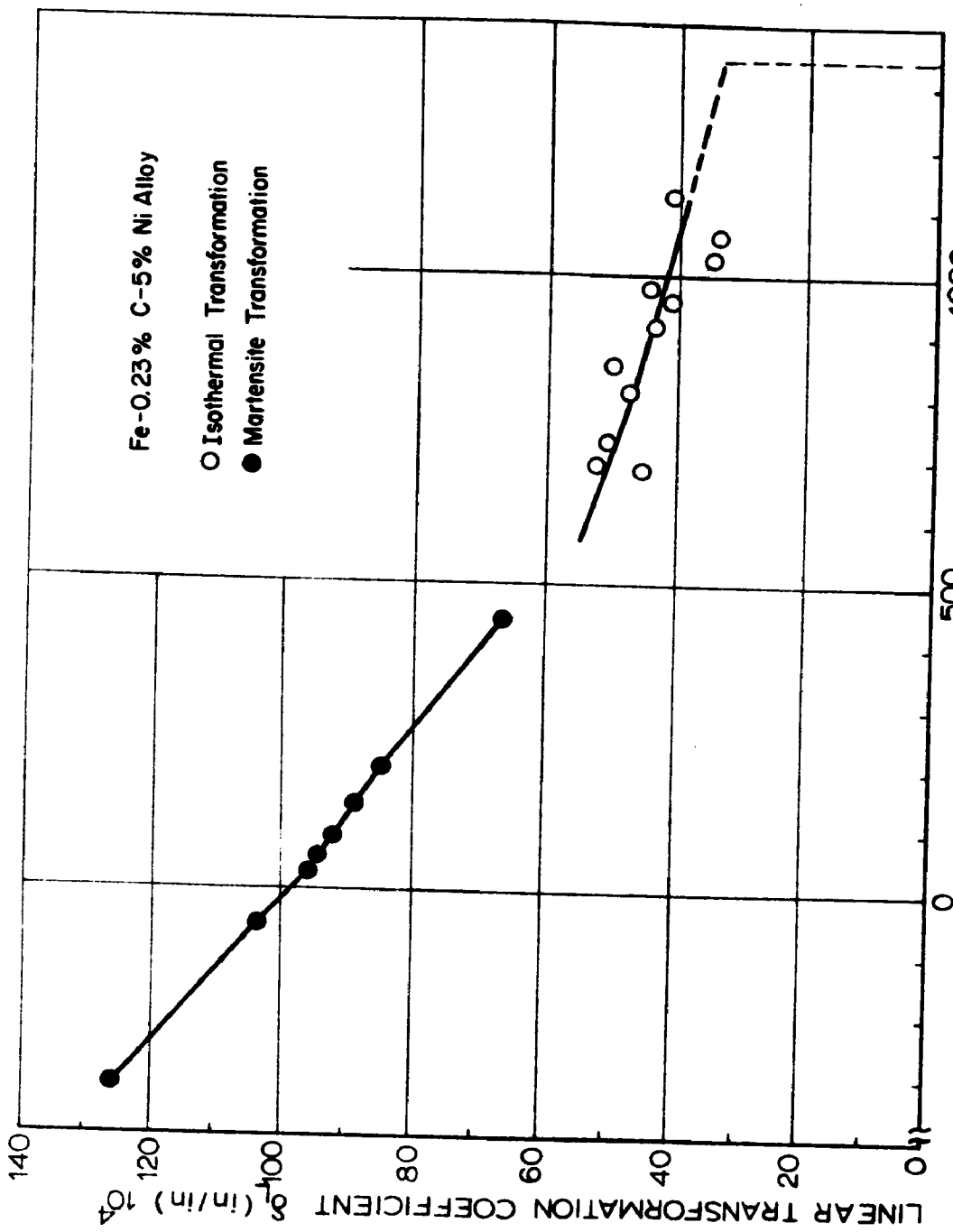


Fig. 8-A. Transformation coefficient, δ_ℓ, vs temperature, 0.23% C-5% Ni

Data for martensite obtained by quenching to successively lower temperatures in one run. See part 4). No separate data for martensite could be obtained near 500°F because of bainite formation.

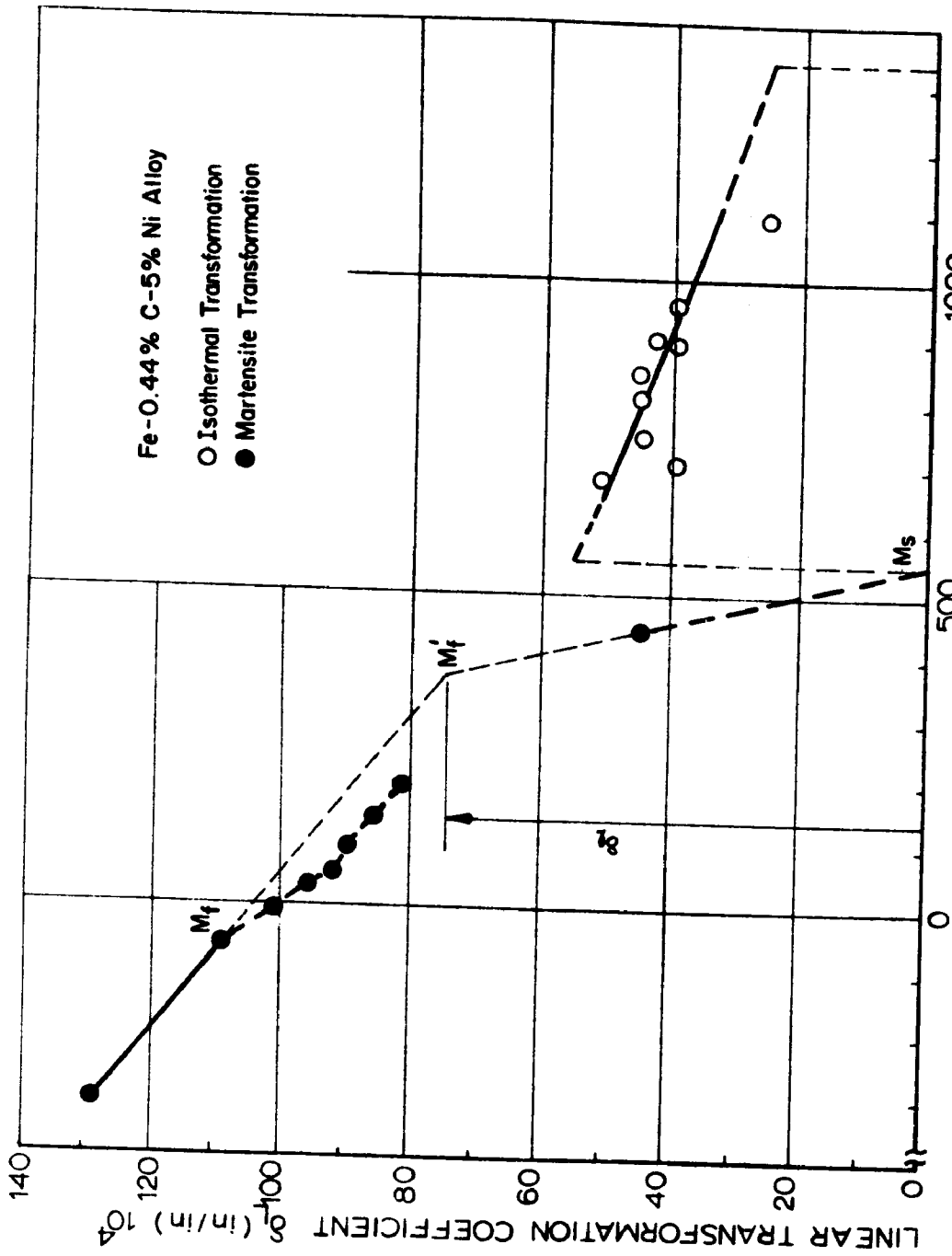


Fig. 8-B. Transformation coefficient, δ_γ, vs temperature, 0.44% C-5% Ni

The dashed line Ms to Mf' was derived from the slope established in Figs. 8-C and 8-D.

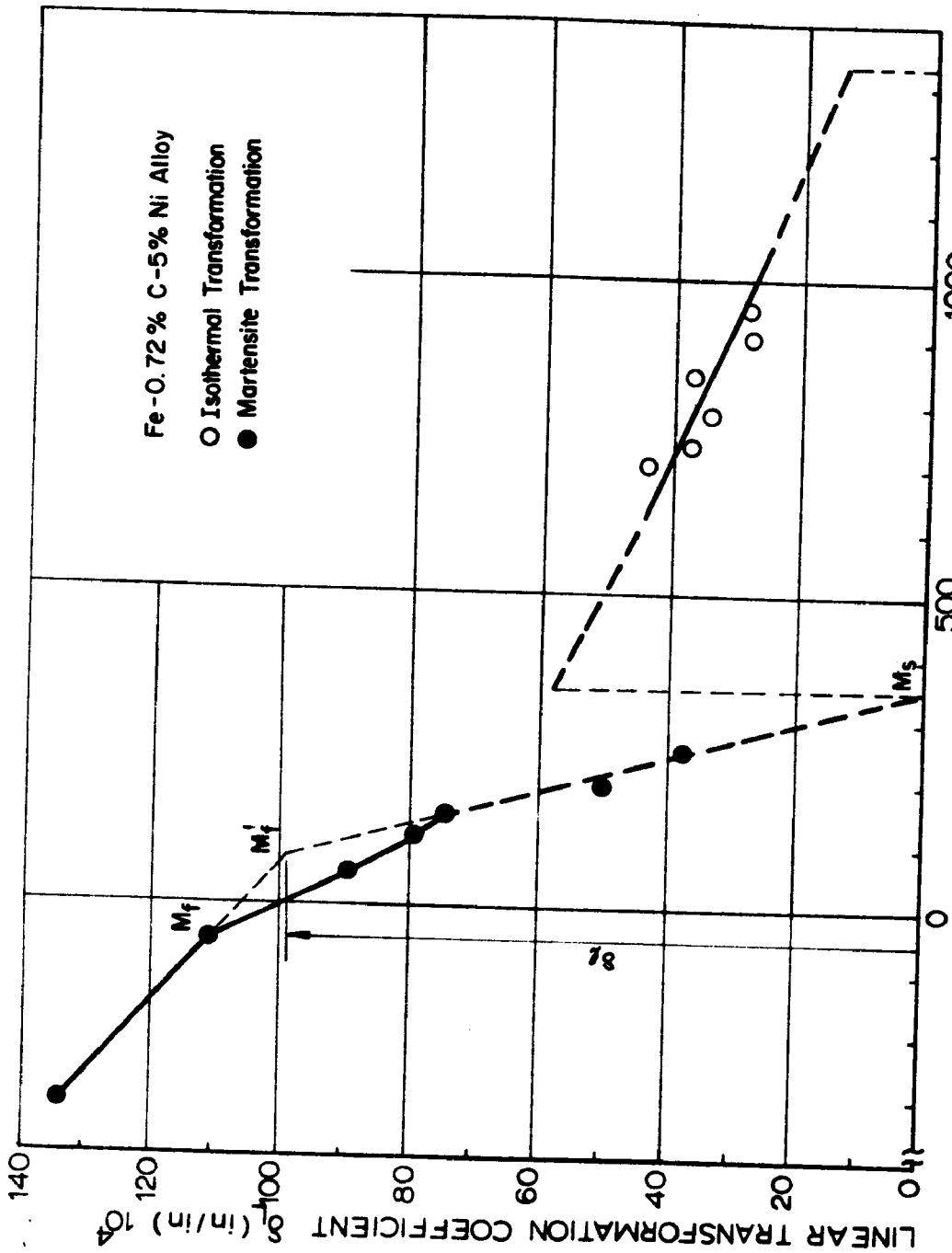


Fig. 8-C. Transformation coefficient, δ_ℓ, vs temperature, 0.72% C-5% Ni

Mf' is the Mf which would probably be obtained if no austenite stabilization took place. Martensite points were obtained on same run using baths at successively lower temperatures.

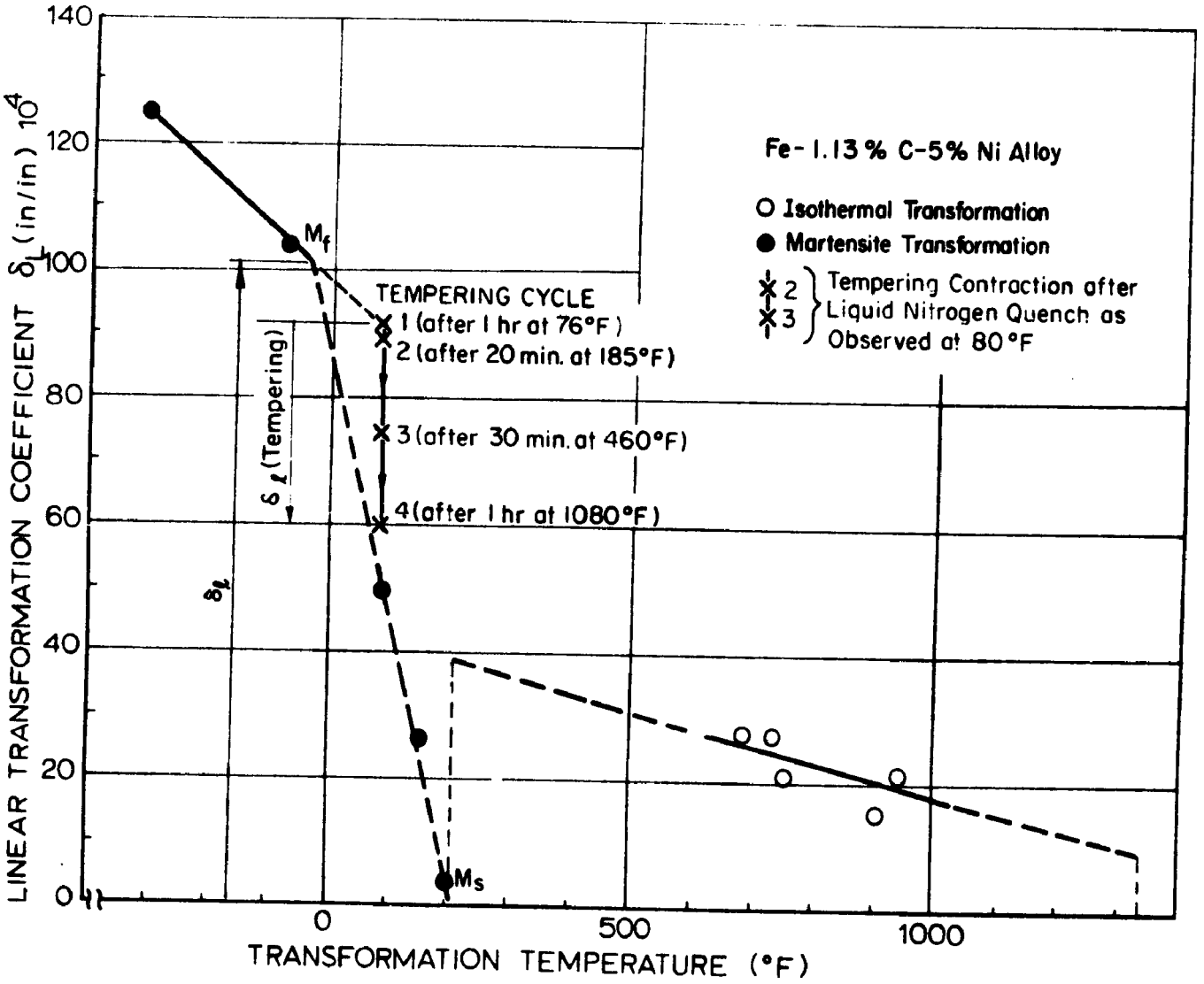


Fig. 8-D. Transformation coefficient, δ_ℓ, vs temperature, 1.13% C-5% Ni

Martensite points were obtained on same run using baths at successively lower temperatures. Tempering cycle (1 hr at 76°F, 20 min at 185°F, 30 min at 460°F, and 1 hr at 1080°F) performed after liquid nitrogen quench indicates a room temperature contraction of 32 x 10^{-4} (in./in.).

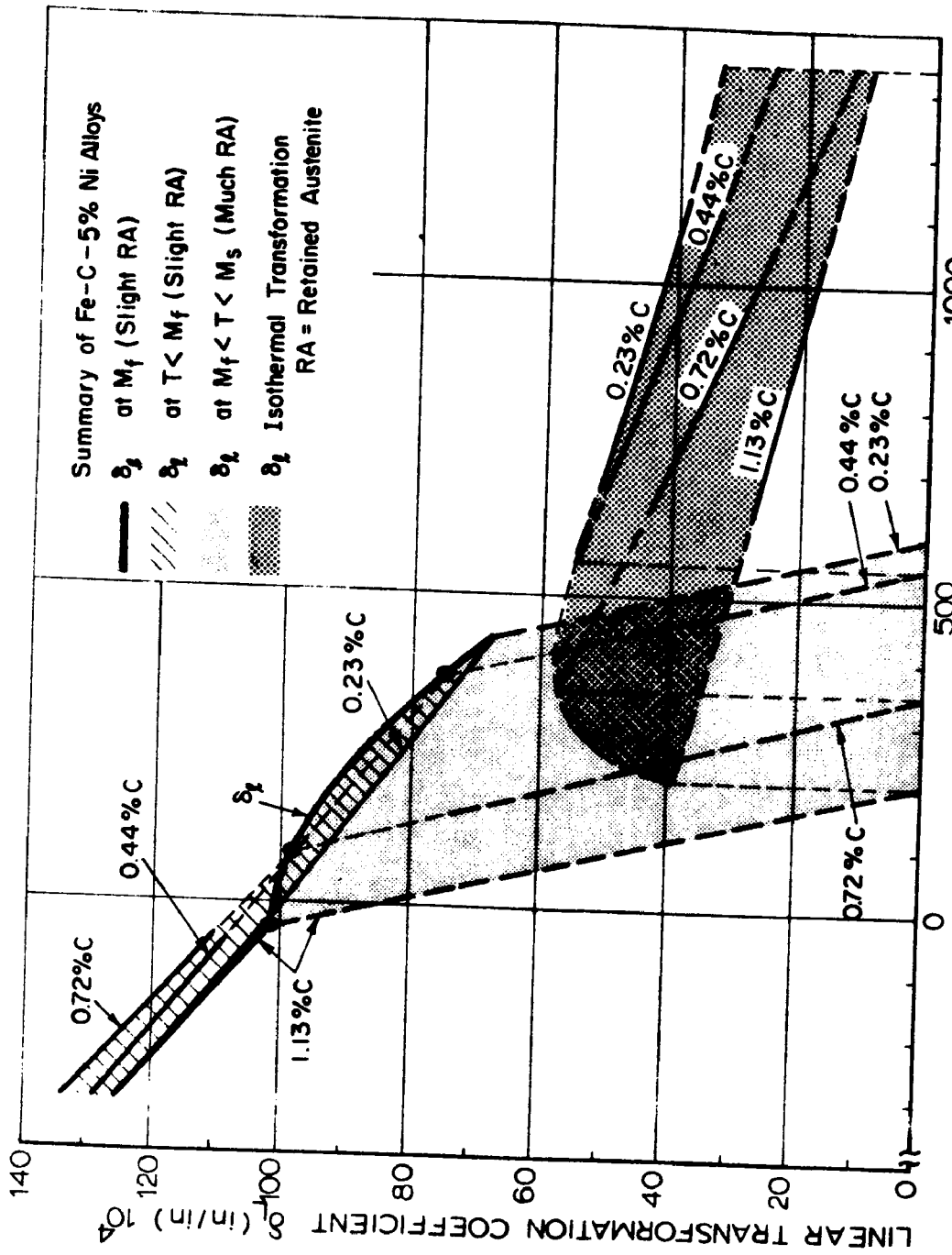


Fig. 8-E. Transformation coefficient, δ_ℓ, vs temperature, all 5% Ni alloys

The heavy line δ_ℓ at Mf is the locus of points of different alloys showing δ_ℓ when the particular alloy reaches Mf temperature (depending upon carbon content).

case the transformation coefficient decreases with increased carbon content, Fig. 11. These series also show an increase of the transformation coefficient with decreased transformation temperature.

The AISI-SAE steels exhibit effects similar to the preceding alloys in Figs. 9 and 10. However, the transformation coefficients measured for 4140 and 8640 are somewhat lower than the ones for other alloys of similar carbon content. This may be attributed to the low austenitizing temperature used, which although adequate to put Fe_3C in solution in γ-Fe, may have been too low to dissolve Mo_2C. This would decrease slightly the volume fraction of the austenite.

The effects of the carbon content and temperature in the pearlite range are summarized in Fig. 11. Despite the large range of alloy content, the data follow the same trend at both 1000 and 1200°F (811 and 922 K).

3) The bainite range

In general the values of the transformation coefficient follow the same trend in the bainite region as in the pearlite range, especially in the upper bainite range,* Figs. 7-10. A deviation from this behavior is observed at the transition temperature between upper and lower bainite, Fig. 12. The transformation coefficient for some alloys shows, with falling temperature, a slight dip followed by

*Approx. 800-1000°F (700-811 K)

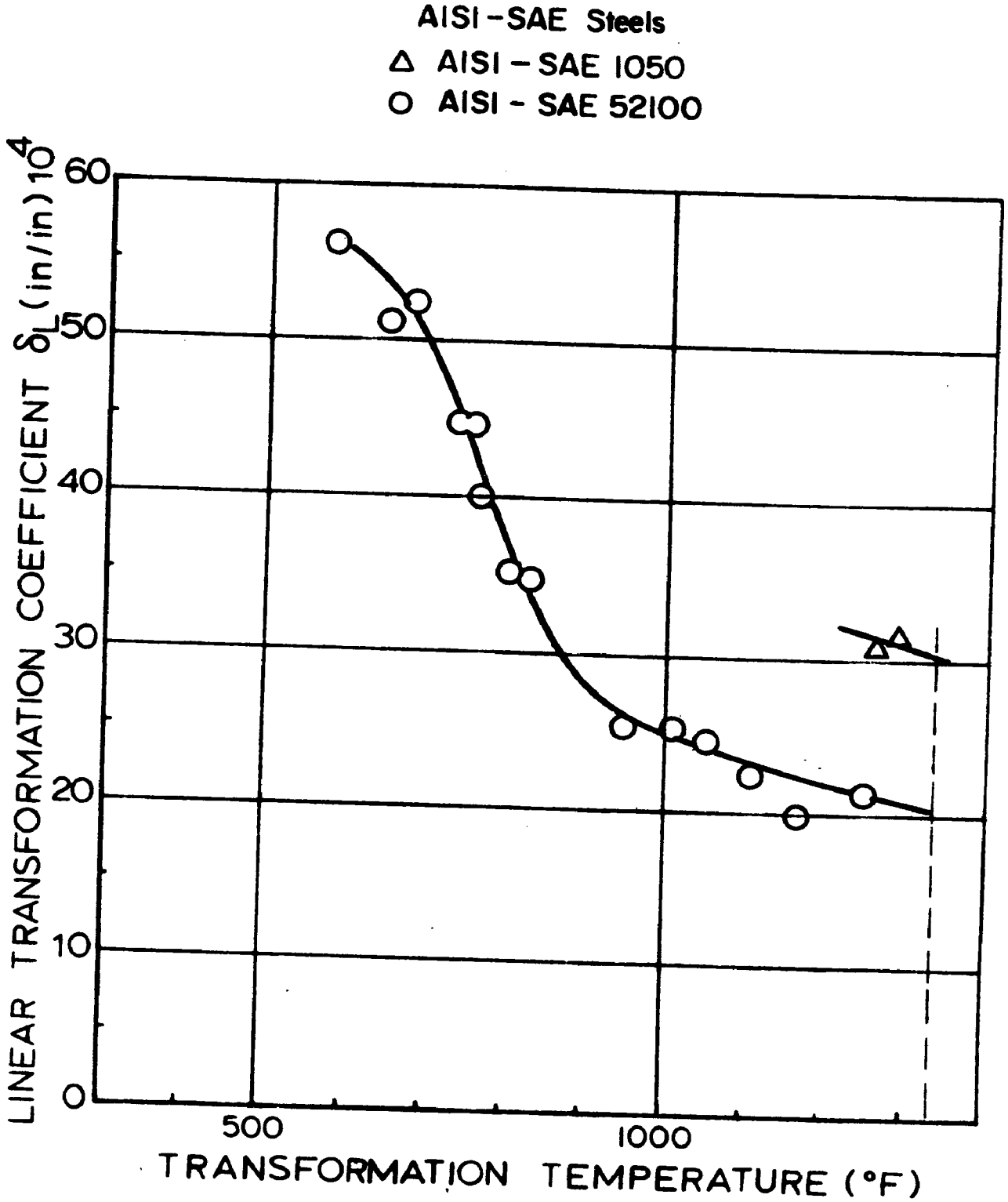


Fig. 9. Transformation coefficient, δ_ℓ, for AISI-SAE 52100 and AISI-SAE 1050 in pearlite and bainite ranges. The sharp rise of δ_ℓ in bainite range of AISI-SAE 52100 is probably due to ferrite supersaturation with carbon (see text pages 65, 86 and 111-112).

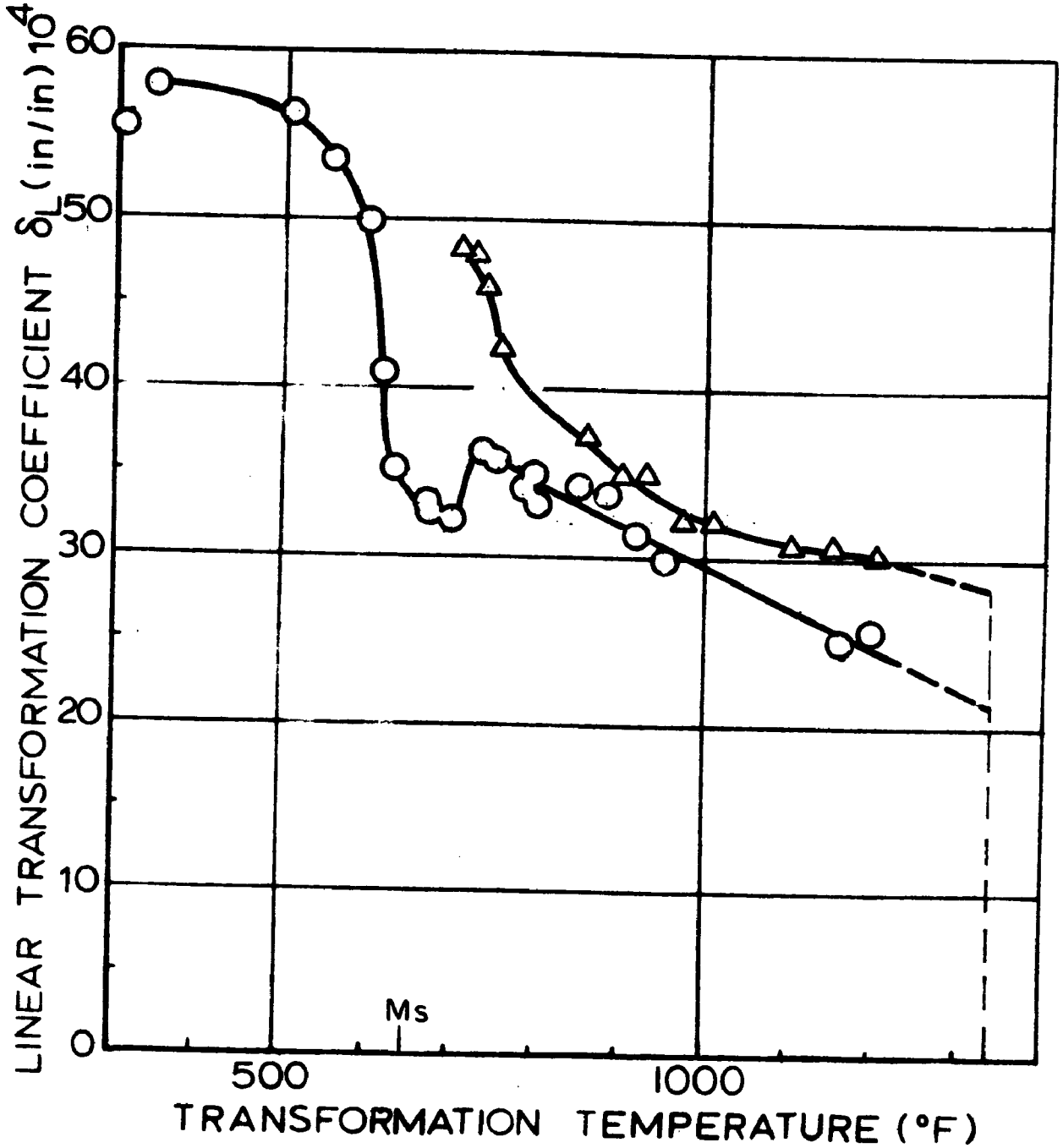
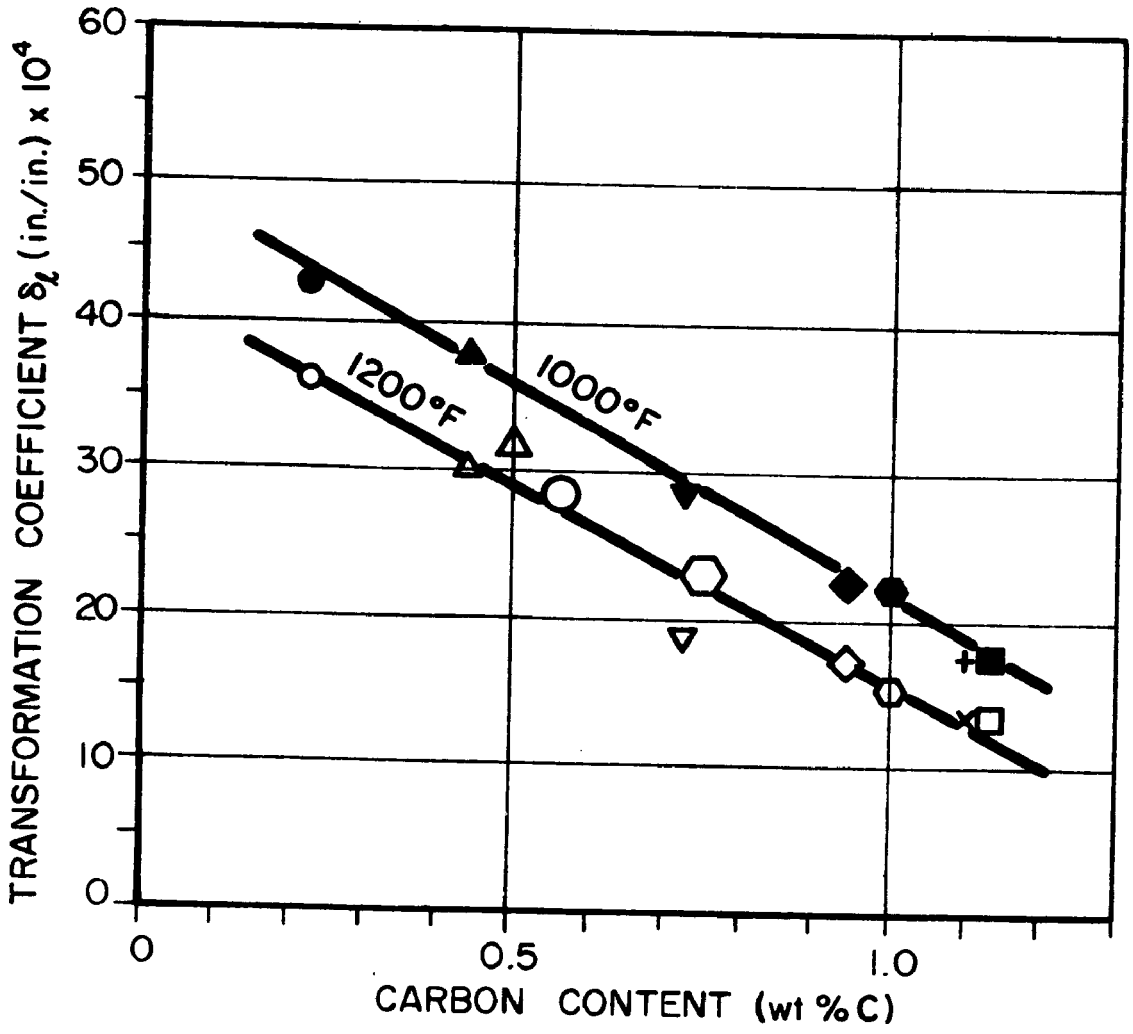


Fig. 10. Transformation coefficient, δ_ℓ, vs temperature for AISI-SAE 4140 and 8640 in pearlite and bainite ranges. Note dip in curve for 4140 followed by rise. (See text pages 65, 86 and 111-112 for bainite discussion.)



	1000°F	1200°F
Fe-0.23%C-5%Ni	●	○
" 0.44 " " "	▲	△
" 0.72 " " "	▼	▽
" 0.13 " " "	■	□
Fe-0.55%C	*	○

	1000°F	1200°F
Fe-0.76%C	*	⬡
Fe-0.94%C	◆	◇
Fe-1.10%C	+	×
SAE 52100	⬢	○
SAE 1050	*	△

Fig. 11. Transformation coefficient, δ_ℓ, in pearlite range vs % C at 1000 (811 K) and 1200°F (922 K). (*) Transformation at 1000°F is too rapid. Note the striking effect of carbon content as opposed to the unappreciable effect of other alloying elements.

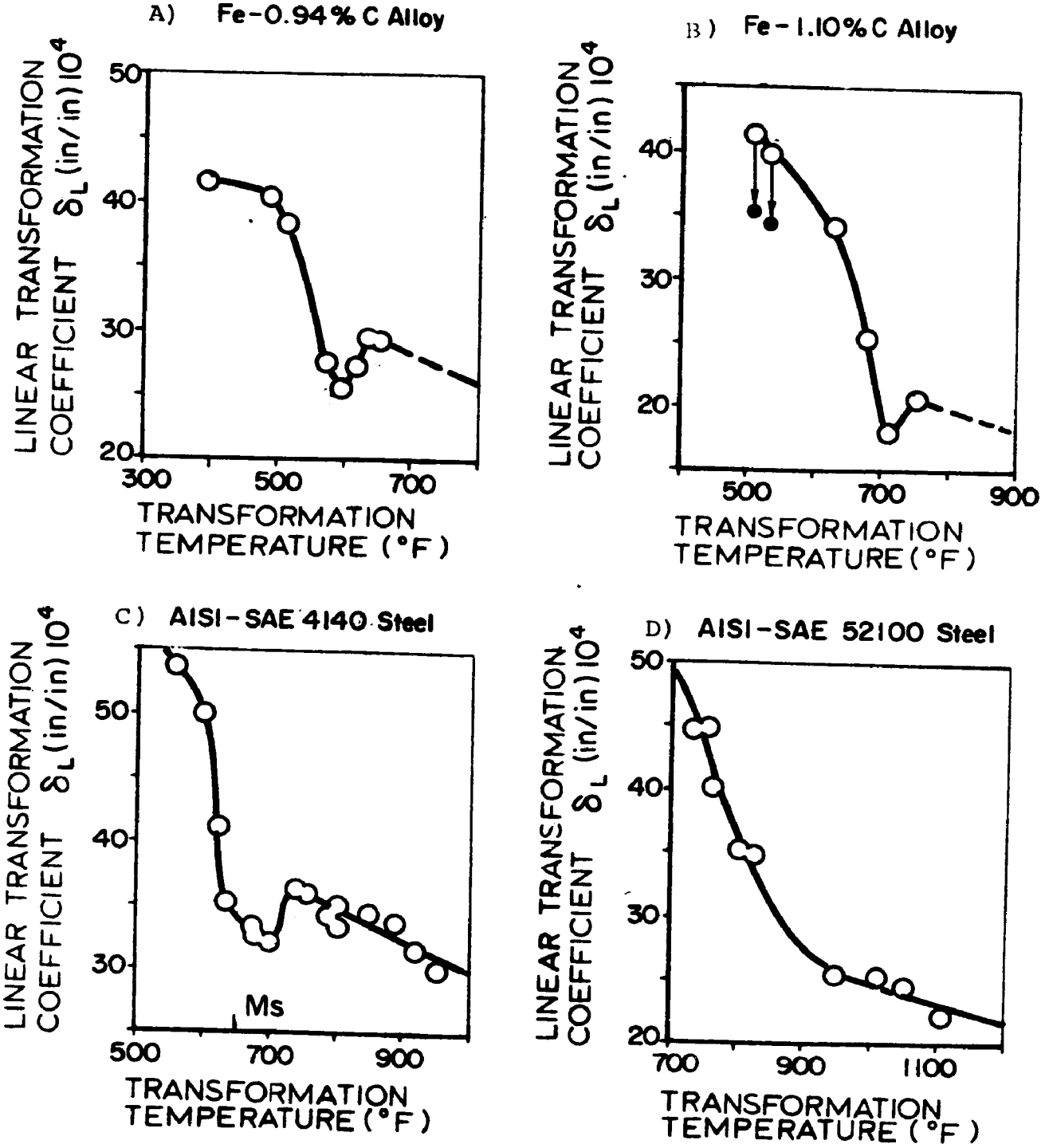


Fig. 12. Transformation coefficient, δ_ℓ, in bainite range showing irregular behavior,

A) Fe-0.94% C alloy; B) AISI-SAE 4140 steel;
C) Fe-1.10% C alloy; D) AISI-SAE 52100 steel

Dark points in B represent length obtained after tempering in bath 10 hr (see Fig. 13). For bainite discussion see text pages 65, 86, and 111-112.

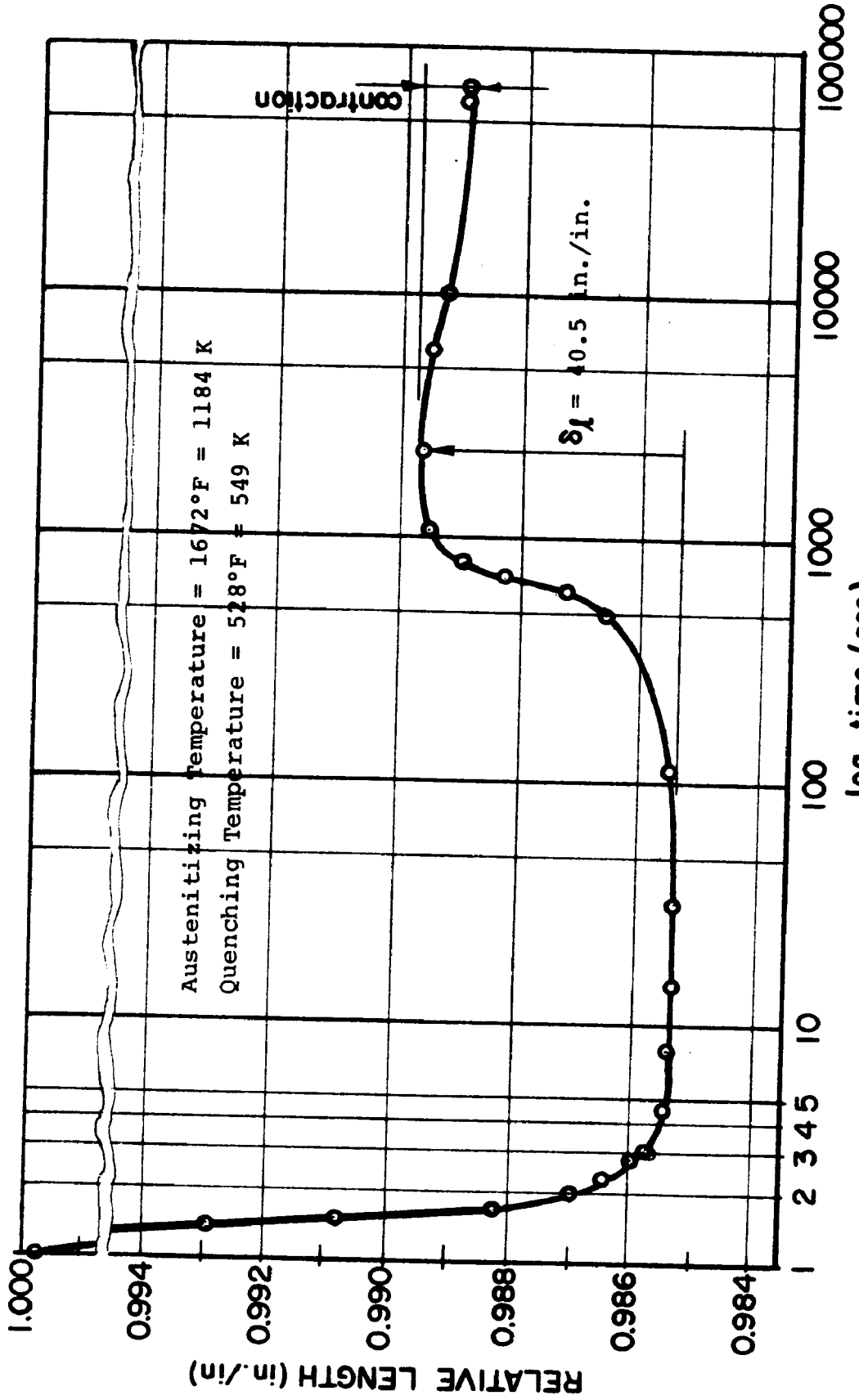


Fig. 13. Relative length vs log time for lower bainite showing tempering. "Tempering" of supersaturated ferrite, ε carbide formation and ε carbide to Fe_3C transformation, probably occurs simultaneously with the γ to αFe transformation. However, the derived contraction is only appreciable after the γ to αFe transformation is finished.

a sharp rise (Fe-0.94% C and AISI-SAE 4140 and probably Fe-1.1% C, Figs. 12-A,B and C). However, other alloys do not exhibit any dip but rather show a continuous increase in transformation coefficient (AISI-SAE 52100, Fig. 12-D).

In all the materials with high carbon content for which the transformation coefficient has been measured in the lower bainite range, the results show a sharp increase above the curve extrapolated from the pearlite range. Another effect is that all these alloys, when transformed in the lower bainite range, show a small slow contraction after the maximum transformation expansion is attained, Fig. 13. The transformation coefficient reported in all cases is the maximum. In one run the experiment was continued for 20 hr (Fe-1.1% C at 520°F, Fig. 12-B and Fig. 13, and the data show a contraction from 41 to 35×10^{-4} (in./in.) or (m/m) and the specimen was still contracting when the run was stopped.

As discussed later this irregular performance in the bainite range is believed to be due to ferrite supersaturation and later "tempering." The dip observed in some cases is suspected as due to the change in carbon content of the last fractions of untransformed austenite, leading to austenite stabilization.

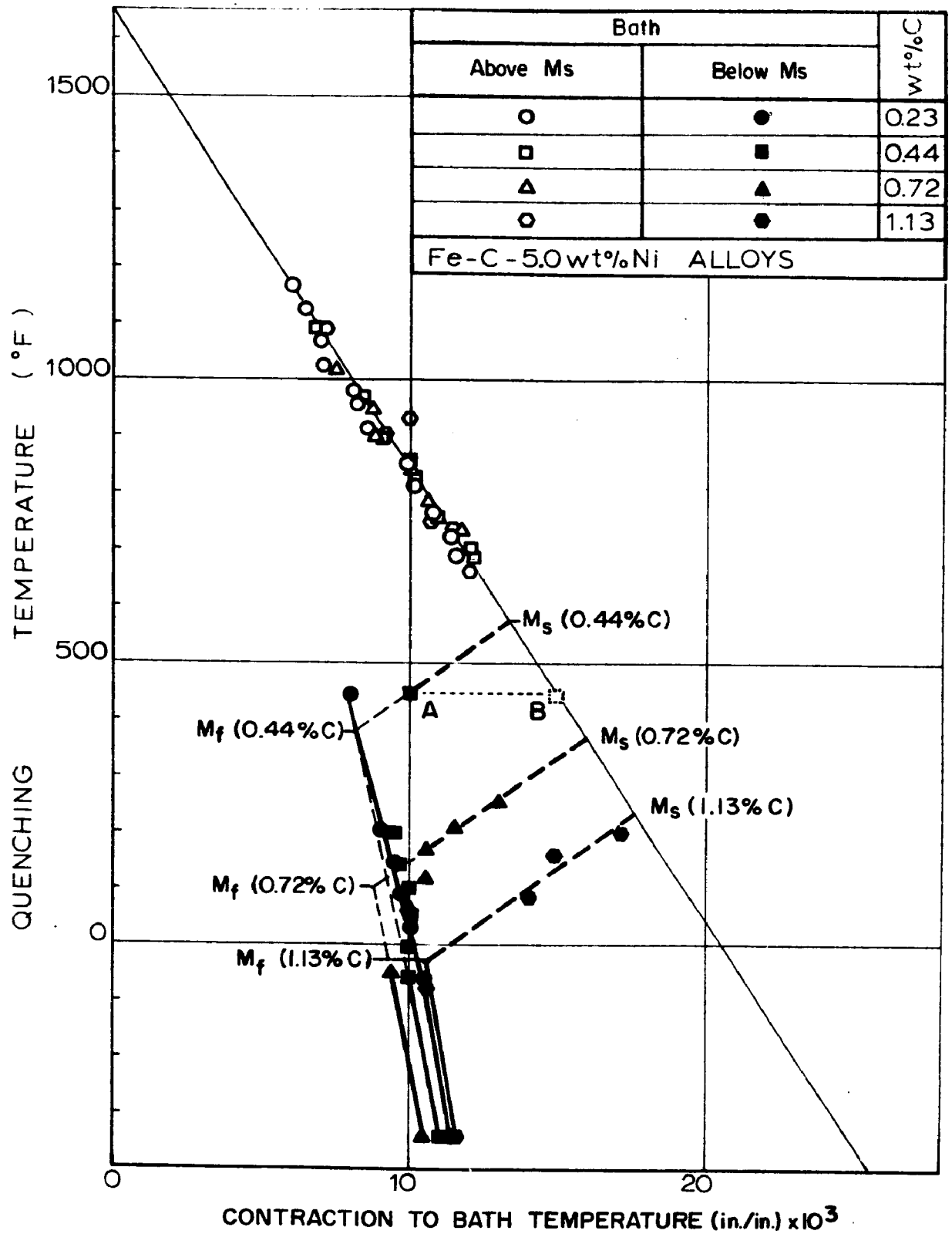


Fig. 14. Overall contraction 1650°F (1172 K) to bath temperature vs quench temperature
Actual austenitizing temperatures corrected to 1650°F. Point B represents contraction expected if no transformation during quench. Point A shows actual contraction decreased by martensite formation (see text, page 73).

4) The martensite range

To avoid misinterpretation it may be well to begin this section by reviewing the differences in dilation to be encountered in austenite to martensite transformation compared with the isothermal data just discussed.

These differences arise from the fact that when a specimen is quenched below the Ms temperature, it will reach the bath temperature partly transformed to martensite. In other words, since it is not possible to suppress martensite transformation when quenching to below Ms, the length change which would be expected from austenite contraction is lessened by an expansion due to the transformation.

To illustrate this effect the data from quenching the iron carbon nickel alloys are given in Fig. 14. The overall change in length, in./in. (m/m), which is obtained during the quench,is plotted against the temperature of the quenching bath used. In the region of the graph above 650°F (616 K) the length change is due simply to austenite contraction as measured in each run before isothermal transformation starts and the graph gives a slope of 12.4×10^{6}/°F (22.3×10^{-6}/K) as expected for austenite.

However, consider the effect of a quench to point A which is below the Ms temperature for this alloy. If only austenite contraction took place during the quench the overall contraction would be 15.0×10^{-3} (in./in.) or (m/m),

point B. However, due to the expansion caused by martensite transformation as the specimen is cooled below the Ms as well as the lower coefficient of contraction of this martensite, the overall length change was only 10.0 x 10^{-3} (in./in.) or (m/m), point A.

As this specimen was quenched to lower temperatures further transformation took place until the Mf was reached. In this range the expansion due to transformation was greater than the contraction at the austenite-martensite mixture due to cooling so that the specimen continued to expand with decreasing temperature until the approximate Mf was reached. Finally upon cooling below Mf, contraction was obtained. The slope of the graph below Mf was less than for austenite because the structure was martensite. (It is recognized also that some retained austenite probably existed below the approximate Mf.) The value of the linear coefficient of expansion of martensite as measured from the data shown in Fig. 14 is 3.8 x 10^{-6}/°F (6.8 x 10^{-6}/K).

With this backgroundthe data of Figs. 8-A,B,C,D may now be discussed. It was decided to concentrate this portion of the work on the Fe-C-5% Ni alloys because of the slow rate of bainite formation in these materials so that the austenite martensite reaction could be isolated for study. In contrast the superimposed bainite reaction

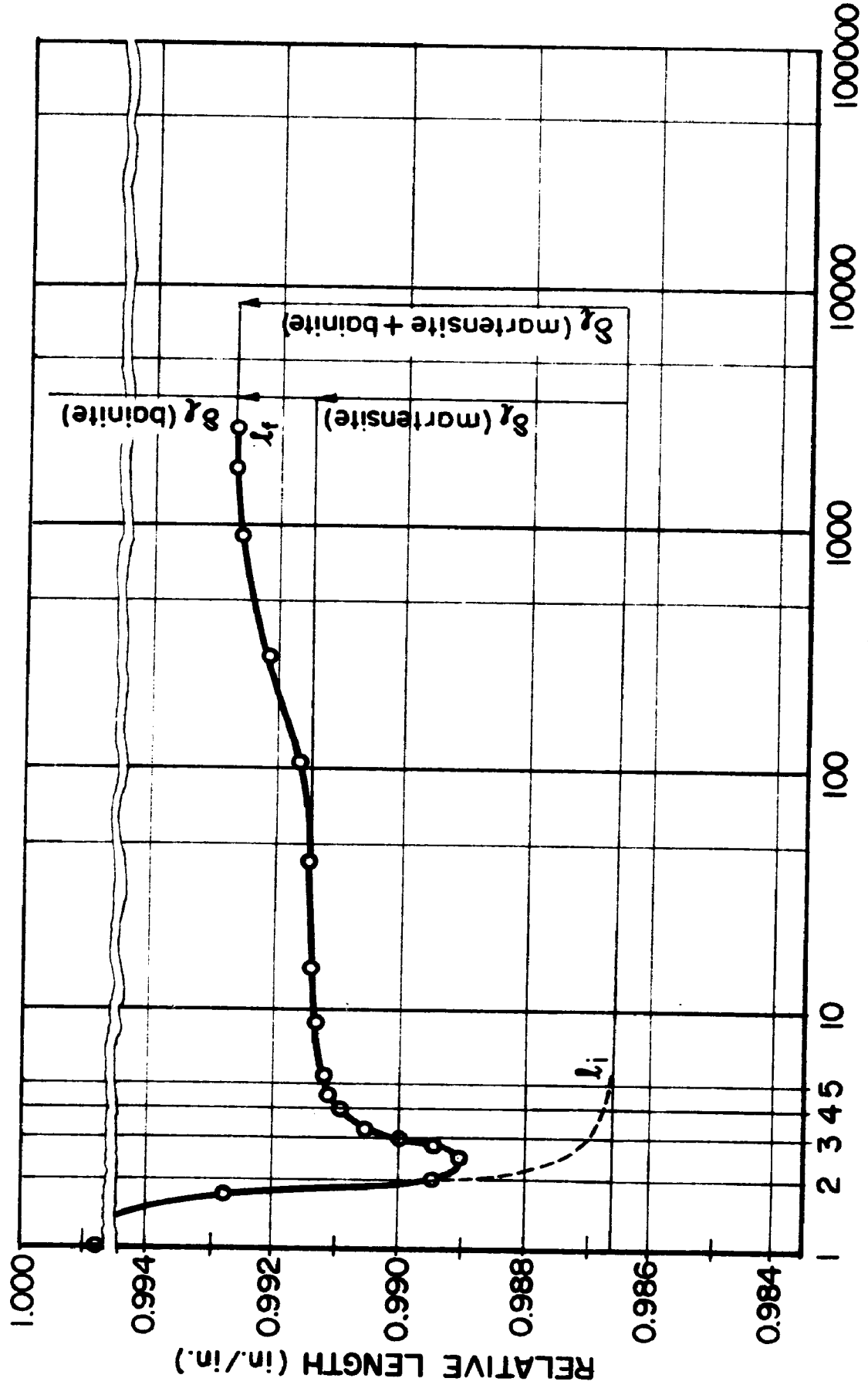


Fig. 15. Relative length vs time curve showing both martensite and bainite formation (AISI-SAE 4140)

in 4140 is shown in Fig. 15. Since the martensite formation in these materials occurs only by reducing the temperature rather than isothermally, it was possible to obtain the transformation characteristics for a number of bath temperatures in a single run. In this procedure the sample was quenched in a lead-tin bath at just above the Ms temperature for example and the normal austenite contraction was obtained. Next the dilatometer was quenched in a bath of water at 200°F (below Ms) and the dial reading noted. Following this other baths of cooler water, chilled acetone and finally liquid nitrogen were used. Due to the effect of time on austenite stabilization the procedure was done rapidly and the time recorded.

The value of the linear transformation coefficient only represents full austenite to martensite transformation at temperatures below the Mf. Therefore at temperatures just below Mf the transformation coefficient represents only the difference between the length of the sample if it were austenite at the bath temperature (calculated value) and the actual length. Below the Mf the value of δ_ℓ continues to increase because the coefficient of expansion of martensite is less than austenite. A small amount of retained austenite may also transform since the approximate Mf temperature is not for 100% martensite.

Fig. 8-D illustrates the contraction due to tempering. Further discussion of this point is made in part C, page 113.

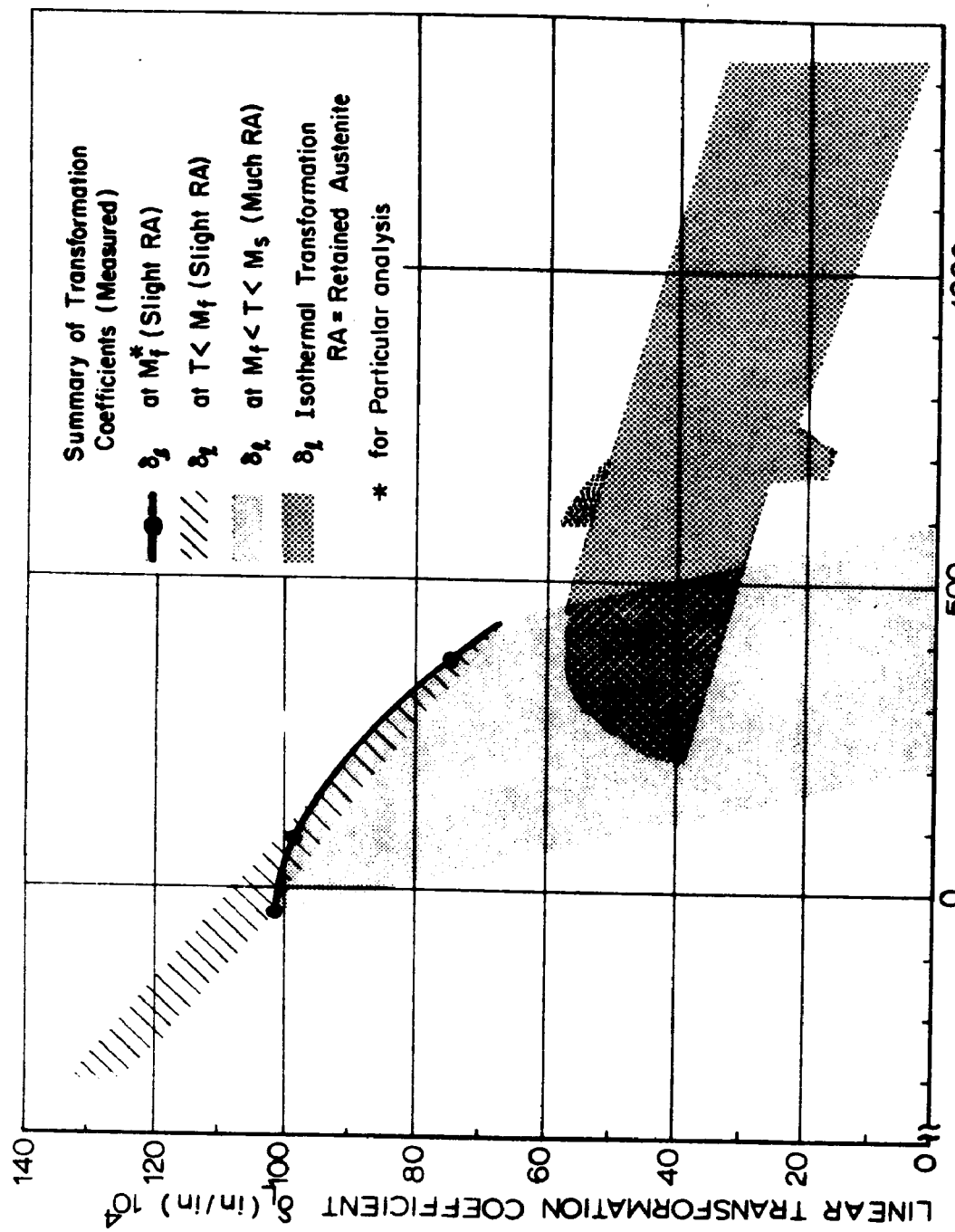


Fig. 16. Summary of transformation coefficient, δ_ℓ, vs temperature of transformation

In comparing the data for the martensite transformation coefficient, Fig. 8-E, in different carbon concentrations, it is found that the results fall in a relatively narrow band. This was not expected because it would be predicted (as shown in Part B) that the higher carbon austenite would transform to more voluminous martensite. Probably the effect which reduces the transformation coefficient for the higher carbon materials is the greater amount of retained austenite in these alloys. It is interesting that this effect has the result of giving about the same δ_ℓ at all carbon levels.

5) Summary of experimental dilatometer data

The transformation coefficient, δ_ℓ, varies greatly depending on the analysis, mainly carbon content and transformation temperature, Fig. 16.

In the pearlite range, 1300 to 1000°F (977 to 811 K) δ_ℓ increases from 12 to 17 x 10^{-4} (in./in.) or (m/m) for a 1.1% C alloy and from 35 to 42 x 10^{-4} (in./in.) or (m/m) for a 0.23% C-5% Ni alloy.

In the bainite range, from 1000°F (811 K) to Ms, δ_ℓ increases from 17 x 10^{-4} (in./in.) or (m/m) at 1000°F (811 K) to about 42 x 10^{-4} (in./in.) or (m/m) at 500°F (533 K) for a 1.1% C Fe-C alloy. The 0.23% C-5% Ni alloy, δ_ℓ increases from 42 x 10^{-4} (in./in.) or (m/m) at 1000°F (811 K) to about 51 x 10^{-4} (in./in.) or (m/m) at 700°F (644 K).

Finally, in the martensite range, δ_{ℓ} varies from 102×10^{-4} (in./in.) or (m/m) for the 1.13% C-5% Ni alloy to 68 (in./in.) or (m/m) for a 0.23% C-5% Ni alloy if the measurement is performed at the observed Mf temperature. However, if the comparison is made at liquid nitrogen temperature [-320°F, (78 K)], δ_{ℓ} increases first from 125×10^{-4} (in./in.) or (m/m) for 0.23% C-5% Ni alloy to 134×10^{-4} (in./in.) or (m/m) for 0.72% C-5% Ni alloy and then decreases to 125×10^{-4} (in./in.) or (m/m) for 1.13% C-5% Ni alloy. Therefore, the most important effect of the carbon content is in controlling the temperature range at which austenite decomposition occurs.

(B) Calculation of volumetric expansion coefficient, δ_V, from lattice parameter data and comparison with dilatometer data

Since the dilatometer provides a relatively simple and flexible method for determining the transformation expansion, it was considered important to compare these data with independent basic data obtained from high temperature x-ray diffraction measurements of the lattice parameter. The x-ray data are more difficult to obtain and the method is not as flexible as the dilatometer and it was considered that if agreement could be obtained for some simple cases, the dilation method would thereby be validated.

In this comparison the lattice parameter data will be used first to calculate δ_V, the volume change due to transformation and then converted to δ_ℓ for comparison. First the δ_V to be expected in going from austenite to mixtures of ferrite, pearlite and carbide will be discussed and then the δ_V for austenite to martensite.

The transformation coefficient can be expressed as the difference between the specific volume of austenite and product phases for the given alloy at the temperature at which the transformation occurs. Since all common phases that exist in steels and Fe-C alloys are crystalline, the specific volume of a given phase can be

computed from the knowledge of its lattice parameter:

$$\bar{V}_i = \frac{AN \cdot v_i}{(n_a \cdot AW_a + n_b AW_b \ldots)}$$

$\bar{V}_i$ = specific volume of the "ith" phase

AN = Avogadro's Number

v_i = unit cell volume of the given phase calculated from its lattice parameter

n = number of atoms of type a per unit cell of the phase

AW_a = atomic weight of the type a atoms, etc.

Therefore the volumetric transformation coefficient can be expressed by:

$$\delta_V = \frac{\bar{V}_P - \bar{V}_A}{\bar{V}_A} = \frac{\bar{V}_P}{\bar{V}_A} - 1$$

where

δ_V = volumetric transforamtion coefficient of a given transformation

$\bar{V}_A$ = specific volume of the initial phase, austenite

$\bar{V}_P$ = specific volume of the product phase or aggregate of phases resulting from the given transformation.

In general, when two or more phases result from austenite decomposition the specific volume of the product is computed from the weight fractions of the individual resulting

phases, f_i^W, and from the specific volumes, $\bar{V}_i$:

$$\bar{V}_p = \sum_{i=1}^{n} (f_i^W \bar{V}_i).$$

Therefore this type of calculation is limited to cases where all these data are available both for the alloy chemistry and for the temperature at which the transformation takes place.

This type of calculation has been performed by means of a digital computer for pure Fe-C alloys assuming different conditions depending on the transformation modes and repeated for all carbon contents and transformation temperatures. Detailed description of the assumptions, computer program used, sample calculations, etc. is given for each case in Appendix II-A,B,C.

The most recent accurate high temperature lattice parameter measurements for ferrite, cementite and austenite have been performed by Ridley and his associates (11,32, 33) who generously provided a copy of their original data, Appendix I. These were used for transformations in the pearlite and bainite ranges. In the martensite range it was necessary to add the data of Roberts for the lattice parameters of martensite.

In all calculations the lattice parameter of austenite, a_A, is obtained by a quadratic extrapolation down to the desired temperature of Ridley and Stuart's (32,33) high temperature data by means of the following

equation, derived as explained in Appendix 1.

$$a_A(\mathring{A}) = 3.5814 + 1.709 \cdot 10^{-2} \cdot (wt\%C) + 7.97 \cdot 10^{-3} \cdot (wt\%C)^2 + 6.7 \cdot 10^{-5} \cdot T + 6.2 \cdot 10^{-9} \cdot T^2 (\pm 0.0010\ \mathring{A})$$

where C is the carbon content in weight percent and T the temperature in °C.

1) Ferrite-Pearlite-Cementite range

As discussed in Appendix 1, the lattice parameters of ferrite and cementite have been calculated from Ridley and Stuart's data (11,33) for a 1.44% C pure Fe-C alloy measured in situ. The following equations were used:

$$a(\mathring{A}) = (2.8655 + 3.36 \cdot 10^{-5} \cdot T + 12.2 \cdot 10^{-9} \cdot T^2) \pm (0.0001\ \mathring{A})$$ for ferrite, and

$$a(\mathring{A}) = (4.5239 + 3.18 \cdot 10^{-5} \cdot T + 19.3 \cdot 10^{-9} \cdot T^2)\ (\pm 0.0004\mathring{A})$$

$$b(\mathring{A}) = (5.0889 - 1.23 \cdot 10^{-5} \cdot T + 86.5 \cdot 10^{-9} \cdot T^2)\ (\pm 0.0004\mathring{A})$$

$$c(\mathring{A}) = (6.7409 + 5.04 \cdot 10^{-5} \cdot T + 65.4 \cdot 10^{-9} \cdot T^2)\ (\pm 0.0005\mathring{A})$$

for cementite. The inverse lever rule applied to the equilibrium Fe-Fe_3C phase diagram has been used to compute the weight fractions of ferrite and cementite. The carbon content in the ferrite has been assumed to follow the equilibrium concentrations reported by Stanley (85) and is given by

$$(wt\ \%\ C)^* = \exp(-8.58 + 6.4 \cdot T \cdot 10^{-3})$$

The carbon content of Fe_3C has been taken as stoichiometric (6.68 wt %).

*Equation obtained by regression of Stanley (85) data.

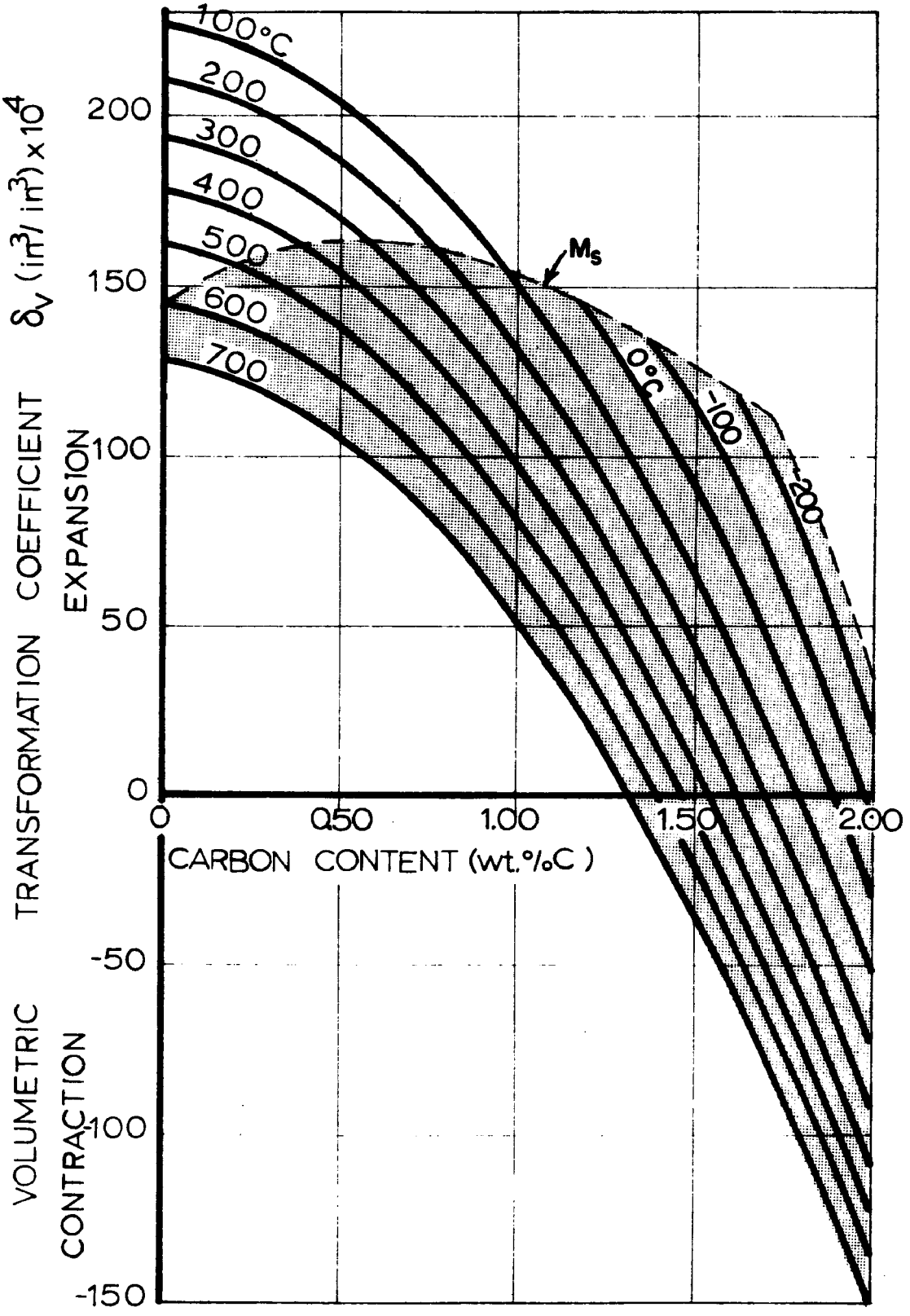


Fig. 17-A. Transformation coefficient in pearlite range, δ_v, (calculated) vs % C
Below temperature range shown by darkened zone martensite rather than isothermal products would be obtained. (See text, page 86)

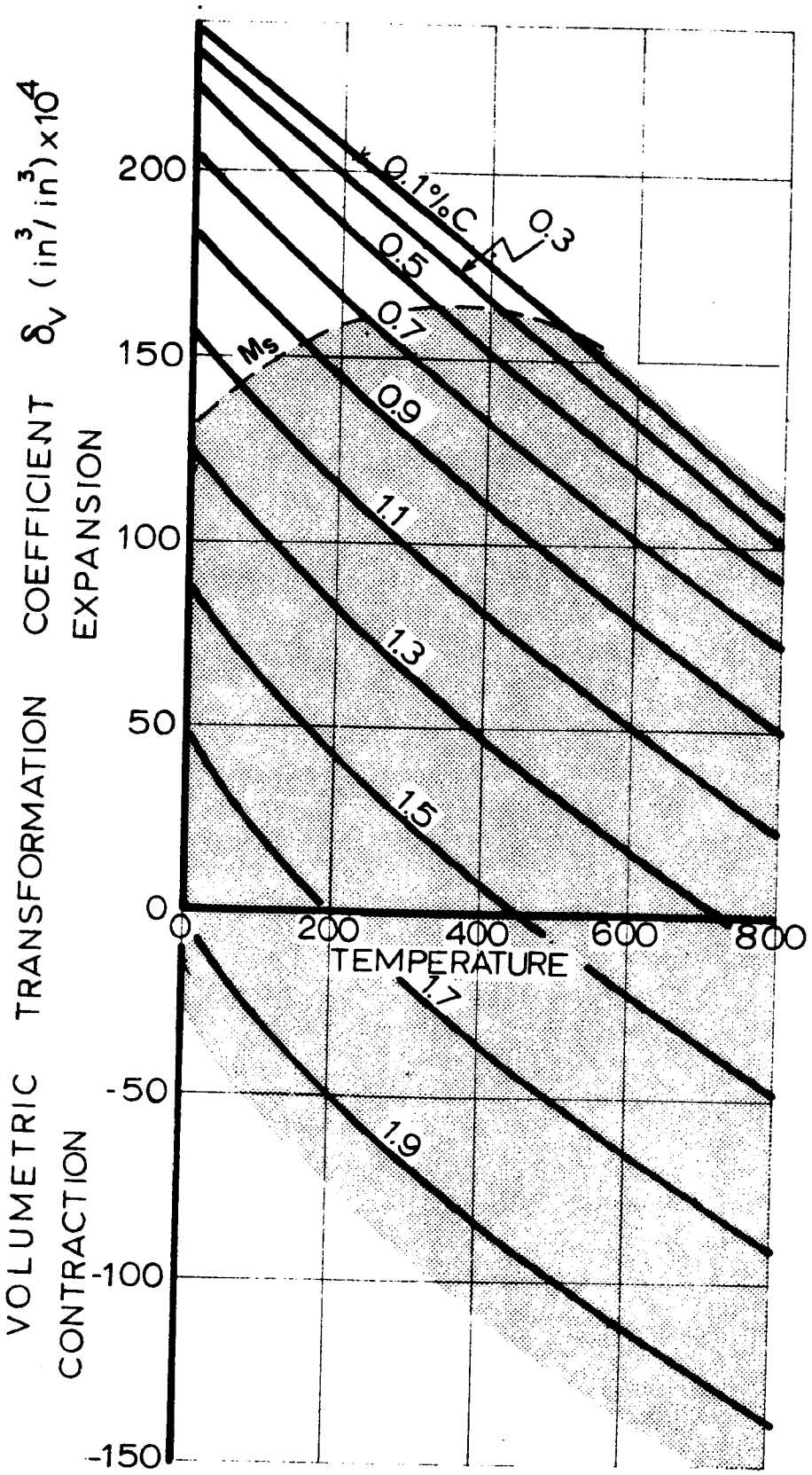


Fig. 17-B. Transformation coefficient in pearlite range, δ_V, (calculated) vs temperature Below temperature range shown by darked zone martensite rather than isothermal products would be obtained. (See text, page 86)

The results of these calculations are shown in Fig. 17-A and B. It is to be emphasized that these calculations assume formation of ferrite and cementite (Fe_3C). Therefore the values are not significant below Ms or if other such phases such as epsilon carbide and supersaturated ferrite are obtained in the bainite range.* The calculations indicate two important relations: 1) The coefficient δ_V decreases with carbon content and becomes negative at higher temperatures and carbon contents; 2) the coefficient increases with decreasing temperature.

2) Bainite range

It is generally agreed that the calculations for "equilibrium" transformation hold also for the upper bainite range, Fig.17A,B. However, there are some data (21) indicating that in the lower bainite region the ferrite is supersaturated with carbon or that the carbide is not Fe_3C. Precise calculations cannot be made of these effects. It would be anticipated therefore that the dilation measurements would not agree exactly in the lower bainite range.

3) Martensite range

The values of the lattice parameters of tetragonal martensite are not as precise as the data for ferrite and carbide. The equations for the "a" and "c" parameters of tetragonal martensite at 25°C are from Roberts (13).

*This region has physical significance only after complete tempering of martensite or supersaturated ferrite has occurred. (See text on page 113.)

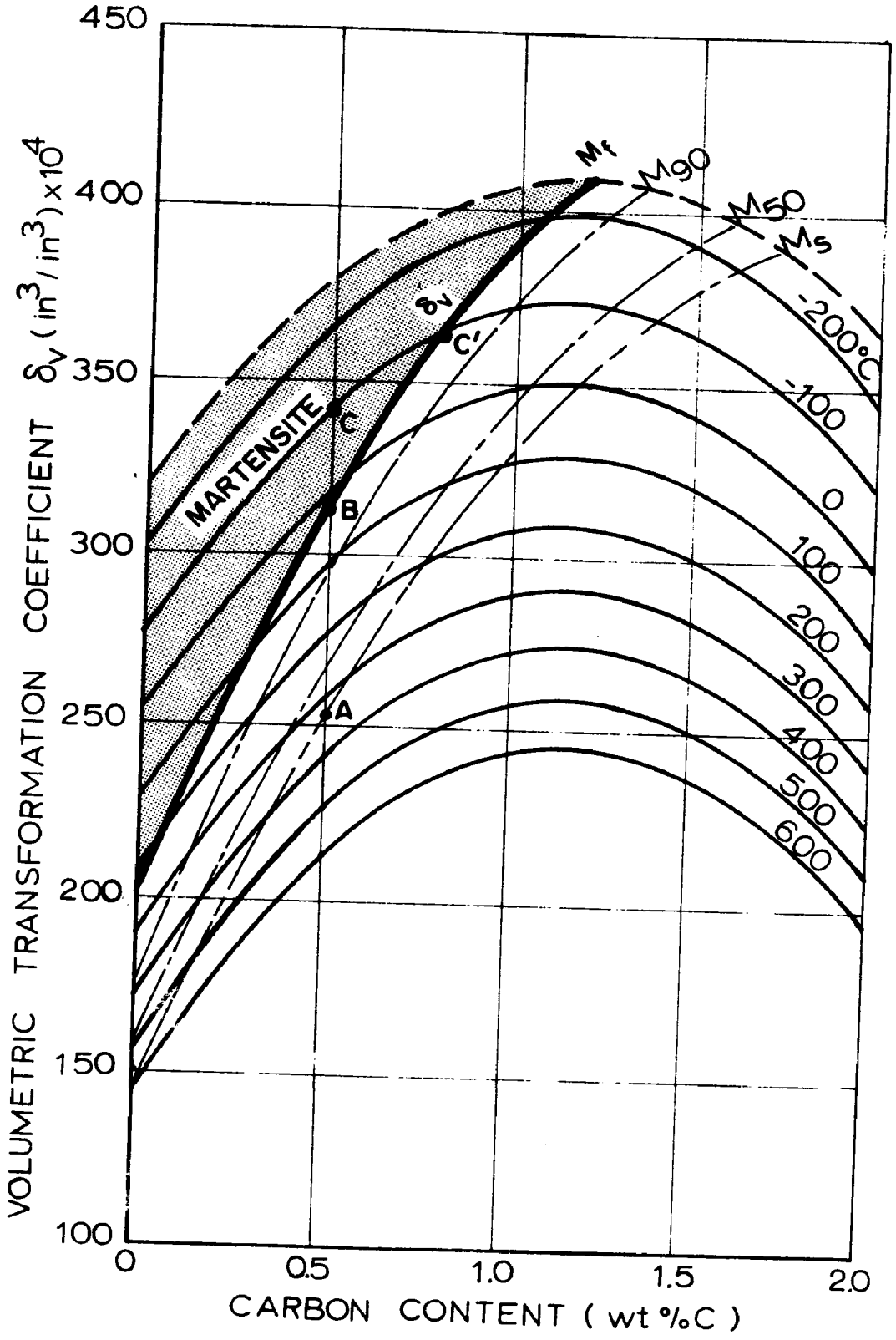


Fig. 18-A. Transformation coefficient in martensite range, δ_V, (calculated) vs % C
Full transformation to martensite only occurs at temperatures shown by darkened zone. (See text, page 89)

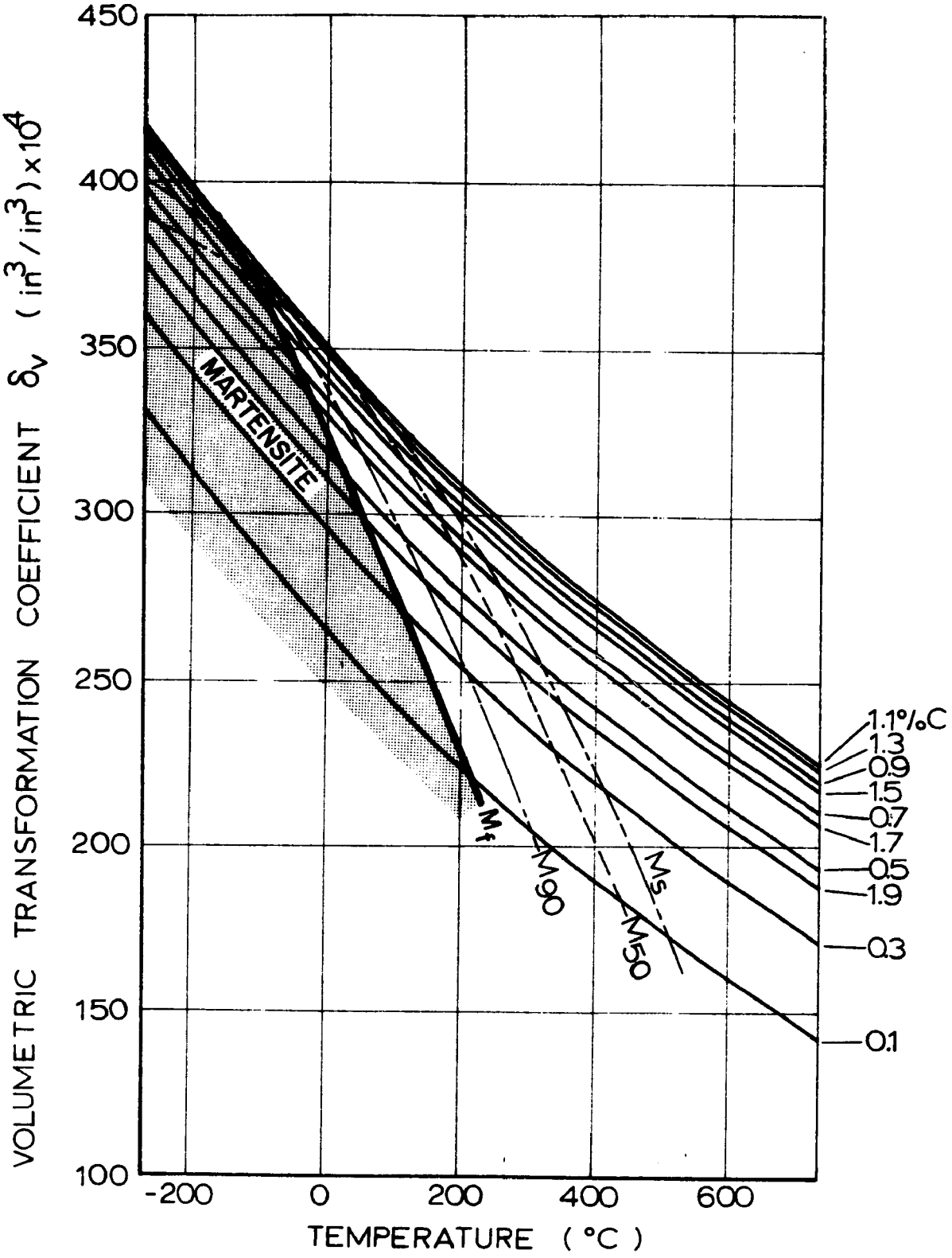


Fig. 18-B. Transformation coefficient in martensite range, δ_V, (calculated) vs temperature

Full transformation to martensite only occurs at temperatures shown by darkened zone. (See text, page 89)

$$a_M(\mathring{A}) = 2.867 - 0.013(\text{wt \% C})$$

$$c_M(\mathring{A}) = 2.867 + 0.116\ (\text{wt \% C})$$

The experimental scatter shown is approximately ± 0.01 Å.

Moreover, no data were found for the coefficient of expansion of martensite. In order to calculate the martensite transformation coefficient at lower and higher temperatures, the volume coefficient of expansion of martensite was assumed to be the same as the ferrite coefficient, obtained from Ridley and Stuart data (33).

The results of the calculations are shown in Fig. 18-A and B. It is to be emphasized that these are theoretical because the values to the right of the line marked Mf would not be obtained during transformation in actual experiments because it is not possible to complete the martensite reaction above the Mf temperature as explained in Part A of the discussion.*

Another point which requires care in interpretation is comparison of δ_V of martensite for different carbon contents. This is quite different than, for example, comparing the transformation coefficients for different carbon contents in the <u>isothermal</u> range because Mf temperatures are different. Therefore, the difference between the coefficient of expansion of ferrite (or martensite) and austenite comes into play, which leads to an increased difference in specific volume, Fig. 18. This is shown by

*This region has physical significance only when virgin martensite can be heated after the quench without tempering.

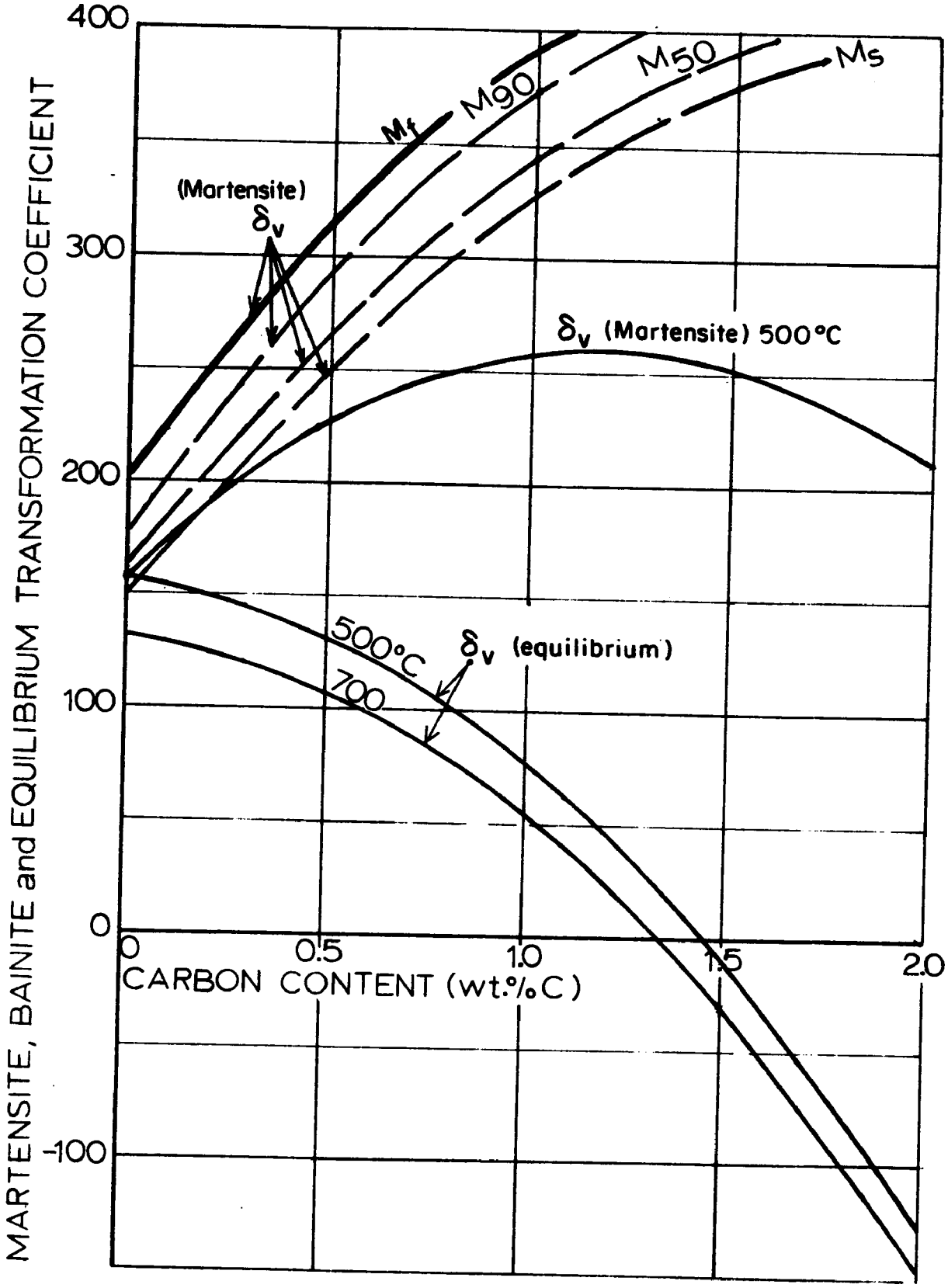


Fig. 19. Comparison of transformation coefficients, δ_V, in pearlite and martensite ranges (both calculated) vs % C

the following example:

Consider first the transformation to martensite in a 0.5% carbon alloy, Fig. 18-A. On cooling, martensite will start to form at point A, Fig. 18-A, and finish at point B giving δ_V of 325 x 10^{-4} ($in.^3/in.^3$) or (m^3/m^3) at 20°C (293 K). In a 0.8% carbon alloy the transformation will not be complete until C' giving δ_V of 370 x 10^{-4} ($in.^3/in.^3$) or (m^3/m^3) at -100°C (173 K). One effect leading to the larger δ_V for the 0.8% carbon alloy is the effect of temperature of measurement. If the 0.5% C alloy is cooled to -100°C (173 K), point C, the apparent δ_V would be 340 x 10^{-4} ($in.^3/in.^3$) or (m^3/m^3), a value closer to the 0.8% C alloy. However, this calculation shows that there is also a real effect due to carbon alone.

Therefore it can be concluded that the carbon concentration increases δ_V in two ways: by lowering the Ms-Mf range and by the effect of carbon in expanding the martensite unit cell.

Summary of calculations of δ_V lattice parameters

The values of δ_V which were calculated for transformation at different temperatures and carbon contents are summarized in Figs. 19-21.

In general for isothermal transformation in the pearlite and bainite ranges the coefficient increases as the temperature is lowered. At a given temperature the lower

the carbon the higher the coefficient.

For martensite transformation also the transformation coefficient is higher as the temperature is lowered. However, the higher the carbon content, the higher the coefficient due to the expansion of the martensite unit cell by carbon and indirectly to the lower Ms-Mf range.

Because of these opposing effects it is shown in Figs. 19-21 that the higher the carbon content, the greater the difference between the transformation coefficients for pearlitic and martensitic transformations. An important consequence of this difference is that it would be expected that when the martensite is fully tempered it assumes the dimensions of the ferrite + carbide equilibrium structure. Therefore, the difference between the "equilibrium" and "martensite" curves is an index of the contraction due to tempering and is highest for higher carbons. This contraction would vary from 0 ($in.^3/in.^3$) if 0% martensite could be formed in pure Fe-C alloys to 260 ($in.^3/in.^3$) [or 0.9% by length] for the tempering of a 1.5% C virgin martensite.

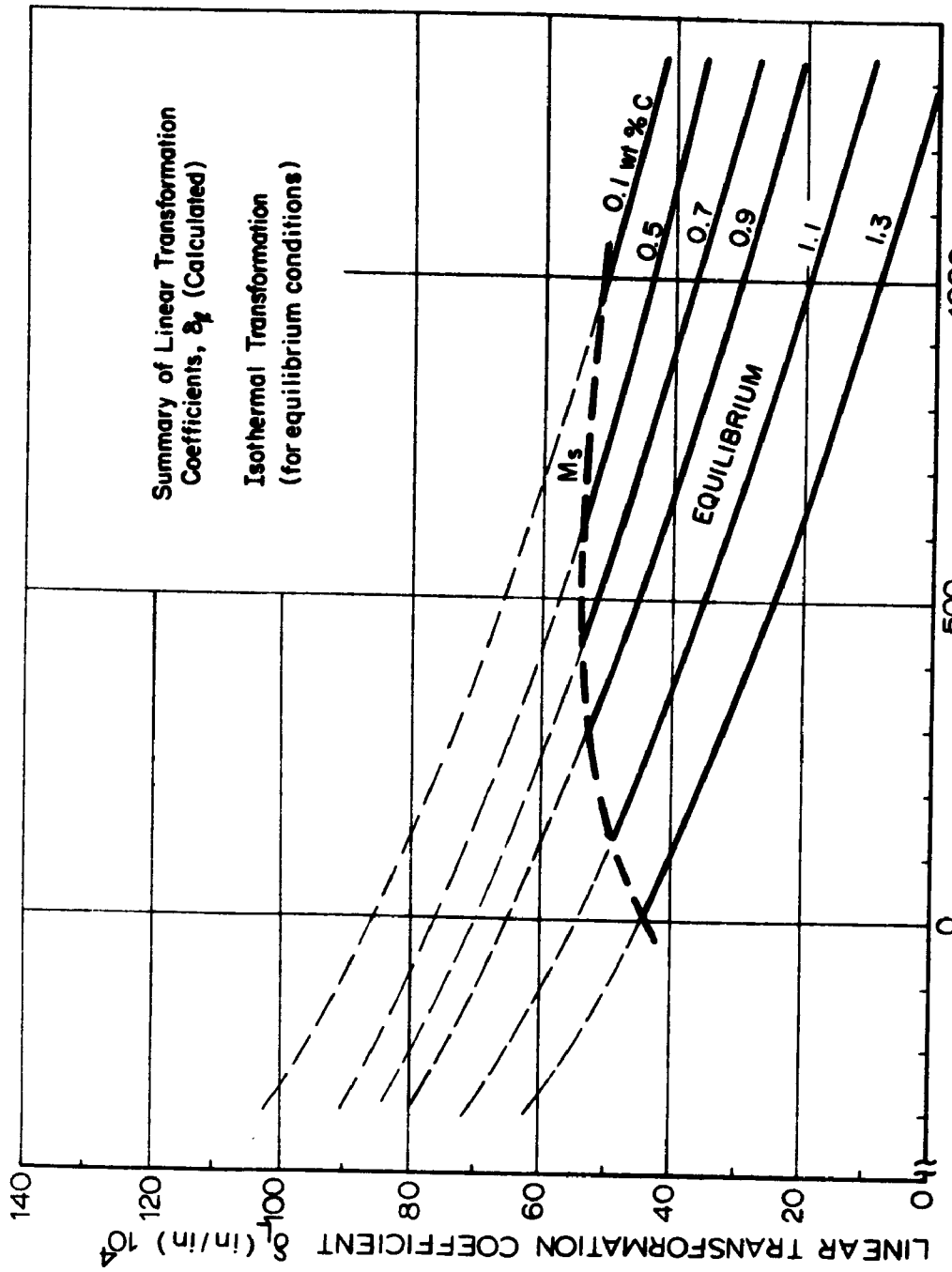


Fig. 20-A. Transformation coefficient, $\delta_{\ell'}$ (calculated) vs temperature in pearlite and upper bainite ranges ($\delta_\ell \cong 1/3\ \delta_V$)

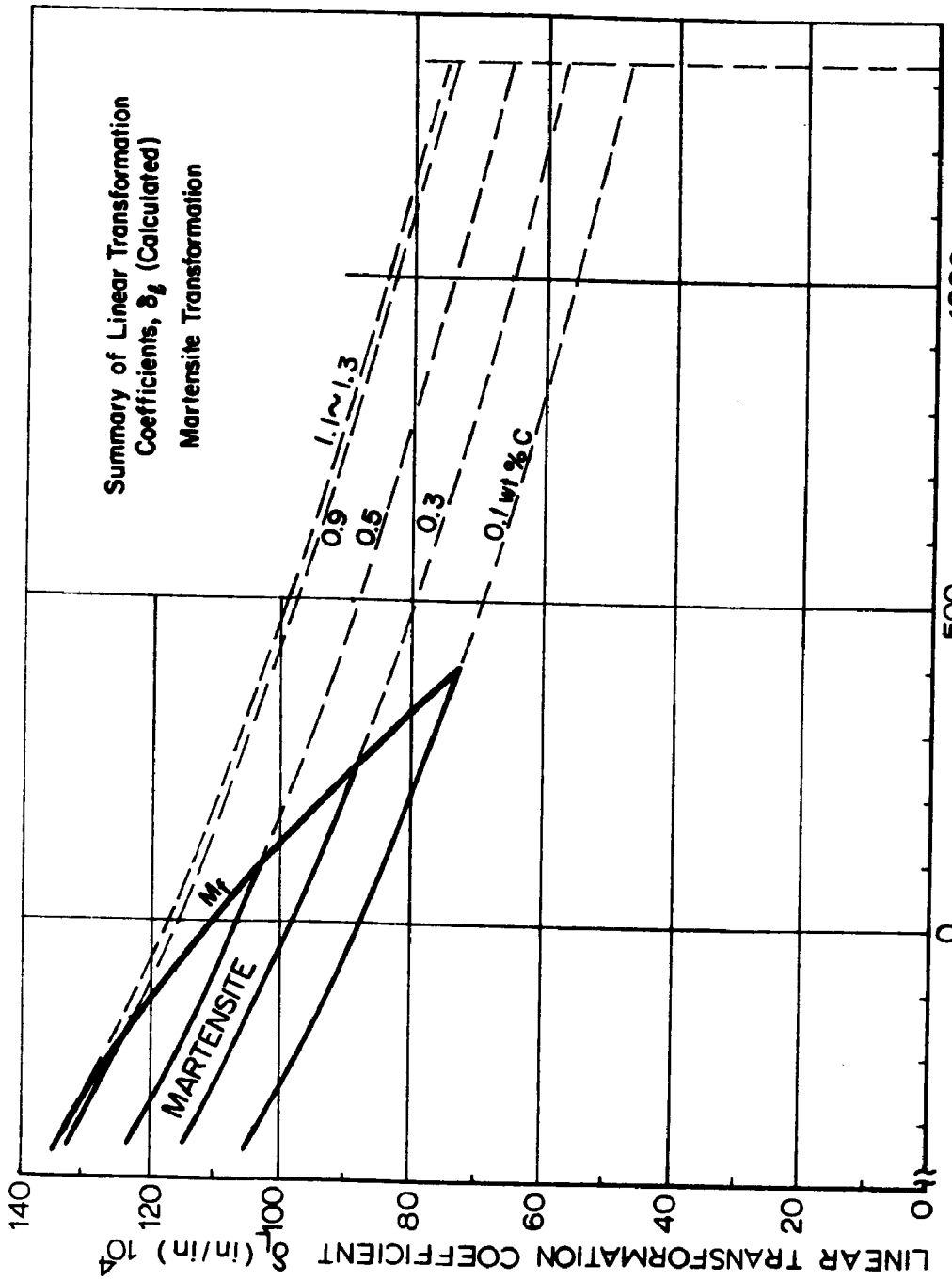


Fig. 20-B. Transformation coefficient, δ_ℓ, calculated vs temperature in martensite range ($\delta_\ell \cong 1/3\ \delta_V$)

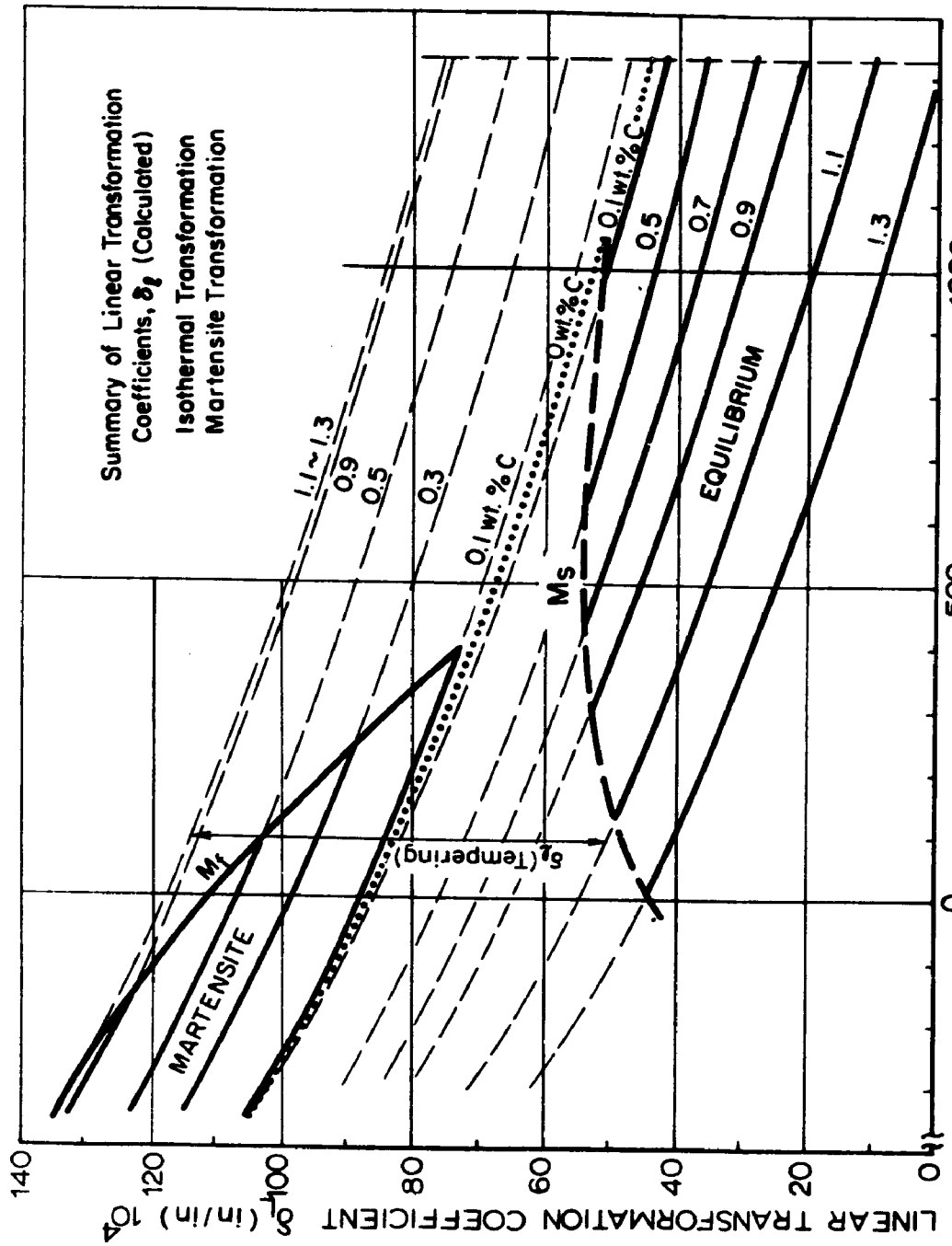


Fig. 21. Comparison of transformation coefficient, δ_ℓ, in pearlite and martensite ranges (both calculated) vs temperature. Full tempering contraction of 100% martensite in a 1.1% C steel at 80°F is 63 x 10^{-4} (in./in.) from these calculations. (See tempering discussion on page 113.)

(C) Comparison of dilation data and results of lattice parameter calculations

In this section first the comparison between calculations and the dilatometric results of the present work is performed. Then the comparison is made with measurements and calculations from other investigators. Then "basic questions" concerning bainite formation are discussed in three points. Finally, martensite transformation is discussed and compared with other investigators' calculations.

In this comparison the linear transformation coefficients, δ_ℓ, are calculated from the volumetric transformation coefficients, δ_V, of section B. The assumption that isotropic length changes occur leads to the following relation:

$$\delta_V = 3\,\delta_\ell + 3(\delta_\ell)^2 + (\delta_\ell)^3$$

For the range of δ_V values obtained, the square and cubic terms can be neglected. Therefore, the calculation of δ_ℓ is:

$$\delta_\ell \cong \frac{1}{3}\,\delta_V$$

Figures 20 and 21 show the results of the calculation for the transformation of austenite to ferrite + cementite and to martensite (obtained from Figs. 17 and 18 by means of $\delta_\ell = \frac{1}{3}\,\delta_V$).

Next, to simplify the comparison, Figs. 22-27 show the same dilatometric measurements discussed in section A,

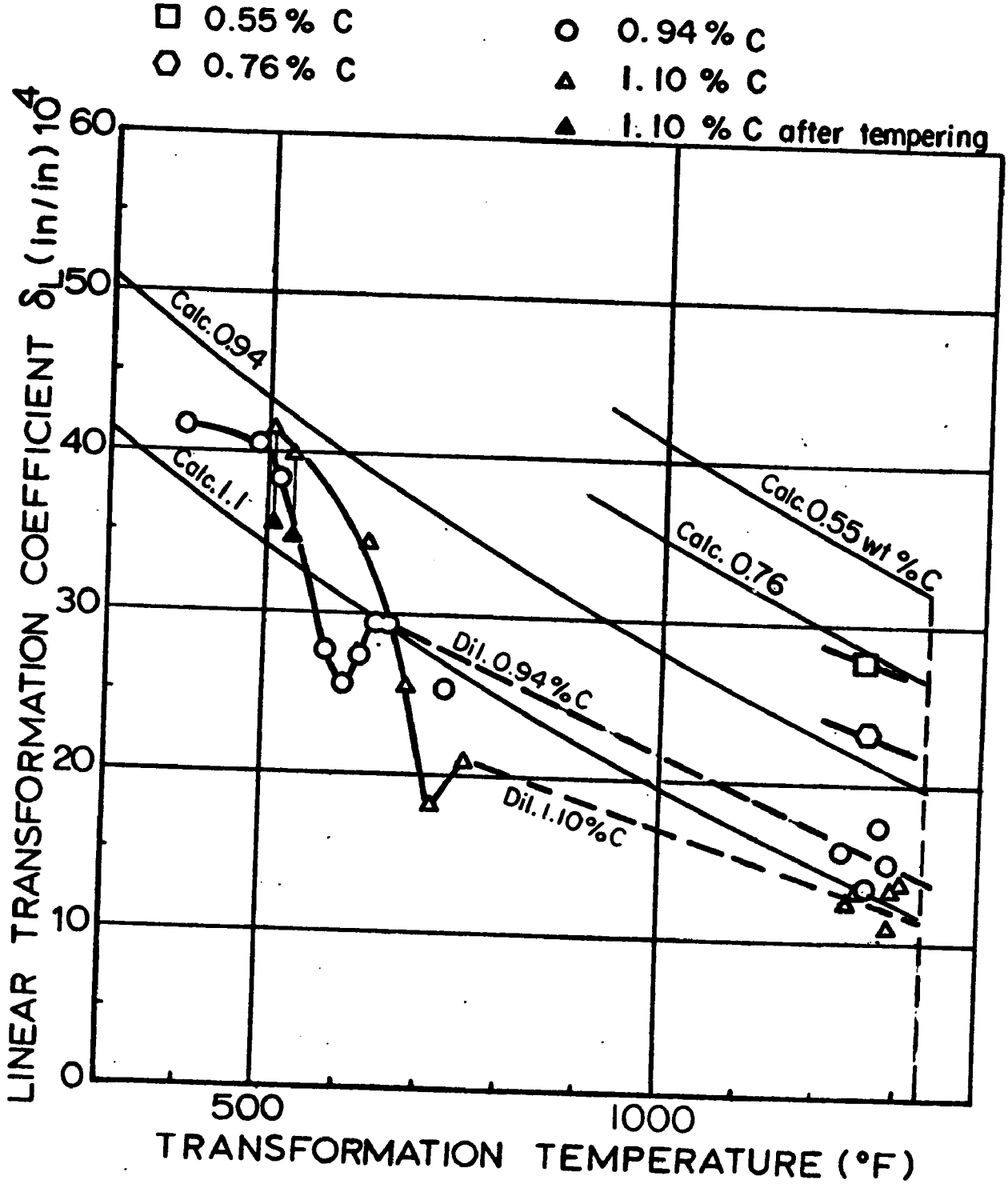


Fig. 22. Comparison of measured and calculated values of δ_ℓ for Fe-C alloys

(See text pages 65, 86, and 111-112 for bainite discussion.)

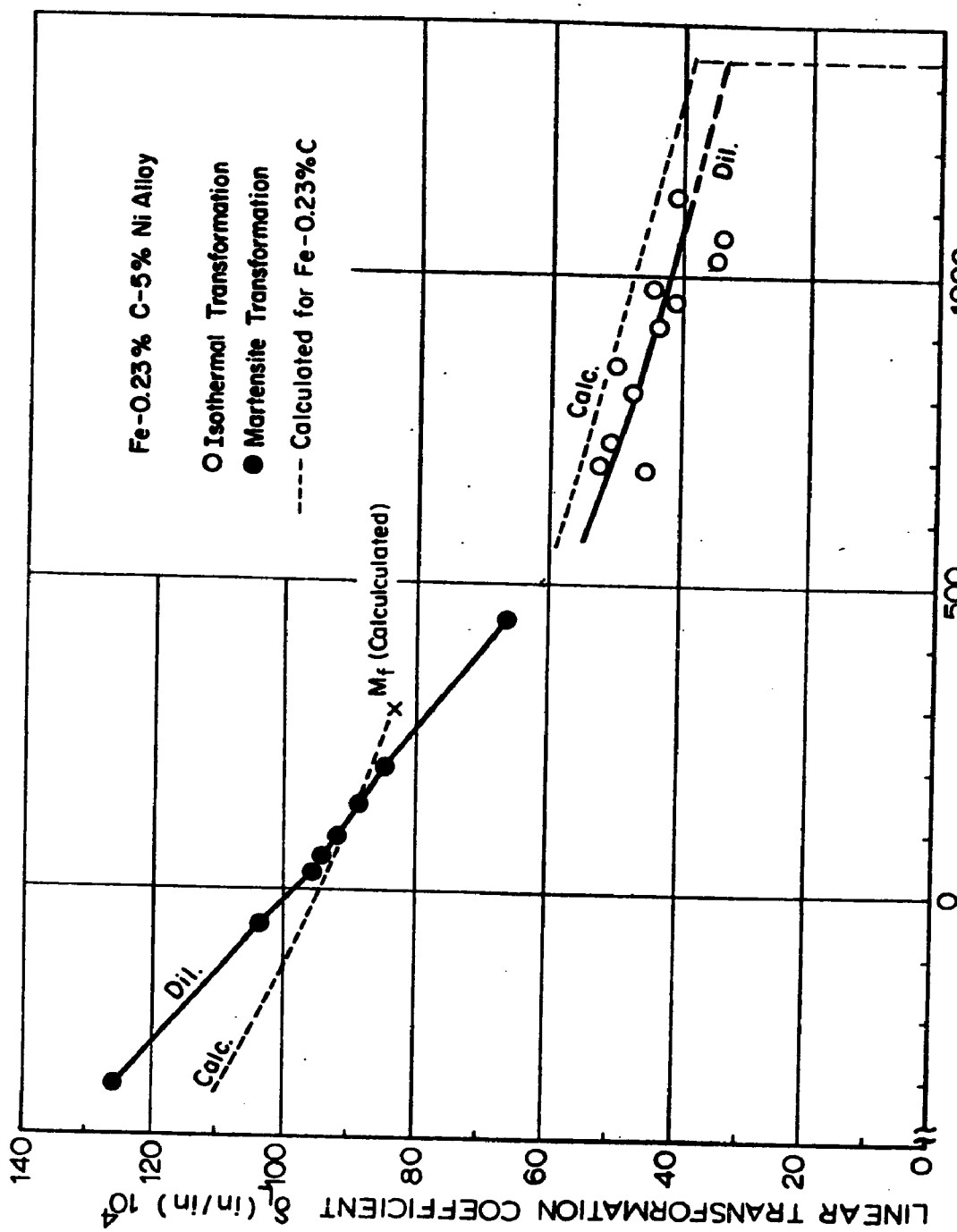


Fig. 23-A. Comparison of measured and calculated values of δ_l for 0.23% C-5% Ni

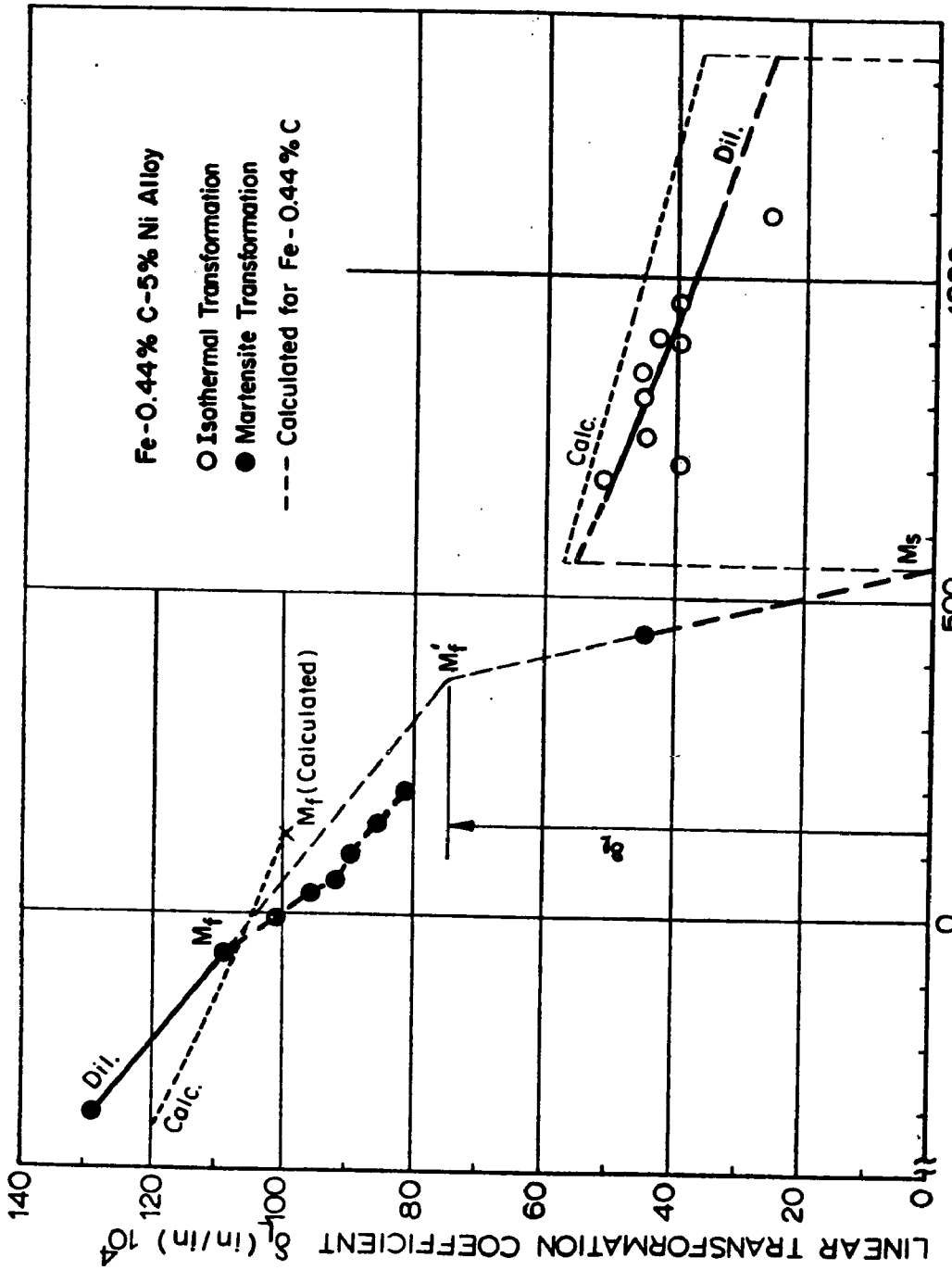


Fig. 23-B. Comparison of measured and calculated values of δ_l for 0.44% C-5% Ni

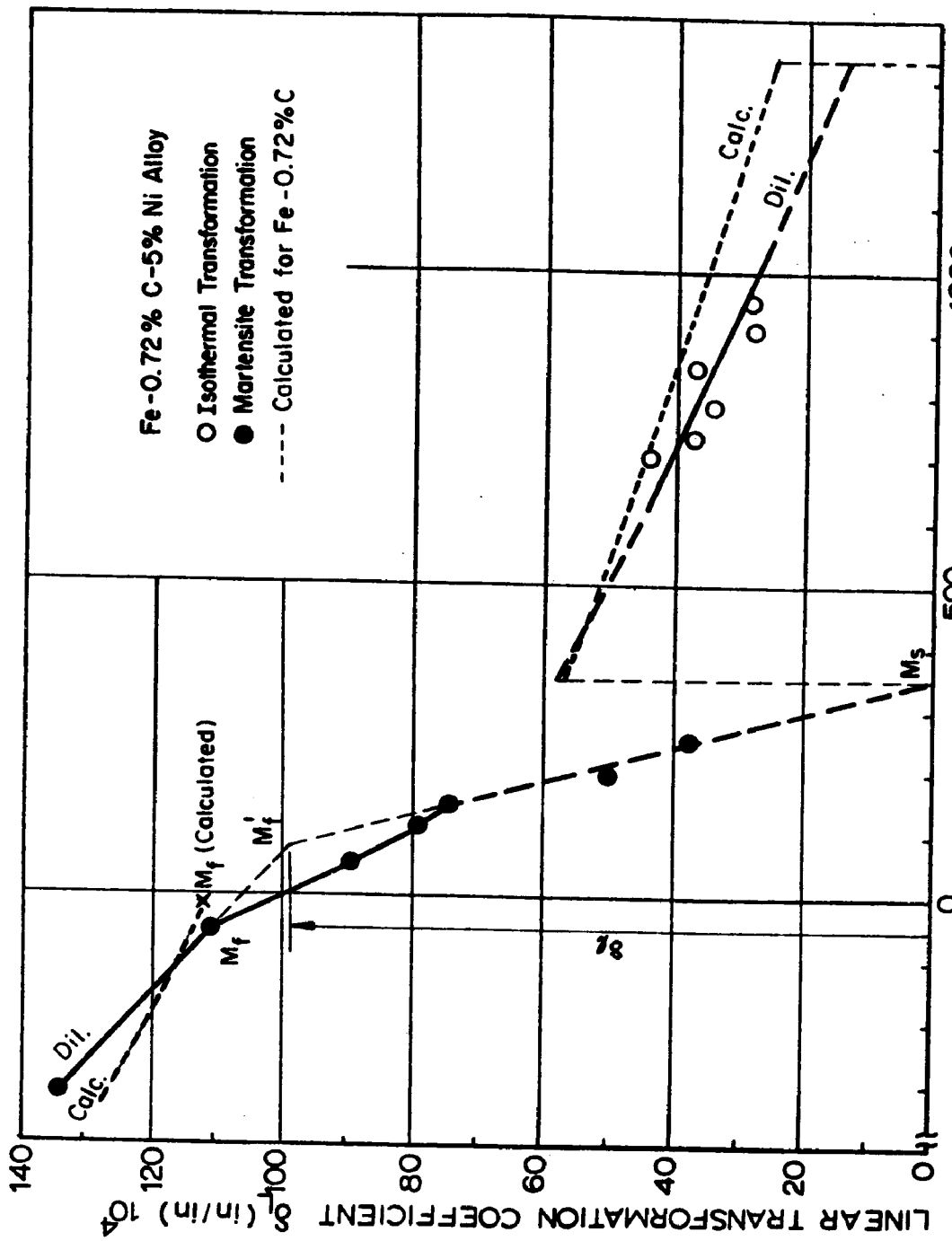


Fig. 23-C. Comparison of measured and calculated values of δ_ℓ for 0.72% C-5% Ni

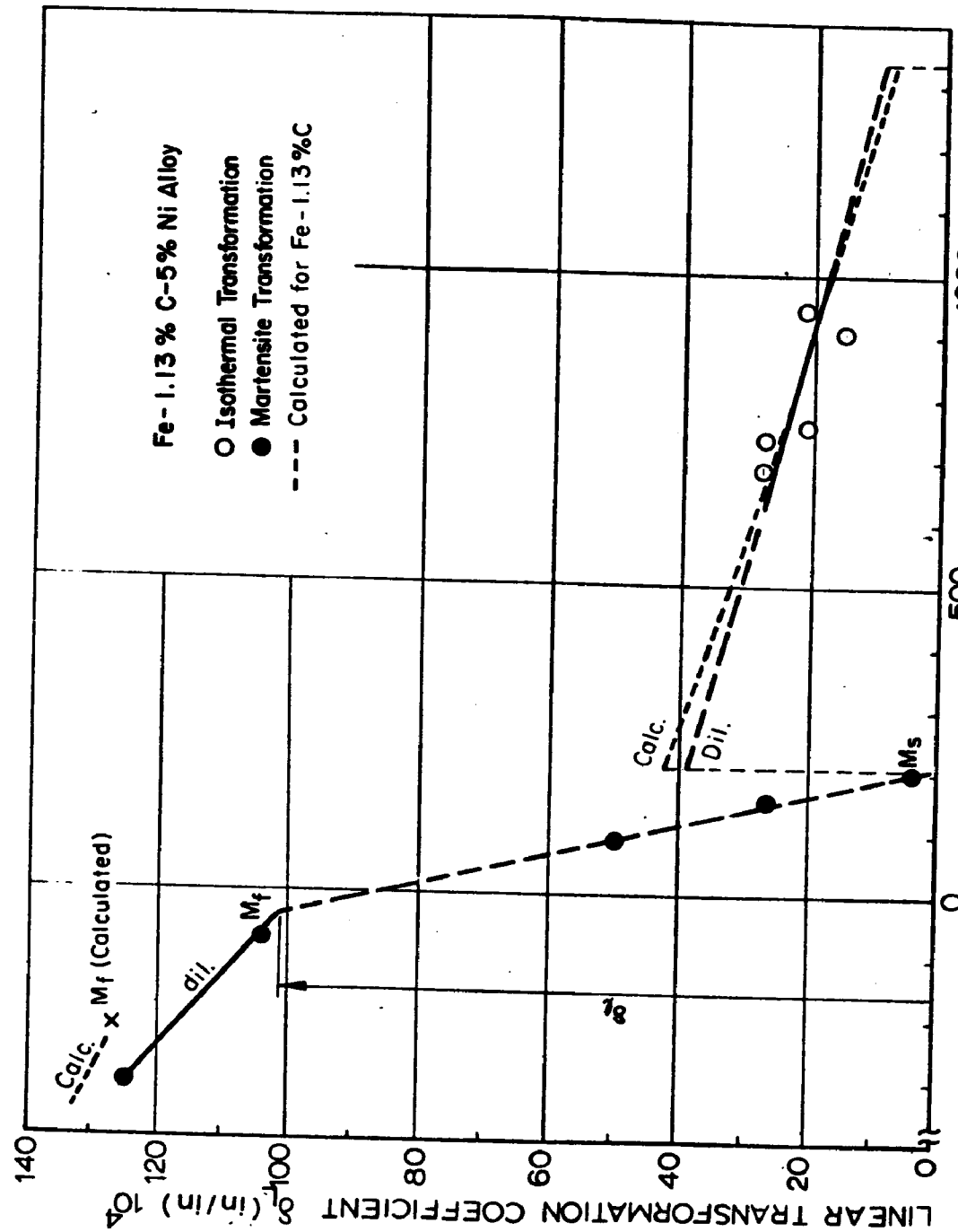


Fig. 23-D. Comparison of measured and calculated values of δ_ℓ for 1.13% C-5% Ni

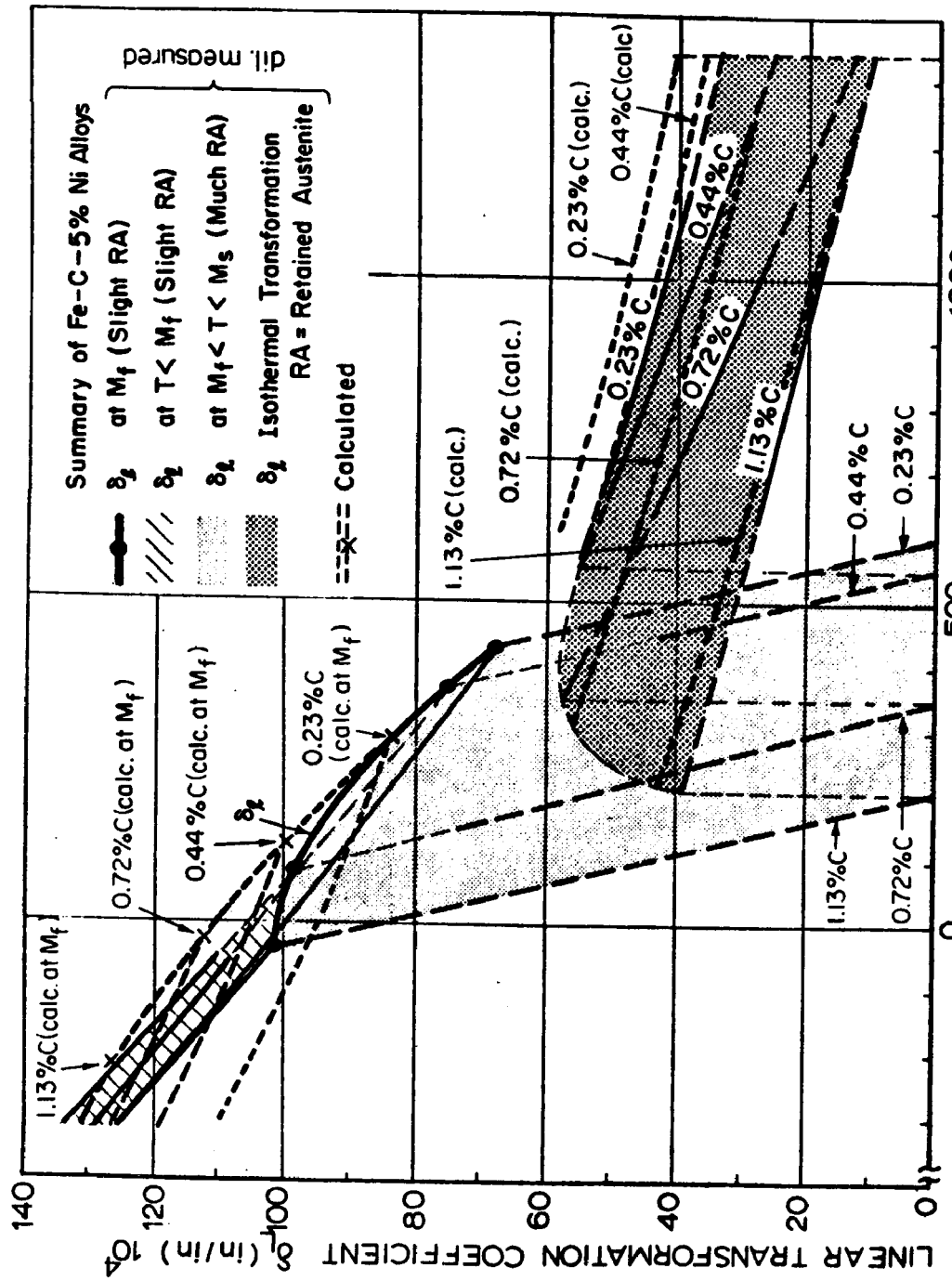


Fig. 23-E. Comparison of measured and calculated values of δ_ℓ for Fe-C-5% Ni alloys

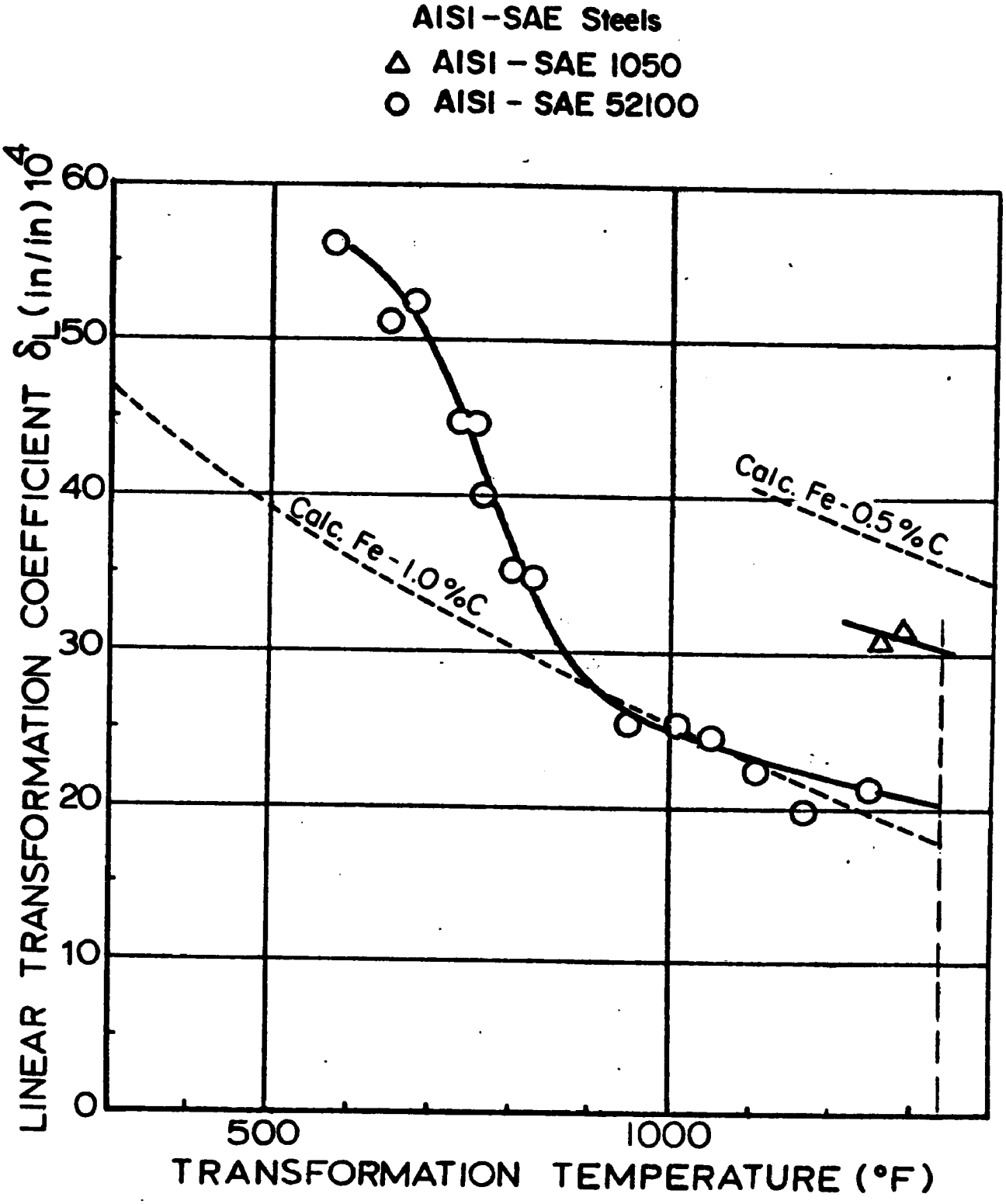


Fig. 24. Comparison of measured and calculated values of δ_ℓ for AISI-SAE 52100 and 1050

(See text pages 65, 86, and 111-112 for bainite discussion.)

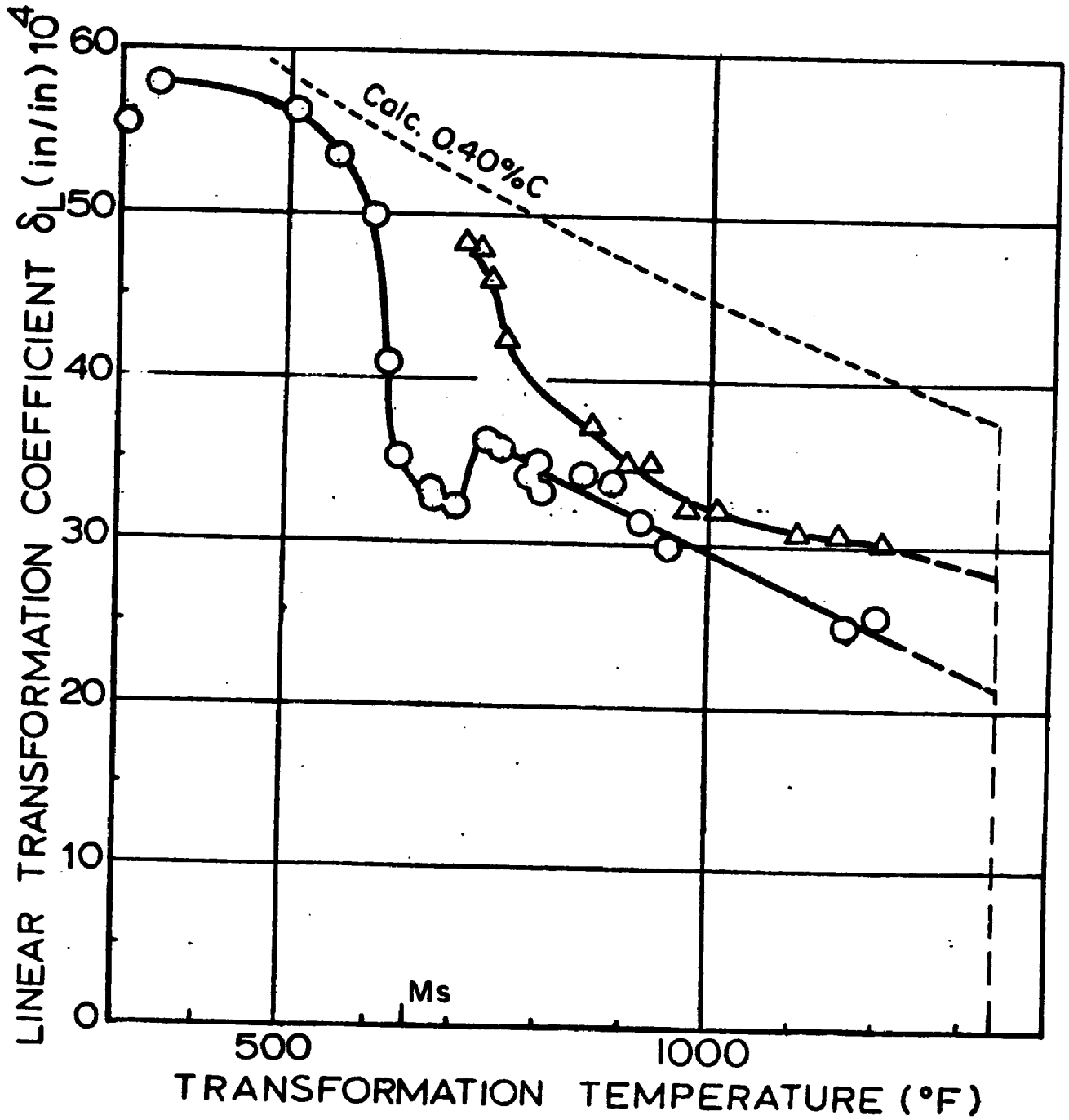


Fig. 25. Comparison of measured and calculated values of δ_ℓ for AISI-SAE 4140 and 8640
(See text pages 65, 86, and 111-112 for bainite discussion.)

Figs. 7-12, together with a line labelled, Calc., that represents the calculated values of δ_ℓ for the same carbon content of the alloy. Since the lattice parameter calculations are valid only for pure Fe-C alloys, a broken line has been used for Fe-C-5% Ni alloys and AISI-SAE steels. However, the data show that the effect of alloying elements is very small compared to the effect of the overall carbon content.

This comparison reveals a good agreement for the ferrite-pearlite-cementite and upper bainite regions. The effects of both temperature and carbon content are consistent as revealed by Fig. 26. The dilatometric data at the lower portion of the upper bainite and lower bainite temperatures exhibit negative and positive deviations (respectively) from the calculations for equilibrium transformations, as summarized in Fig. 27.
Finally, reasonably good overall agreement is obtained for martensite transformation when each alloy is considered separately as a function of the temperature. However, the effect of the carbon content cannot be compared accurately because the retained austenite and tempering effects are not taken into account in the calculations due to the lack of quantitative data, Fig. 28.

A summary of all these effects is given in Fig. 28 indicating the results of both the measurements and calculations (for the range 0.23 to 1.1% C). This shows a reasonable agreement both for the equilibrium and martensite

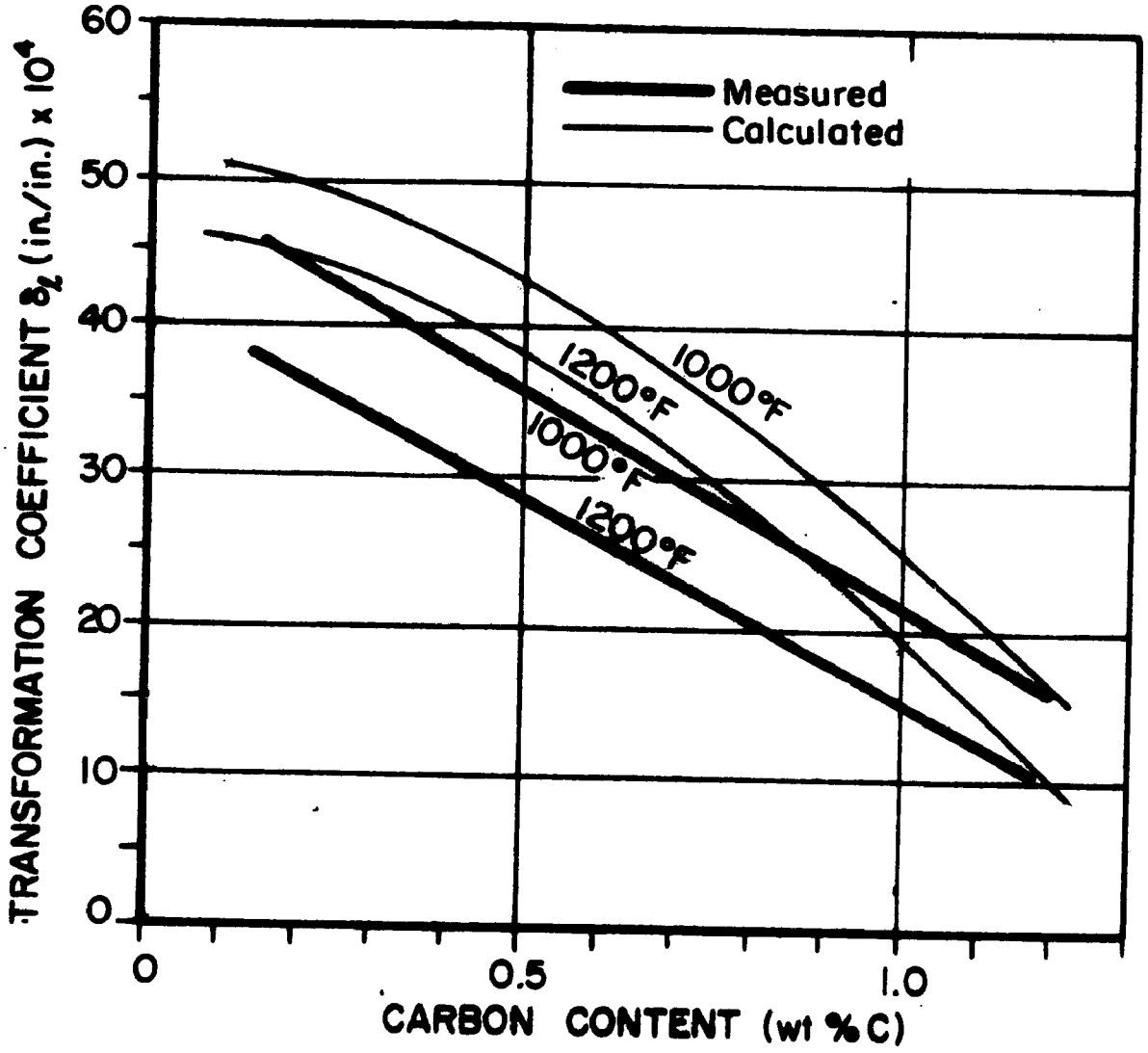


Fig. 26. Comparison of measured and calculated values of δ_ℓ vs % C at 1000°F (811 K) and 1200°F (922 K).

Data for "measured" curve from Fig. 11. Both measurements and calculations show an important effect of the % C upon δ_ℓ.

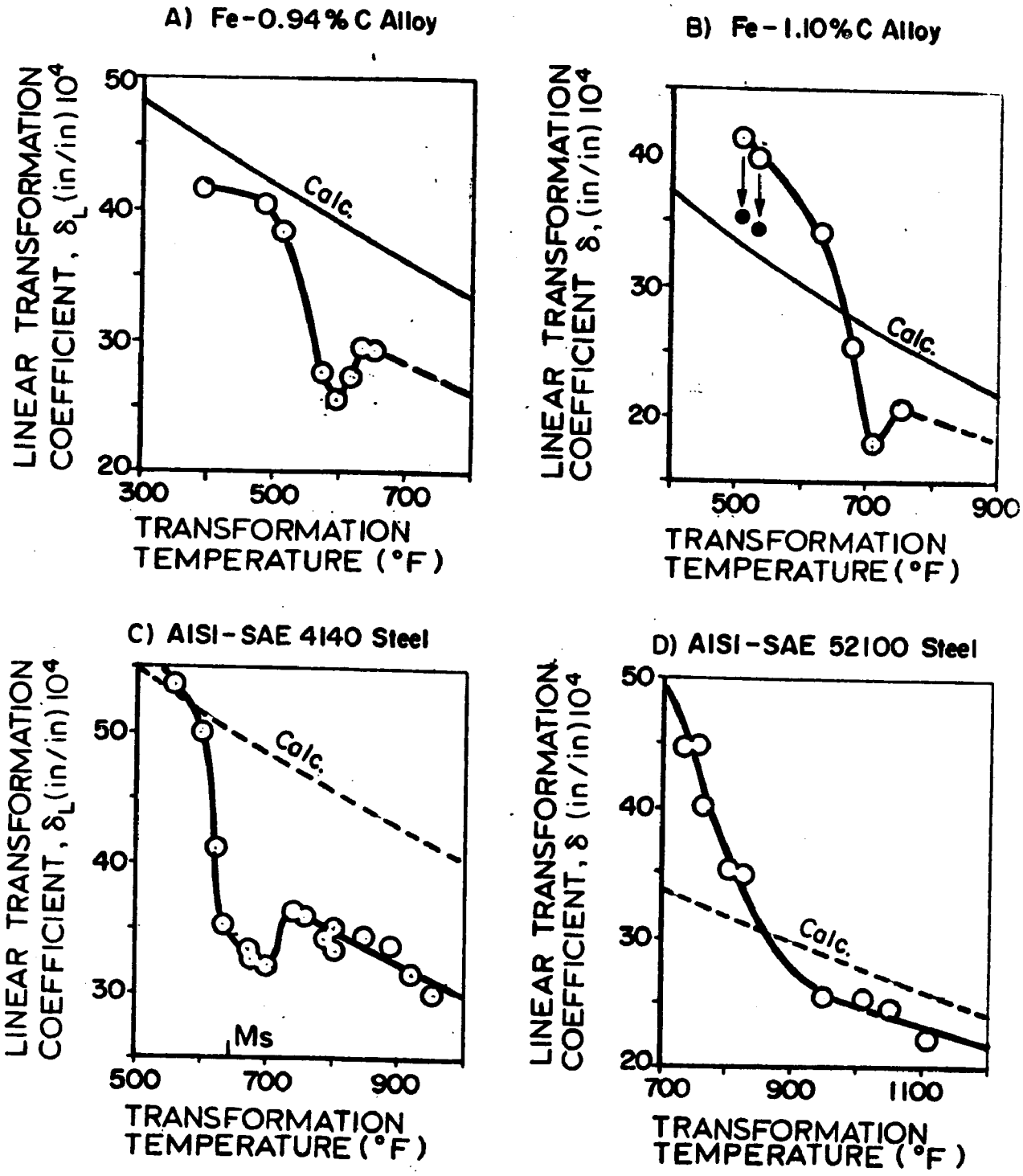


Fig. 27. Comparison of measured and calculated values of δ_ℓ in bainite region showing irregular behavior. Both positive and negative deviations are found in the bainite range. This is probably due to ferrite supersaturation with carbon and austenite retention respectively. (See text on pages 65, 86 and 111-112 for bainite discussion.)

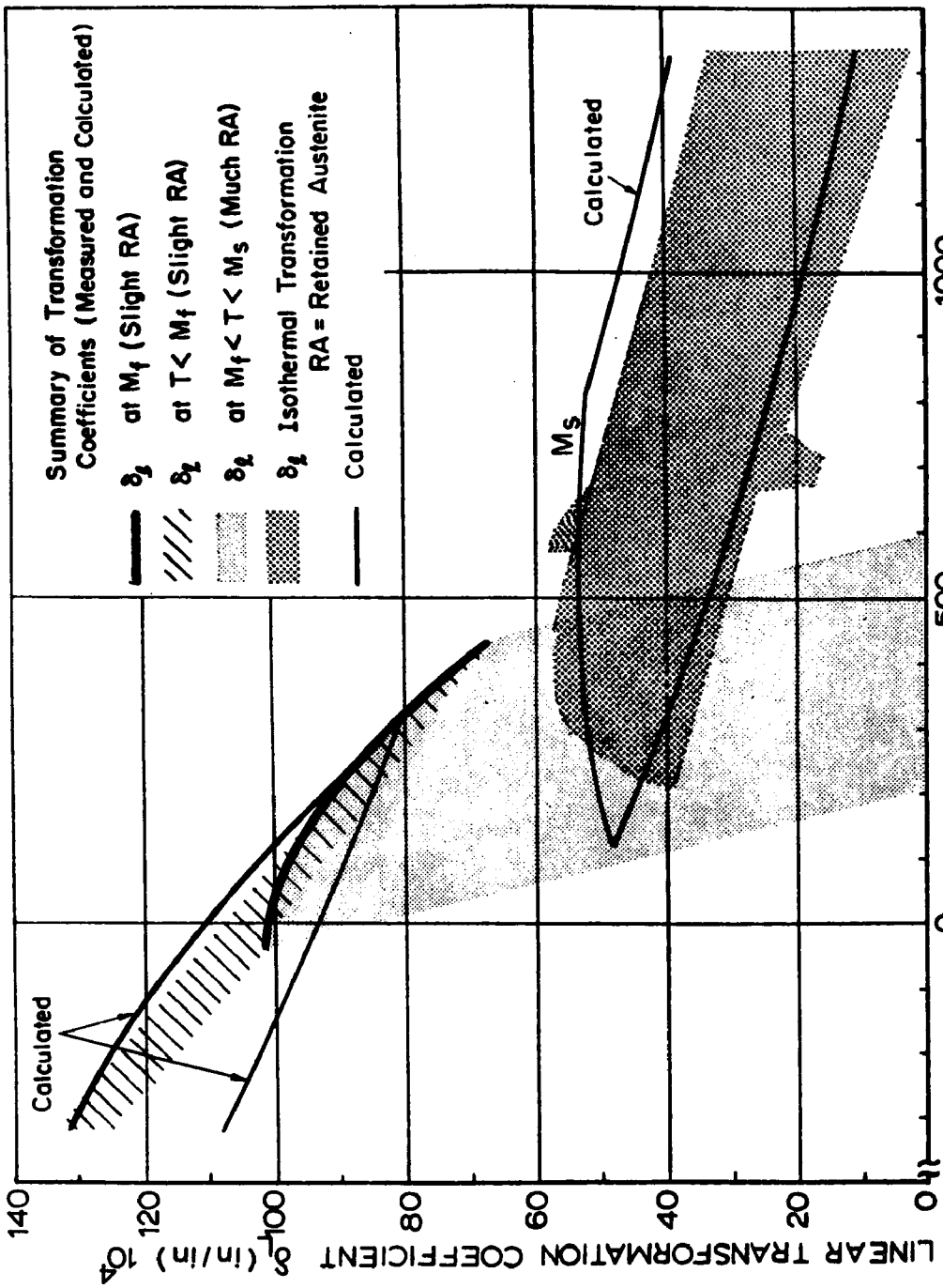


Fig. 28. Summary of measured and calculated values of δ_t vs temperature of transformation

transformations except in the lower bainite range as mentioned earlier and discussed in pages 111-112.

Next it is of interest to compare at this point the results of dilatometric measurements performed by other investigators.

Flinn et al. (2)have reported a series of relative length curves from which the transformation coefficient can be computed. Figure 29 shows these calculations from the reported data for two steels, (Steel A: 0.3 C-1.63 Mn-0.49 Si-0.44 Cr-0.33 Mo, and Steel B: 1.04 C-0.29 Mn-0.17 Si-0.05 Ni-0.04 Cr), together with the overall area covered by the measurements performed in the present work. Also the results of the calculations from lattice parameters are included for 0.3 and 1.04% carbon.

Reasonable agreement is found in the pearlite and upper bainite regions. The lower bainite regions of both steels show positive deviations from the calculated lines in agreement with the findings of the present work.

Hehemann(21) has measured the transformation coefficient of an AISI-SAE 4340 steel at the bainite range. Figure 28 shows his results together with calculated and measured values of δ_ℓ from the present work. Again in this case first a negative and then an positive deviation is found. The negative deviation occurs in the temperature range where Heheman reports incomplete transformation, above 752°F (673 K). At lower temperatures,

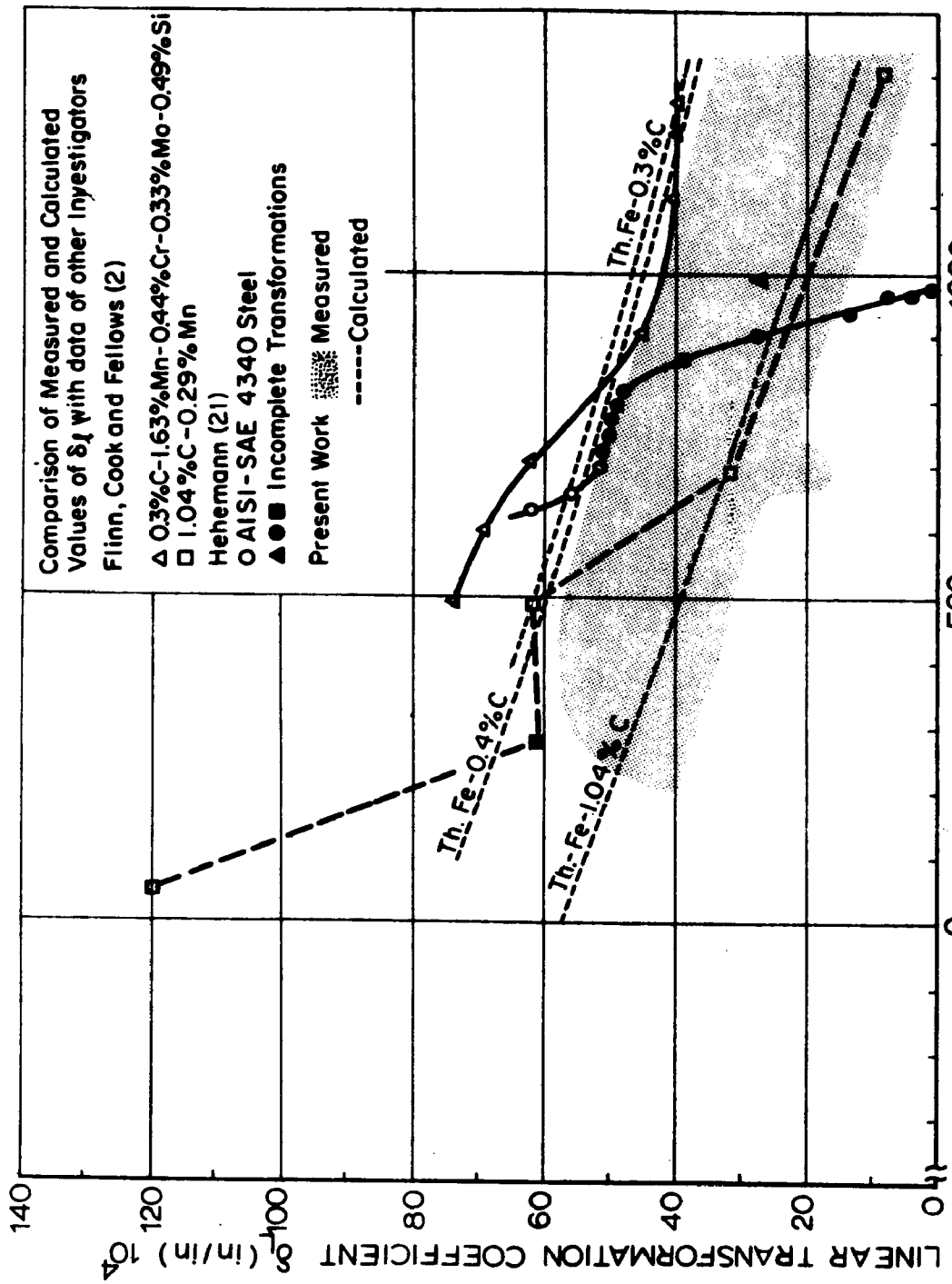


Fig. 29. Comparison of measured and calculated values of δ_ℓ with data of other investigators

however, complete austenite decomposition occurs and the transformation coefficient indicates a tendency toward the positive deviations.

Therefore the higher transformation coefficient values found in the present work at the lower bainite region are also revealed from an examination of the data of Flinn (2) and Hehemann (21) data.

Next, the differences between the δ_ℓ values measured vs. calculated are greatest in certain portions of the bainite range. In addition the trends of the deviations are consistent and correlate qualitatively with recent investigations of the theory of bainite formation. First it may be helpful to review the present understanding of the structure of bainite as the isothermal transformation temperature is lowered to below the pearlite range.

1) Upper bainite formed adjacent to the pearlite-ferrite range has a different microstructural appearance (feathery) but the crystal structures of the phases are still ferrite and Fe_3C (65-71).

2) Toward the lower end of upper bainite the transformation time increases, the product becomes coarsely acicular and some austenite persists after very long isothermal transformation times (69, 72-82).

3) In the lower bainite field the product is finely acicular, similar in appearance to martensite. Supersaturated ferrite and another form of carbide

(epsilon) are reported (83,84). It is also stated that the epsilon carbide will transform to Fe_3C with prolonged holding and cause contraction after and probably during the bainite transformation expansion (21).

Regarding point 1, the dilation measurements of δ_ℓ would be expected to correlate well with the calculated values and this is indeed observed, Figs. 22-25.

Regarding point 2, the dilation data for δ_ℓ at the lower end of upper bainite formation are lower than expected in some cases. This would correlate with the presence of retained austenite which would lead to a lower than expected value of δ_ℓ, Figs. 27-A,B and C.

Regarding point 3, the formation of supersaturated ferrite and ε carbide would lead to larger than calculated values of δ_ℓ as obtained. Also the contraction accompanying the transformation of ε carbide to Fe_3C is observed in all cases but indicated only in Fig. 27-B.

As discussed under Future Work in D, it is suggested that it would be of theoretical interest to perform accurate determinations of retained austenite and to investigate the lattice parameter of bainite carefully to evaluate these indications.

Finally, Fig. 30 is included to show the effect of carbon content upon the dimensional changes found in martensite transformation. It is a summary of the extrapolated measurements and lattice parameter calculations at room temperature. The extrapolation to room

temperature of the measured transformation coefficients at Mf is performed by means of the slopes of the δ_ℓ vs. temperature curves, between Mf and -320°F (78 K), Figs. 8-A,B,C and D. These are the best data of the coefficient of expansion of martensite available.

The calculated line is taken from Fig. 18-A. Figure 30 also shows the results of Magee and Davies (56) calculations from the same source of lattice parameter data. The difference in slope between the calculated lines is probably due to the models assumed to fit Ridley and Stuart data of the austenite lattice parameter. An overall agreement is evident from Fig. 30. However, the slightly lower measured δ_ℓ value for the 1.13% C alloy is due to incomplete austenite decomposition.

The comparison of δ_V at 20°C illustrates the effect of carbon in expanding the martensite unit cell and isolates it from its effect on δ_ℓ by lowering Ms-Mf range. However, this is true only at low carbon content levels, where the percent retained austenite is small. This effect is further explained by the contraction found in tempering of martensite*to an aggregate of equilibrium ferrite and cementite, Fig. 8-D. The difference between calculations of Fig. 21 and measurements of Fig. 8-D might be due to both incomplete martensite formation and incomplete tempering of it.

*The contractions due to bainite tempering (Figs. 13 and 27-B) also support this point.

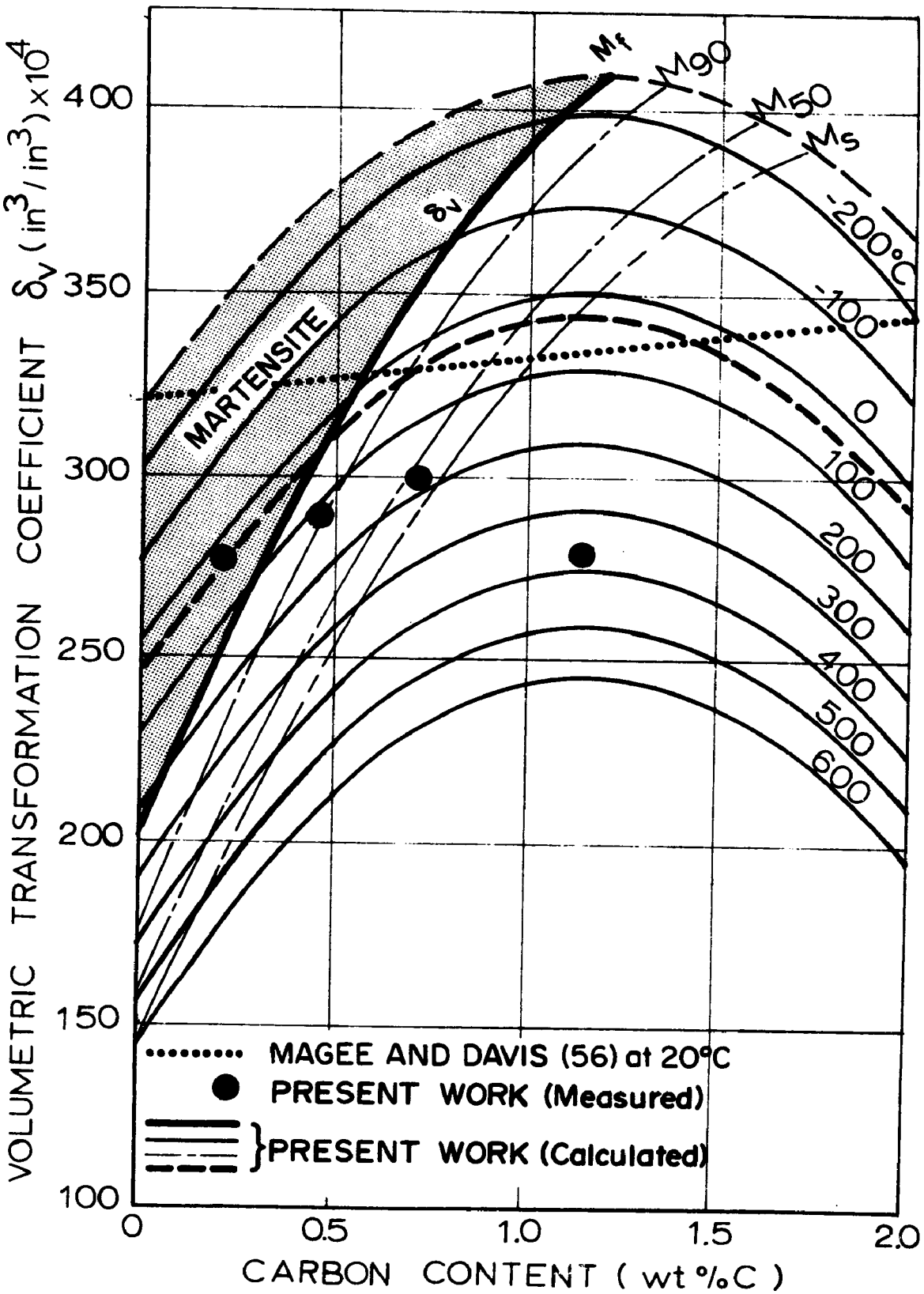


Fig. 30. Comparison of measured and calculated values of δ_ℓ for martensite at RT with other investigators

Note overall agreement of measurement data and calculated values. (Negative deviation at 1.13% C probably due to retained austenite.)

(D) Significance of the data, applications, suggestions for future work

At this point it is interesting to consider both the engineering implications of the data as well as some of the interesting basic questions raised by the experiments.

Engineering applications

The data indicate that the expansion accompanying the transformation of austenite is generally of a magnitude which can contribute to distortion, residual stresses and cracking during cooling. For example, if a typical δ_ℓ of 30×10^{-4} led to elastic strain of the same amount this would be equivalent to a (unaxial) stress of 90,000 psi (620 MN/m^2). It is recognized that this stress would not develop if an entire component transformed at the same time but this is rarely the case. The quench will usually lead to transformation at different times in different regions of a part. Therefore if the transformation takes place in one region before another, some corresponding deformation is forced in the other. In the case of a quenched bar, for example, these effects lead to circumferential tensile stress in the outer layer. These effects are well known but now that data are available for different

analyses and temperatures, the effects of composition and quenching technique in actual cases can be estimated.

Another application of the data is in understanding the stress build-up in composites. These materials range from a simple carburized case hardened gear to centrifugally cast bi-metal pipes or rolls. In these cases it is important to know the δ_ℓ as a function of both composition and temperature. Often,for example, a small expansion takes place due to pearlite transformation in the low alloy inner shell and a later very large expansion due to martensite in the outer layer. The final state of stress depends on the time and magnitude of the transformations and the plastic and elastic behavior of the materials.

Other cases involving a composition gradient include the use of hard facing materials in welding and assemblies of structures with different alloys. In addition there are many applications involving heating by braking or intermittent service at elevated temperatures in which the dilation coefficient should be an important factor in evaluating materials.

There are many other steels and other alloys for which δ_ℓ data should be obtained. Although a wide range of compositions was investigated, it should be realized that these covered only the low alloy steels. Additional data should be obtained for the high speed steels, special high strength alloys such as HY 130, HY 150, alloy

cast irons and maraging and precipitation hardening high alloy steels in order to understand distortion and residual stresses in these materials.

Basic questions

Finally the interesting correlation between consistently abnormal values of δ_{ℓ} in the bainite range with determinations of the accompanying changes in the fine structure of the bainite would be of theoretical interest.

Also, in the martensite range the correlation of quantity of retained austenite, lattice parameter measurements of martensite and dilatometric measurements of δ_{ℓ} would be interesting.

V. CONCLUSIONS

1. Using an especially designed quenching dilatometer the transformation coefficient, δ_ℓ, has been determined for a wide range of Fe-C alloys and steels as a function of temperature.

2. The data indicate that substantial variations in δ_ℓ occur depending upon carbon content, the type of transformation and temperature.

3. The differences in the effect of carbon in the higher temperature pearlite-ferrite range and in the martensite range are striking. In the pearlite range the higher the carbon content, the lower the value of δ_ℓ, while in the martensite range, increasing the carbon increases δ_ℓ.

4. Values of δ_ℓ were calculated from basic lattice parameter data which were available for special cases of pure Fe-C alloys. Good general agreement with the measurements from the dilatometer was obtained.

5. In the bainite range consistent deviations between the measured and calculated values of δ_ℓ were found. These may be explained qualitatively on the basis of known differences in structure and probably chemistry between certain bainites and the ferrite and cementite structures used as a basis for the calculations.

6. The calculations from lattice parameters show the unexpected result that high carbon-high temperature transformation of austenite can exhibit an overall contraction.

7. The values of δ_{ℓ} for the wide range of Fe-C alloys and commercial steels provide a basis for understanding the distortion, cracking and residual stresses encountered in commercial heat treatment and in intermittent service at elevated temperatures.

APPENDIX 1. REGRESSION ANALYSIS

In order to calculate the transformation coefficients from the available x-ray data, an equation describing the lattice parameter temperature and carbon content dependence is required.

The equation estimate of this relationship is obtained by the least squares method. In all cases the model assumed for the data is both quadratic in temperature and carbon content,

$$a = a_o + a_1 T + a_2 T^2 \tag{1}$$

or

$$a = a_o + a_1 C + a_2 C^2 + a_3 T + a_4 T^2 \tag{2}$$

where a is the lattice parameter value for the temperature T in °C and the carbon content C in weight %, and a_i are the coefficients estimated by the least square method. If $a(T_i)$ is the lattice parameter measured at the temperature T_i and a_i is the estimate obtained from equation (1), then the coefficients of this equation should be such that the following is true:

$$S = \sum (a_i - a(T_i))^2 = 0 \tag{3}$$

$$S = \sum (a_o + a_1 T_i + a_2 T_i^2 - a(T_i))^2 = 0 \tag{4}$$

The derivative of S with respect to a_o, a_1 and a_2 are also equal to zero and they give a set of three linear

equations with three unknowns, a_o, a_1 and a_2.

$$\begin{aligned} n\,a_o + \sum (T_i)\,a_1 + \sum (T_i^2)\,a_2 &= \sum a(T_i) \\ \sum (T_i)\,a_o + \sum (T_i^2)\,a_1 + \sum (T_i^3)\,a_2 &= \sum (a(T_i)\,T_i) \\ \sum (T_i^2)\,a_o + \sum (T_i^3)\,a_1 + \sum (T_i^4)\,a_2 &= \sum (a(T_i)\,T_i^2) \end{aligned} \qquad (5)$$

In the same way, calling $a(T_i,C_i)$ the lattice parameter measured at the temperature T_i for the alloy containing C_i weight percent carbon and a_i the estimate obtained from equation (2), and going through the same arguments that lead to equations (3), (4) and (5), a set of five independent linear equations with five unknowns, a_o, a_1, a_2, a_3 and a_4, is obtained.

$$\left.\begin{aligned} n\,a_o+\sum(C_i)a_1+\sum(C_i^2)a_2+\sum(T_i)a_3+\sum(T_i^2)a_4 &= \sum a(T_i,C_i) \\ \sum(C_i)a_o+\sum(C_i^2)a_1+\sum(C_i^3)a_2+\sum(T_iC_i)a_3+\sum(T_i^2C_i)a_4 &= \sum(C_i a(T_i,C_i)) \\ \sum(C_i^2)a_o+\sum(C_i^3)a_1+\sum(C_i^4)a_2+\sum(T_iC_i^2)a_3+\sum(T_i^2C_i^2)a_4 &= \sum(C_i^2 a(T_i,C_i)) \\ \sum(T_i)a_o+\sum(T_iC_i)a_1+\sum(T_iC_i^2)a_2+\sum(T_i^2)a_3+\sum(T_i^3)a_4 &= \sum(T_i a(T_i,C_i)) \\ \sum(T_i^2)a_o+\sum(T_i^2C_i)a_1+\sum(T_i^2C_i^2)a_2+\sum(T_i^3)a_3+\sum(T_i^4)a_4 &= \sum(T_i^2 a(T_i,C_i)) \end{aligned}\right\} \qquad (6)$$

A computer program was developed to solve the set of equations (5) or (6) and therefore find the solution to the coefficients of equations (1) and (2) from the set of "n" experimentally determined lattice parameters (Appendix 3).

This type of calculation was first applied to the data available from Ridley and Stuart from the personal

communication (33), Table 10, to obtain the coefficients of the quadratic equations for austenite,ferrite and cementite, Table 11.

For the case of austenite this calculation was done in two ways: a) using the quadratic model in the temperature (only) for the data available for each Fe-C alloy taken individually, and b) using the quadratic model both in the temperature and carbon content for all the data available for different Fe-C alloys, Table 11-A. Next the calculation is performed for the data of the two types of pure α-Fe and ferrite in a 1.44% C Fe-C alloy, by means of the quadratic model in the temperature, Table 11-B. Finally, the data for pure α-Fe, ferrite and both extracted cementite and cementite in situ (in a 1.44% C Fe-C alloy) have been regressed again using the quadratic model in the temperature, Table 11-C and D.

Table 10. Lattice Parameter Data from Ridley and Stuart (33)

(A) Lattice Parameter of α-Fe

1) Johnson-Matthey Spectrographically Pure Iron

Composition: O_2 Mn,Si,Mg,Al,Cu,Ag

Wt%: 0.012 <0.02 total

Temp. °C	Lattice Parameter Å	Specimen Number	Temp. °C	Lattice Parameter Å	Specimen Number
22	2.8663	1	734	2.8967	2
78	2.8682	1	747	2.8974	2
159	2.8711	1	765	2.8979	2
223	2.8736	1	774	2.8979	2
376	2.8800	1	793	2.8984	2
549	2.8876	1	802	2.8988	2
660	2.8930	1	810	2.8994	2
751	2.8975	1	822	2.8998	2
896	2.9037	1	23	2.8662	2
23	2.8663	2	715	2.8957	3
448	2.8830	2	831	2.9002	3
601	2.8903	2	842	2.9008	3
652	2.8927	2	858	2.9016	3
677	2.8937	2	871	2.9021	3
688	2.8944	2	888	2.9029	3
704	2.8953	2	23	2.8664	3
718	2.8960	2			

Table 10 (cont.)

Japanese Electrolytic Iron

Composition:	O_2	C	Si	Co	Mn, Pb, W, Nb, Al, Ni	Mo, Ti, Sn, Cu, Al, V	Pb, B
Wt%:	0.040	0.006	0.016	0.010	<0.005 each	<0.002 each	<0.01 each

Temp. °C	Lattice Parameter Å	Temp. °C	Lattice Parameter Å
19	2.8660	758	2.8977
540	2.8871	780	2.8980
630	2.8914	799	2.8988
700	2.8949	821	2.8997
734	2.8966	832	2.9002
740	2.8969	20	2.8662

α-Fe in Equilibrium with Fe_3C in a 1.44% C Steel

Temp. °C	Lattice Parameter
24	2.8664
127	2.8699
174	2.8717
256	2.8748
337	2.8782
454	2.8834
538	2.8872
669	2.8933
719	2.8960

Table 10 (cont.)

(B) Lattice Parameter Data for Fe_3C

1) Extracted Fe_3C

a) SPECIMEN 1

TEMPERATURE °C.	'a'	'b'	'c'
23	4.5246	5.0864	6.7423
148	4.5290	5.0893	6.7495
267	4.5341	5.0921	6.7587
364	4.5378	5.0953	6.7681
496	4.5442	5.1039	6.7827
565	4.5482	5.1098	6.7897

b) SPECIMEN 2

TEMPERATURE °C.	'a'	'b'	'c'
23	4.5246	5.0883	6.7423
63	4.5259	5.0888	6.7453
214	4.5313	5.0911	6.7548
346	4.5364	5.0951	6.7656
423	4.5411	5.0988	6.7714
657	4.5553	5.1235	6.8038

2) Fe_3C in ferrite (1.44% C steel)

TEMPERATURE °C.	'a'	'b'	'c'
24	4.5246	5.0883	6.7424
127	4.5279	5.0887	6.7485
174	4.5298	5.0900	6.7519
256	4.5326	5.0916	6.7577
337	4.5371	5.0952	6.7655
454	4.5428	5.1016	6.7779
538	4.5466	5.1081	6.7867
669	4.5556	5.1245	6.8053

Table 10 (cont.)

(C) Lattice Parameters of Austenites

1) Fe-0.32% C

TEMPERATURE °C	LATTICE PARAMETER Å	TEMPERATURE °C	LATTICE PARAMETER
832	3.6473	1048	3.6650
865	3.6505	1083	3.6682
922	3.6544	1140	3.6720
980	3.6593	1186	3.6764

2) Fe-0.62% C

TEMPERATURE °C	LATTICE PARAMETER Å	TEMPERATURE °C	LATTICE PARAMETER
825	3.6555	1007	3.6688
870	3.6592	1067	3.6735
935	3.6636	1076	3.6741
986	3.6675		

3) Fe-0.86% C

TEMPERATURE °C	LATTICE PARAMETER Å	TEMPERATURE °C	LATTICE PARAMETER
817	3.6610	987	3.6737
870	3.6660	1042	3.6781
940	3.6693	1120	3.6842

Table 10 (cont.)

4) Fe-1.02% C

TEMPERATURE °C	LATTICE PARAMETER Å	TEMPERATURE °C	LATTICE PARAMETER
830	3.6657	955	3.6753
861	3.6694	1015	3.6807
870	3.6696	1062	3.6839
908	3.6719	1111	3.6886
925	3.6740		

5) Fe-1.15% C

TEMPERATURE °C	LATTICE PARAMETER Å	TEMPERATURE °C	LATTICE PARAMETER Å
920	3.6812	1065	3.6901
951	3.6826	1096	3.6943
960	3.6840	1124	3.6961
1002	3.6882	1169	3.7023

6) Fe-1.44% C

TEMPERATURE °C	LATTICE PARAMETER Å	TEMPERATURE °C	LATTICE PARAMETER Å
991	3.6945	1130	3.7063
1027	3.6979	1156	3.7073
1089	3.7024	1185	3.7100

Table 10 (cont.)

7) PURE IRON

Data of Basinski and of Goldschmidt Converted to Å

BASINSKI (22)		GOLDSCHMIDT (36)	
TEMPERATURE °C	LATTICE PARAMETER Å	TEMPERATURE	LATTICE PARAMETER Å
916	3.6468	912	3.6466
923	3.6471		
950	3.6496	926	3.6484
1074	3.6598	999	3.6528
1184	3.6696	1113	3.6623

Table 10. Lattice Parameter Data from Ridley and Stuart (33)

(A) Lattice Parameter of α-Fe

1) Johnson-Matthey Spectrographically Pure Iron

Composition: O_2 Mn,Si,Mg,Al,Cu,Ag

Wt%: 0.012 <0.02 total

Temp. °C	Lattice Parameter Å	Specimen Number	Temp. °C	Lattice Parameter Å	Specimen Number
22	2.8663	1	734	2.8967	2
78	2.8682	1	747	2.8974	2
159	2.8711	1	765	2.8979	2
223	2.8736	1	774	2.8979	2
376	2.8800	1	793	2.8984	2
549	2.8876	1	802	2.8988	2
660	2.8930	1	810	2.8994	2
751	2.8975	1	822	2.8998	2
896	2.9037	1	23	2.8662	2
23	2.8663	2	715	2.8957	3
448	2.8830	2	831	2.9002	3
601	2.8903	2	842	2.9008	3
652	2.8927	2	858	2.9016	3
677	2.8937	2	871	2.9021	3
688	2.8944	2	888	2.9029	3
704	2.8953	2	23	2.8664	3
718	2.8960	2			

Table 10 (cont.)

2) Japanese Electrolytic Iron

Composition:	O_2	C	Si	Co	Mn, Pb, W, Nb, Al, Ni	Mo, Ti, Sn, Cu, Al, V	Fb, B
Wt%:	0.040	0.006	0.016	0.010	<0.005 each	<0.002 each	<0.01 each

Temp. °C	Lattice Parameter Å	Temp. °C	Lattice Parameter Å
19	2.8660	758	2.8977
540	2.8871	780	2.8980
630	2.8914	799	2.8988
700	2.8949	821	2.8997
734	2.8966	832	2.9002
740	2.8969	20	2.8662

3) α-Fe in Equilibrium with Fe_3C in a 1.44% C Steel

Temp. °C	Lattice Parameter
24	2.8664
127	2.8699
174	2.8717
256	2.8748
337	2.8782
454	2.8834
538	2.8872
669	2.8933
719	2.8960

Table 10 (cont.)

(B) Lattice Parameter Data for Fe_3C

1) Extracted Fe_3C

a) SPECIMEN 1

TEMPERATURE °C.	'a'	'b'	'c'
23	4.5246	5.0884	6.7423
148	4.5290	5.0893	6.7495
267	4.5341	5.0921	6.7587
364	4.5378	5.0953	6.7681
496	4.5442	5.1039	6.7827
565	4.5482	5.1098	6.7897

b) SPECIMEN 2

TEMPERATURE °C.	'a'	'b'	'c'
23	4.5246	5.0883	6.7423
63	4.5259	5.0888	6.7453
214	4.5313	5.0911	6.7548
346	4.5364	5.0951	6.7656
423	4.5411	5.0988	6.7714
657	4.5553	5.1235	6.8038

2) Fe_3C in ferrite (1.44% C steel)

TEMPERATURE °C.	'a'	'b'	'c'
24	4.5246	5.0883	6.7424
127	4.5279	5.0887	6.7485
174	4.5298	5.0900	6.7519
256	4.5326	5.0916	6.7577
337	4.5371	5.0952	6.7655
454	4.5428	5.1016	6.7779
538	4.5466	5.1081	6.7867
669	4.5556	5.1245	6.8052

Table 10 (cont.)

(C) Lattice Parameters of Austenites

1) Fe-0.32% C

TEMPERATURE °C	LATTICE PARAMETER Å	TEMPERATURE °C	LATTICE PARAMETER
832	3.6475	1048	3.6650
865	3.6505	1083	3.6682
922	3.6544	1140	3.6720
980	3.6593	1186	3.6764

2) Fe-0.62% C

TEMPERATURE °C	LATTICE PARAMETER Å	TEMPERATURE °C	LATTICE PARAMETER
825	3.6555	1007	3.6688
870	3.6592	1067	3.6735
935	3.6636	1076	3.6741
986	3.6675		

3) Fe-0.86% C

TEMPERATURE °C	LATTICE PARAMETER Å	TEMPERATURE °C	LATTICE PARAMETER
817	3.6610	987	3.6737
870	3.6660	1042	3.6781
940	3.6693	1120	3.6842

Table 10 (cont.)

4) Fe-1.02% C

TEMPERATURE °C	LATTICE PARAMETER Å	TEMPERATURE °C	LATTICE PARAMETER
830	3.6657	955	3.6753
861	3.6694	1015	3.6807
870	3.6696	1062	3.6839
908	3.6719	1111	3.6886
925	3.6740		

5) Fe-1.15% C

TEMPERATURE °C	LATTICE PARAMETER Å	TEMPERATURE °C	LATTICE PARAMETER Å
920	3.6812	1065	3.6926
951	3.6826	1096	3.6943
960	3.6840	1124	3.6961
1002	3.6882	1189	3.7023

6) Fe-1.44% C

TEMPERATURE °C	LATTICE PARAMETER Å	TEMPERATURE °C	LATTICE PARAMETER Å
991	3.6945	1130	3.7063
1027	3.6979	1156	3.7073
1089	3.7024	1185	3.7100

Table 10 (cont.)

7) PURE IRON

Data of Basinski and of Goldschmidt Converted to Å

BASINSKI (22)		GOLDSCHMIDT (36)	
TEMPERATURE °C	LATTICE PARAMETER Å	TEMPERATURE	LATTICE PARAMETER Å
916	3.6468	912	3.6466
923	3.6471		
950	3.6496	926	3.6484
1074	3.6598	999	3.6528
1184	3.6696	1113	3.6623

Table 11. Regression analysis

(A) Austenites (for each carbon content separately)

Model*: $a_A = a_o + a_1 T + a_2 T^2$ (Å)

	Carbon content of α-Fe (wt %)					
	0.00%C	0.32%C	0.62%C	0.86%C	1.02%C	1.17%C	1.44%C
a_o	3.63001 (1)						
	3.59095 (2)	3.58286	3.59779	3.62314	3.61658	3.61453	3.56930
	3.64702 (3)	(4)	(4)	(4)	(4)	(4)	(4)
$a_1 \cdot 10^5$	-3.20 (1)						
	4.20 (2)	7.51	6.76	2.60	4.64	6.79	16.65
	-6.23 (3)	(4)	(4)	(4)	(4)	(4)	(4)
$a_2 \cdot 10^7$	5.52 (1)						
	2.06 (2)	0.311	0.310	2.55	1.63	0.474	-4.04
	6.83 (3)	(4)	(4)	(4)	(4)	(4)	(4)
σ	±0.00038 (1)						
	±0.00014 (2)	±0.00034	±0.00017	±0.00063	±0.00053	±0.00063	±0.00039
	±0.00047 (3)						
N	9 (1)						
	5 (2)	8	7	4	9	8	6
	4 (3)						

*Temperatures in °C; (1) From Basinski and Goldschmidt data together; (2) From Basinski data alone; (3) From Goldschmidt data alone; (4) From Ridley data alone.

Table 11. (cont.)

(B) Austenites (for all carbon contents together - except points for pure iron)

Model: $a_A = a_o + a_1C + a_2C^2 + a_3T + a_4T^2$ (Å)

C is the weight percent of carbon and T the temperature in °C.

$a_o = 3.58142$

$a_1 = 1.709 \cdot 10^{-2}$

$a_2 = 7.97 \cdot 10^{-3}$ $\quad \sigma = \pm 0.00096$

$a_3 = 6.7 \cdot 10^{-5}$ $\quad N = 44$ (from Ridley data)

$a_4 = 6.2 \cdot 10^{-9}$

(C) Ferrite

Model: $a_F = a_o + a_1T + a_2T^2$ (Å)

T is the temperature in °C.

	Johnson Matthey Spectrographically Pure Iron				Japanese Electrolytic Iron	Ferrite in a 1.44% C Fe-C Alloy
	Spec.#1	Spec.#2	Spec.#3	Summary		
a_o	2.86523	2.86526	2.86542	2.86518	2.86530	2.86550
$a_1 \cdot 10^5$	3.70	4.00	4.28	3.93	3.96	3.36
$a_2 \cdot 10^9$	7.14	3.02	-0.86	4.00	3.34	12.16
σ	±0.00030	±0.00039	±0.00013	±0.00038	±0.00038	±0.0001
N	9	17	7	31	9	12

Table 11. (cont.)

(D) Cementite

Model: $a_C = a_o + a_1T + a_2T^2$ (Å)

$b_C = b_o + b_1T + b_2T^2$ (Å)

$c_C = c_o + c_1T + c_2T^2$ (Å)

T is the temperature in °C.

	Extracted Cementite			Cementite in a 1.44% C Fe-C Alloy
	Spec.#1	Spec.#2	Summary	
a_o	4.52391	4.52511	4.52415	4.52391
$a_1 \cdot 10^5$	3.18	2.51	2.64	2.93
$a_2 \cdot 10^8$	1.93	3.40	3.06	2.81
σ	±0.00025	±0.00031	±0.00049	±0.00048
N	6	6	12	8
b_o	5.08887	5.08948	5.08953	5.08942
$b_1 \cdot 10^5$	-1.23	-2.25	-2.23	-2.00
$b_2 \cdot 10^8$	8.65	11.23	10.83	10.62
σ	±0.00042	±0.00100	±0.00113	±0.00087
N	6	6	12	8
c_o	6.74089	6.74223	6.74172	6.74136
$c_1 \cdot 10^5$	5.04	3.57	4.14	4.65
$c_2 \cdot 10^8$	6.54	8.74	7.94	7.27
σ	±0.00052	±0.00108	±0.00088	±0.00041
N	6	6	12	8

APPENDIX 2

CALCULATION OF TRANSFORMATION DILATION FROM X-RAY LATTICE PARAMETER DATA

The volumetric transformation coefficient has been defined as

$$\delta_V = \frac{\Delta V}{V_i} = \frac{V_f - V_i}{V_i} \qquad (1)$$

where δ_V is the volume change per unit volume and ΔV is the total volume change due to the transformation of a volume V of the given material (V_f is the final volume and V_i the initial).

Since the weight W of the material transforming does not change during transformation, it is possible to express δ_V in terms of the specific volumes of the phases.

$$\delta_V = \frac{\frac{V_f}{W} - \frac{V_i}{W}}{\frac{V_i}{W}} = \frac{\bar{V}_f - \bar{V}_i}{\bar{V}_i} \qquad (2)$$

where $\bar{V}_f$ and $\bar{V}_i$ are the final and initial specific volumes. The specific volume of materials having crystalline atomic arrangement can be calculated from the knowledge of their unit cell lattice parameters by the following equation:

$$\bar{V}_i = \frac{AN \cdot v_i}{n_a \cdot AW_a + n_b \cdot AW_b + \ldots} \qquad (3)$$

where $\bar{V}_i$ is the specific volume in (cm^3/gm) of phase i, AN is the Avogadro's Number in (number of atoms/mole), v_i is the unit cell volume in (cm^3) and n_a is the number

of atoms of the "a" kind per unit cell with atomic weight AW_a in (gm/mole). Therefore, the specific volume as defined by equation (3) has the dimensions of (cm^3/gm).

Since phase transformations in steels involve only crystalline phases, their specific volumes can be computed by means of equation (3), provided the lattice parameters of the initial and final phases are known at the temperature the phase transformation occurs and for the chemical composition of the alloy (basically its carbon content).

First, part A, the calculation of the transformation coefficient for pearlitic transformations has been performed. The assumption that equilibrium ferrite and stoichiometric Fe_3C are the product phases of a pearlitic reaction is made.

In bainitic transformations only the product phases of upper bainite are known to be ferrite and cementite. Lower bainite product phases are known to be supersaturated ferrite and ε carbide. It has also been shown that the transformation of ε to Fe_3C eventually occurs. However, the degree of carbon supersaturation is not well known. Moreover, no accurate data for the ε carbide coefficient of expansion are found in the literature. Therefore the only data available are for upper bainite and are the same calculations performed for transformations in the pearlite range. In other

words the only difference between pearlitic and upper bainitic transformations is the morphology of their product phases,not in the unit cells involved.

The calculations of the martensitic transformation coefficients, part B, are performed assuming that transformation goes to completion and that the product phase is virgin martensite (no allowance is made for tempering.)

It is important to emphasize that these calculations are only valid for the conditions established by the set of assumptions described in each case.

Another important point to emphasize is that slight variations in the chemistry of the alloy during actual transformations, especially in the carbon content of the phases, might affect the comparison of dilation measurements and calculations.

Finally, no allowance is made for (a) elastic strains that might affect the lattice parameter, or (b) for differences in the density of lattice imperfections between the initial and final phases, such as vacancies, dislocations, etc.

Although bainitic and martensitic transformations result in mixtures of equilibrium and non-equilibrium phases or mixtures of two types of non-equilibrium phases, the calculation of these two extreme situations is of great significance because it defines an upper and lower limit to the transformation dilation. Therefore, hybrid

transformations should give volume changes between the values for complete equilibrium and those for complete non-equilibrium.

A) EQUILIBRIUM TRANSFORMATIONS (Ferrite, Pearlite, Cementite)

1) Computation Procedure

In this case the initial phase is austenite and the final is an aggregate of ferrite and cementite. Therefore, $\bar{V}_i = \bar{V}_A$.

$$\bar{V}_f = \frac{V_f}{W} = \frac{V_F + V_C}{W} = \frac{W_F \cdot \bar{V}_F + W_C \cdot \bar{V}_C}{W} = f_F^W \cdot \bar{V}_F + f_C^W \cdot \bar{V}_C \qquad (4)$$

where $\bar{V}_i$ and $\bar{V}_f$ are the initial and final specific volumes, $\bar{V}_A$, $\bar{V}_F$ and $\bar{V}_C$ are the specific volumes of austenite, ferrite and cementite respectively, V_f is the final total volume of the weight W of the material undergoing transformation, V_F and V_C are the volumes of ferrite and cementite such that $V_f = V_F + V_C$, W_F and W_C are the ferrite and cementite weights such that $W = W_F + W_C$, and finally f_F^W and f_C^W are the weight fractions of ferrite and cementite. Therefore, from equation (2)

$$\delta_V = \frac{f_F^W \cdot \bar{V}_F + f_C^W \cdot \bar{V}_C - \bar{V}_A}{\bar{V}_A} \qquad (5)$$

$$\delta_V = f_F^W \cdot \frac{\bar{V}_F}{\bar{V}_A} + f_C^W \cdot \frac{\bar{V}_C}{\bar{V}_A} - 1 \qquad (6)$$

To solve equation (6), weight fractions of ferrite and cementite and specific volume ratios of ferrite to austenite and cementite to austenite should be computed.

Assuming equilibrium conditions, ferrite and cementite weight fractions can be computed from the lever rule by:

$$f_F^w = \frac{6.68 - C}{6.68 - C^F} \; ; \quad f_C^w = 1 - f_F^w \qquad (7)$$

where C is the weight percent carbon of the Fe-C alloy, C^F is the carbon content of ferrite and 6.68 the weight percent carbon in cementite as calculated from stoichiometry.

2) Derivation of the equations of the specific volume ratio

By means of equation (3) the specific volumes of austenite, ferrite and cementite can be calculated as follows:

$$\bar{V}_A = \frac{AN \cdot V_A}{n_{Fe}^A \cdot AW_{Fe} + n_C^A \cdot AW_C}$$

$$\bar{V}_F = \frac{AN \cdot V_F}{n_{Fe}^F \cdot AW_{Fe} + n_C^F \cdot AW_C} \qquad (8)$$

$$\bar{V}_C = \frac{AN \cdot V_C}{n_{Fe}^C \cdot AW_{Fe} + n_C^C \cdot AW_C}$$

AN = Avogadro's Number (# atoms/mole)

AW_{Fe}, AW_C = Atomic Weights of Iron and Carbon (gm/mole)

V_A, V_F and V_C = Unit Cell Volumes of Austenite, Ferrite and Cementite (cm^3)

$n_{Fe}^A = 4$ = # of Iron Atoms per Austenite Unit Cell

n_C^A = # of Carbon Atoms per Austenite Unit Cell

$n_{Fe}^F = 2$ = # of Iron Atoms per Ferrite Unit Cell

n_C^F = # of Carbon Atoms per Ferrite Unit Cell

$n_{Fe}^C = 12$ = # of Iron Atoms per Cementite Unit Cell

$n_C^C = 4$ = # of Carbon Atoms per Cementite Unit Cell

The unit cell volumes of austenite, ferrite and cementite can be calculated from their lattice parameters as follows:

$$V_A = a_A^3; \quad V_F = a_F^3; \quad V_C = a_C \cdot b_C \cdot c_C$$

where a_A = lattice parameter of austenite

a_F = lattice parameter of austenite

a_C, b_C and c_C = lattice parameters of cementite.

Now an equation has to be derived to compute n_C^F and n_C^A. Taking 100 gm of material as the basis for the calculation, and knowing that the weight of a single carbon atom is given by the ratio of the atomic weight of carbon to Avogadro's Number

$$\frac{AW_C}{AN} = \frac{(\text{gm C/mole})}{(\text{\# of atoms/mole})} = \frac{\text{gm}}{\text{C atom}},$$

the weight percent of carbon can be calculated by

$$\%C = C = \frac{n_C \cdot \left(\frac{AW_C}{AN}\right)}{100} \cdot 100$$

If the unit cell is taken as the basis, then

$$\%C = C = \frac{n_C \cdot \left(\frac{AW_C}{AN}\right)}{W_{uc}} \cdot 100$$

where W_{uc} is the unit cell weight in grams. A similar relation can be derived for iron,

$$\%Fe = Fe = \frac{n_{Fe} \cdot \frac{AW_{Fe}}{AN}}{W_{uc}} \cdot 100$$

Taking the ratio of the carbon to the iron percents,

$$\frac{\%C}{\%Fe} = \frac{C}{Fe} = \frac{n_C}{n_{Fe}} \cdot \frac{AW_C}{AW_{Fe}}$$

$$n_C = (C/Fe) \cdot (AW_{Fe}/AW_C) \cdot n_{Fe} \qquad (9)$$

By means of this equation, the number of carbon atoms in austenite and ferrite unit cells can be calculated:

$$n_C^A = \left(\frac{C^A}{Fe^A}\right) \cdot \left(\frac{AW_{Fe}}{AW_C}\right) \cdot n_{Fe}^A$$

$$n_C^F = \left(\frac{C^F}{Fe^F}\right) \cdot \left(\frac{AW_{Fe}}{AW_C}\right) \cdot n_{Fe}^F \qquad (10)$$

Now it is possible to go back to the equations of the specific volume (8) and insert the corresponding values of the iron and carbon atoms per unit cell as in equation (10):

$$\bar{V}_A = \frac{AN \cdot V_A}{4.AW_{Fe} + \left(\frac{C^A}{Fe^A}\right) \cdot \left(\frac{AW_{Fe}}{AW_C}\right) \cdot 4 \cdot AW_C}$$

$$\bar{V}_A = \frac{AN \cdot V_A}{4\ AW_{Fe}\left[1 + \left(\frac{C^A}{Fe^A}\right)\right]}$$

$$\bar{V}_F = \frac{AN \cdot V_F}{2.AW_{Fe} + \left(\frac{C^F}{Fe^F}\right) \cdot \left(\frac{AW_{Fe}}{AW_C}\right) \cdot 2 \cdot AW_C}$$

$$\bar{V}_F = \frac{AN \cdot V_F}{2.AW_{Fe}\left[1 + \left(\frac{C^F}{Fe^F}\right)\right]}$$

$$\bar{V}_C = \frac{AN \cdot V_C}{12 \cdot AW_{Fe} + 4 \cdot AW_C}$$

$$\bar{V}_C = \frac{AN \cdot V_C}{4.AW_{Fe}\left(3 + \frac{AW_C}{AW_{Fe}}\right)}$$

Therefore the ratio of the specific volumes $\bar{V}_F/\bar{V}_A$, $\bar{V}_C/\bar{V}_A$ and $\bar{V}_C/\bar{V}_F$ can be computed as follows:

$$\frac{\overline{V}_F}{\overline{V}_A} = \frac{\dfrac{AN \cdot V_F}{2.AW_{Fe} \cdot \left[1 + \left(\dfrac{C^F}{Fe^F}\right)\right]}}{\dfrac{AN \cdot V_A}{4.AW_{Fe} \cdot \left[1 + \left(\dfrac{C^A}{Fe^A}\right)\right]}}$$

$$\frac{\overline{V}_F}{\overline{V}_A} = 2 \cdot \frac{\left[1 + \left(\dfrac{C^A}{Fe^A}\right)\right] \cdot V_F}{\left[1 + \left(\dfrac{C^F}{Fe^F}\right)\right] \cdot V_A} \qquad (11)$$

$$\frac{\overline{V}_C}{\overline{V}_A} = \frac{\dfrac{AN \cdot V_C}{4.AW_{Fe} \cdot \left[3 + \left(\dfrac{AW_C}{AW_{Fe}}\right)\right]}}{\dfrac{AN \cdot V_A}{4.AW_{Fe} \cdot \left[1 + \left(\dfrac{C^A}{Fe^A}\right)\right]}}$$

$$\frac{\overline{V}_C}{\overline{V}_A} = \frac{\left[1 + \left(\dfrac{C^A}{Fe^A}\right)\right] \cdot V_C}{\left[3 + \left(\dfrac{AW_C}{AW_{Fe}}\right)\right] \cdot V_A} \qquad (12)$$

3) Assumptions

During the derivation of these equations several assumptions have been made and these should be summarized:

Assumption 1: The carbon content of cementite has been calculated from stoichiometry.

Assumption 2: Ferrite and cementite weight fractions have been calculated for the equilibrium conditions predicted by the Fe-C equilibrium phase diagram.

Assumption 3: The carbon solubility of ferrite is taken from the experimental curve of the equilibrium phase diagram and is given by C_F = exp

Assumption 4: Austenite decomposition goes to 100% completion.

Assumption 5: 100% solution of carbon in austenite happened during austenitization.

4) Results

The lattice parameter equations have been obtained by a regression analysis of the x-ray data of Ridley (33), assuming that points fit a quadratic model both in their temperature and carbon content dependence (Appendix 1).

The austenite lattice parameter equation derived from x-ray data for all available carbon contents gives a more consistent extrapolation for lattice parameters at the low range of temperatures, below the eutectoid temperature, where austenite decomposition takes place.

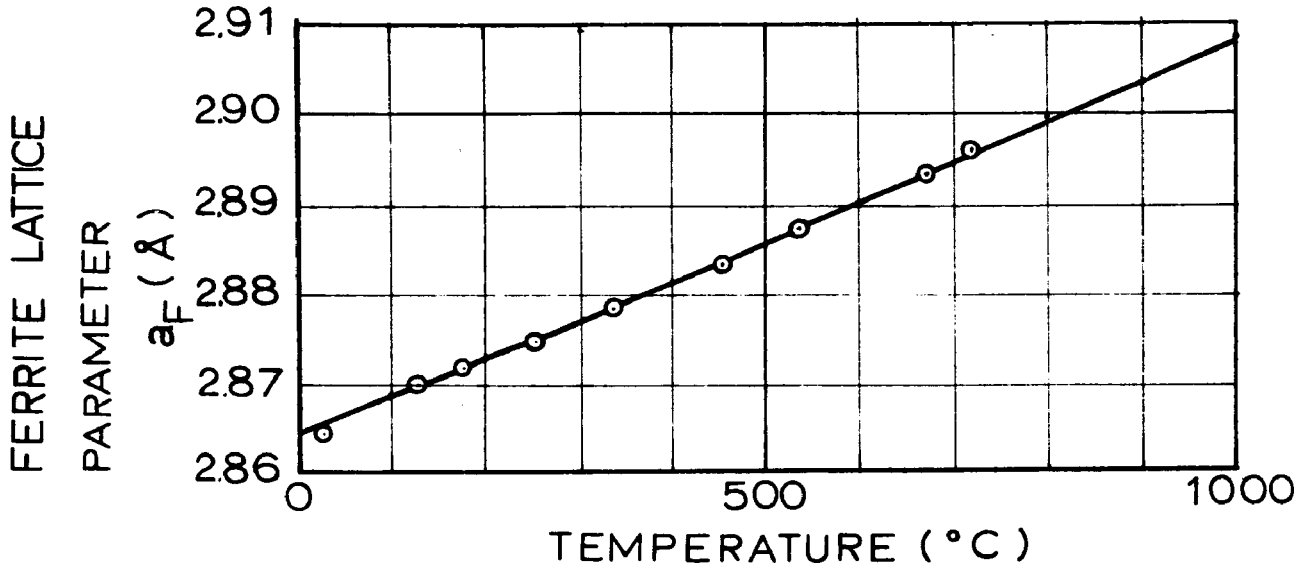


Fig. 31. Lattice parameter of ferrite (1.44% C alloy) vs temperature (Ridley and Stuart, 33)

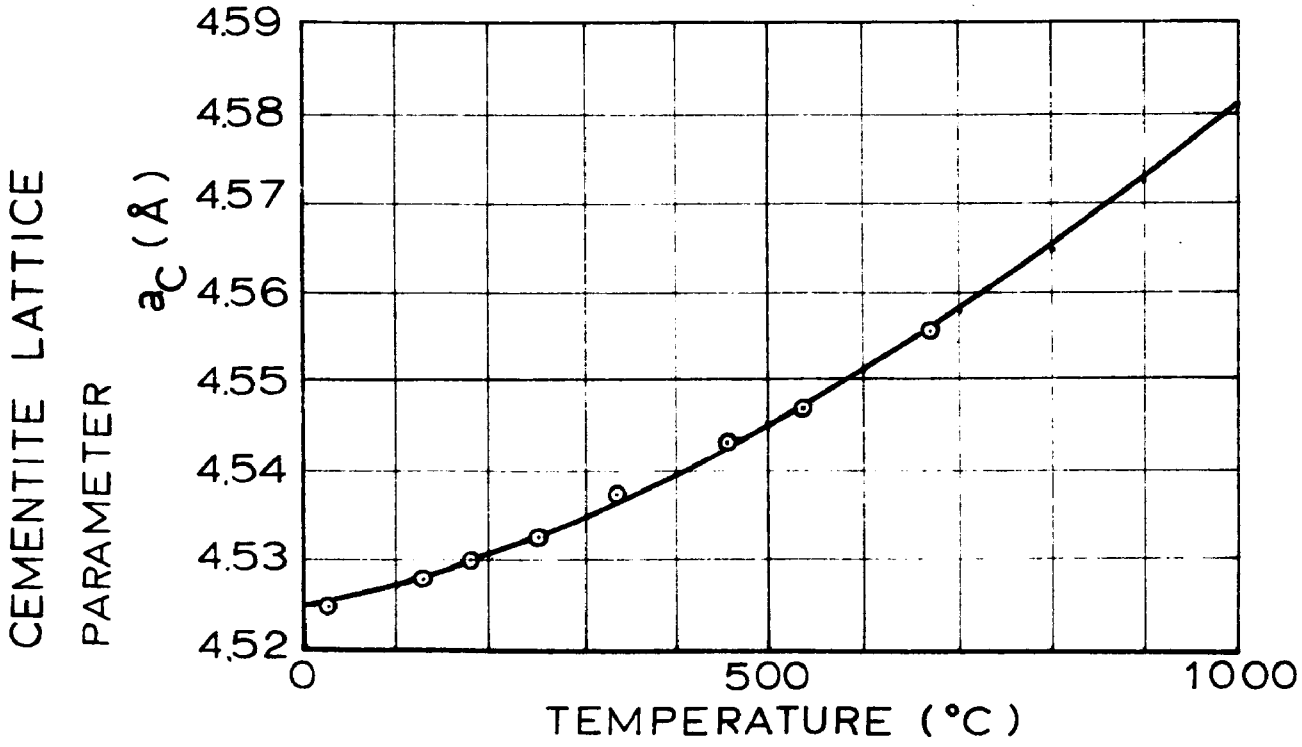


Fig. 32-A. "a" lattice parameter of cementite (1.44% C alloy) vs temperature (33)

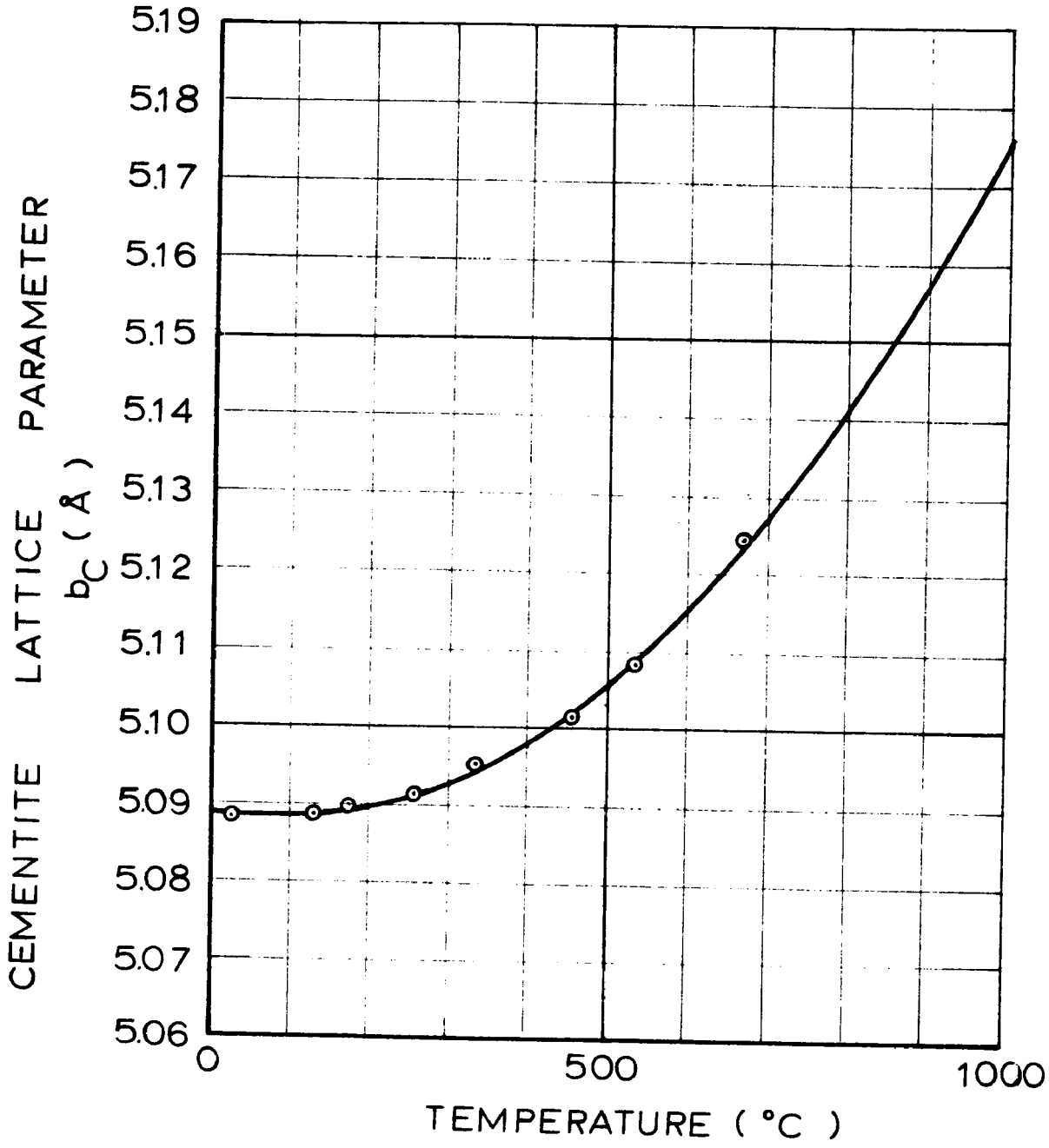


Fig. 32-B. "b" lattice parameter of cementite (1.44% C alloy) vs temperature (33)

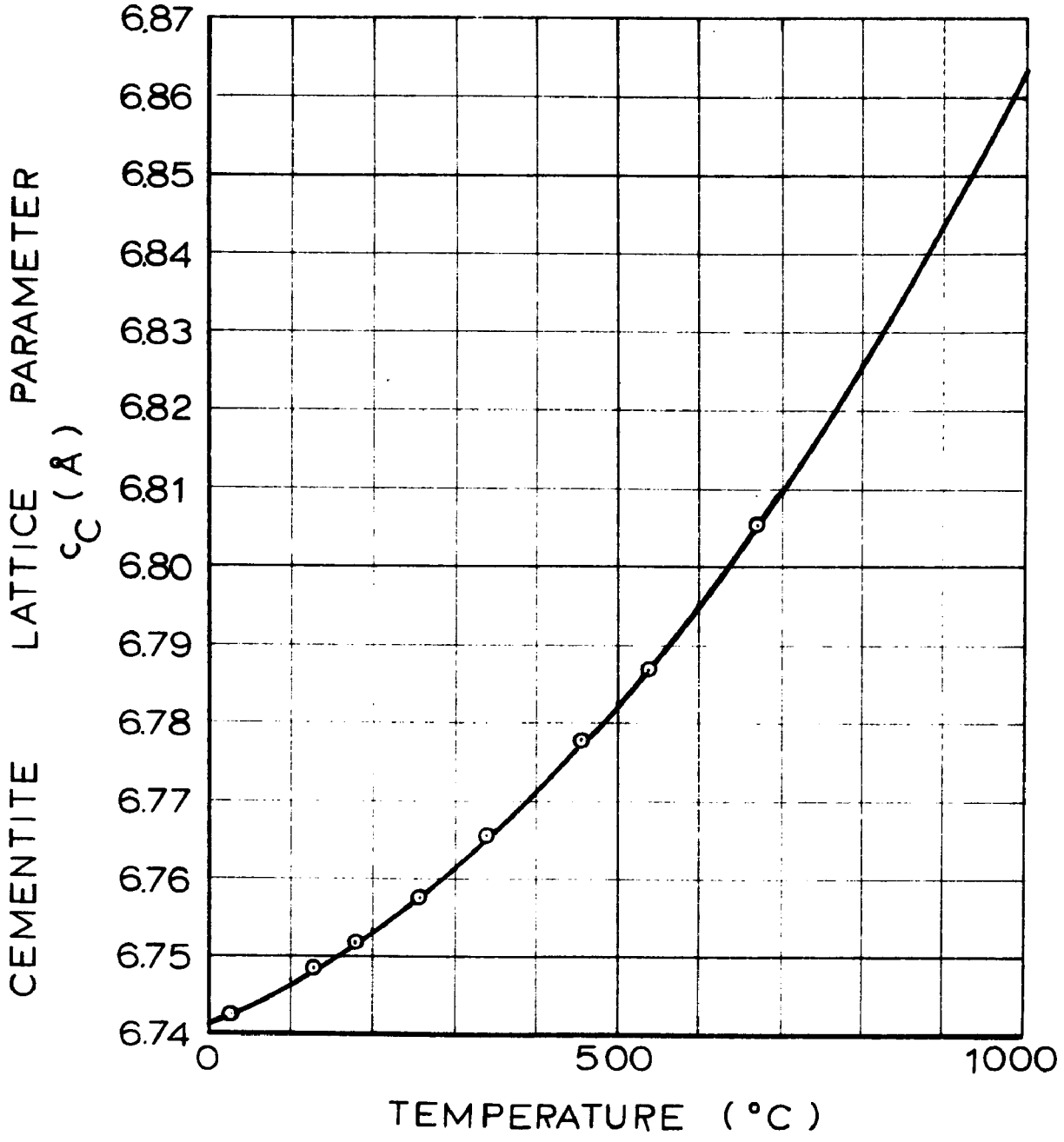


Fig. 32-C. "c" lattice parameter of cementite (1.44% C alloy) vs temperature (33)

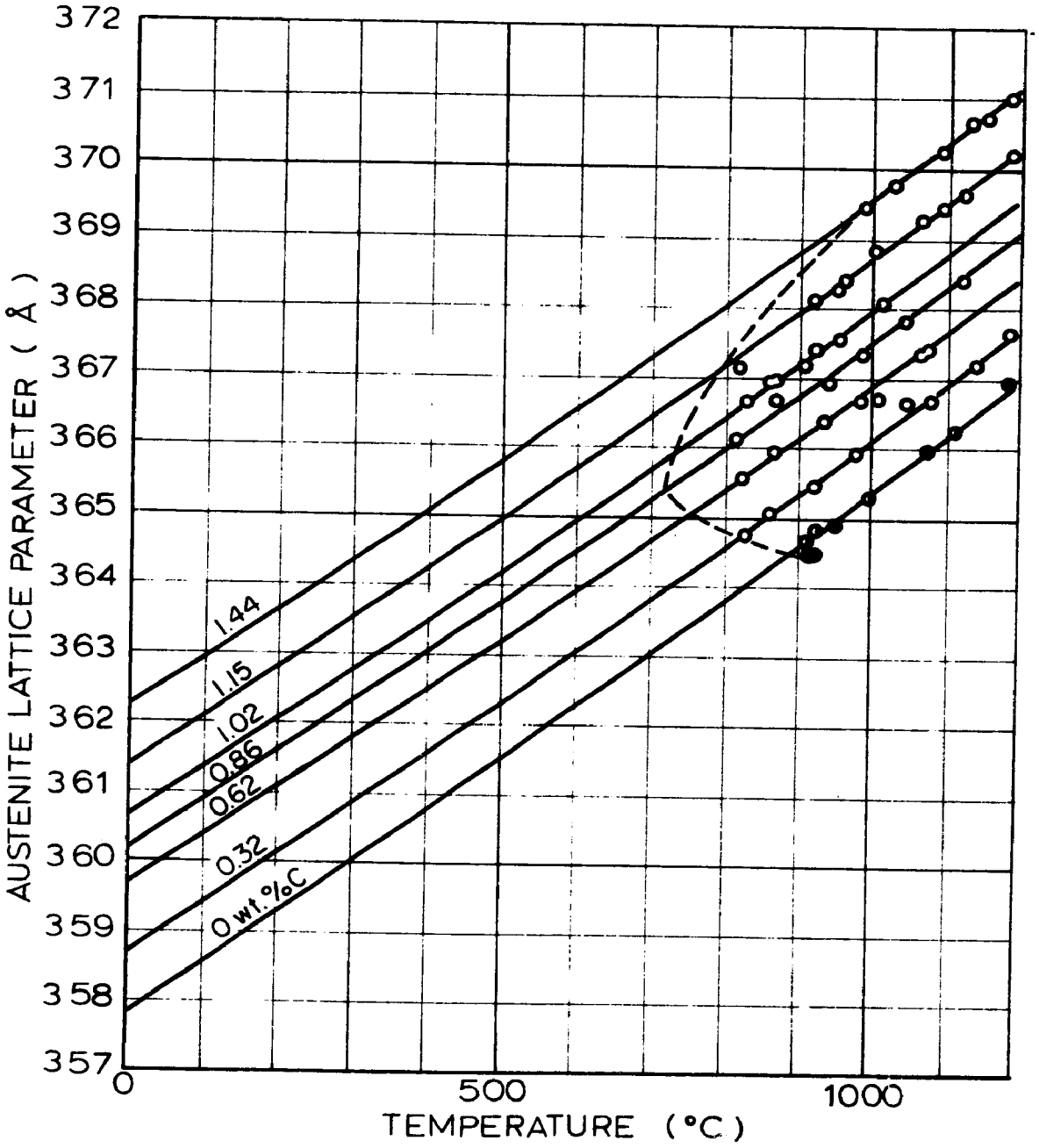


Fig. 33-A. Lattice parameter of austenite of different carbon contents vs temperature (33)

Dashed line shows limit of austenite stability.

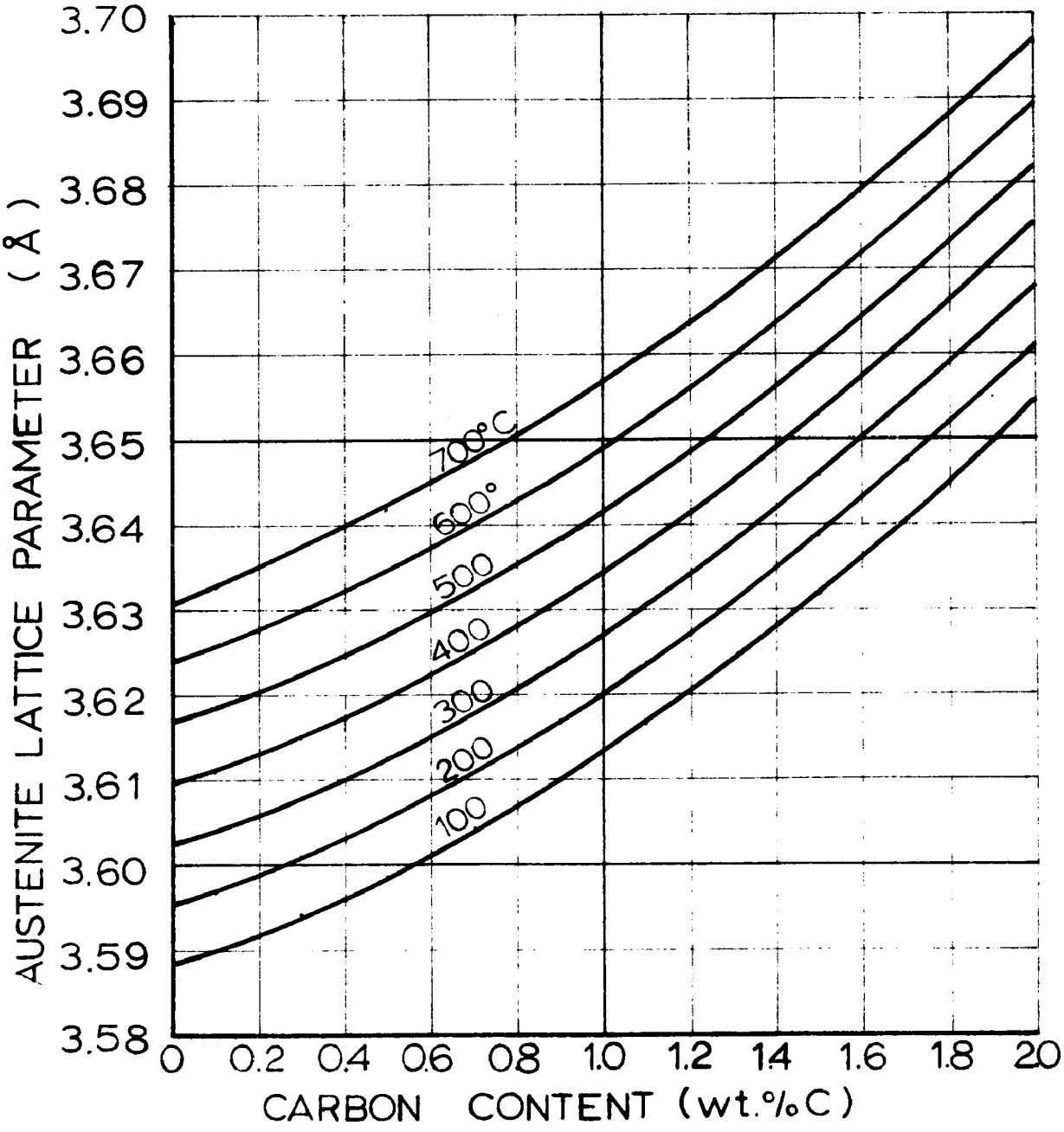


Fig. 33-B. Lattice parameter of austenite of different carbon contents vs % C (33)

Austenite Lattice Parameter Equation (Fig. 33 A and B)

$$a_A(\pm 0.001\ \mathring{A}) =$$

$$= 3.5814 + 1.709 \cdot C \cdot 10^{-2} + 7.97 \cdot C^2 \cdot 10^{-3} +$$

$$+ 6.7 \cdot T \cdot 10^{-7} + 6.2 \cdot T^2 \cdot 10^{-9} \qquad (13)$$

The lattice parameter numbers obtained are in $\mathring{A}$, C is the carbon content in weight percent and T the temperature in °C.

Both the ferrite and cementite lattice parameter equations are based on ferrite and cementite in equilibrium in a 1.44% C steel.

Ferrite Lattice Parameter Equation (Fig. 31)

$$a_F(\pm 0.000\ \mathring{A}) = 2.8655 + 3.96 \cdot T \cdot 10^{-5} + 3.34 \cdot T^2 \cdot 10^{-9} \qquad (14)$$

Cementite Lattice Parameter Equations
(Fig. 32-A,B and C)

$$a_C(\pm 0.000\ \mathring{A}) = 4.5239 + 2.93 \cdot T \cdot 10^{-5} + 2.81 \cdot T^2 \cdot 10^{-8}$$

$$b_C(\pm 0.000\ \mathring{A}) = 5.0894 - 2.00 \cdot T \cdot 10^{-5} + 10.62 \cdot T^2\ \ 10^{-8} \qquad (15)$$

$$c_C(\pm 0.000\ \mathring{A}) = 6.7414 + 4.65 \cdot T \cdot 10^{-5} + \ 7.27 \cdot T^2\ \ 10^{-8}$$

A regression analysis has been performed to obtain a single equation describing the transformation coefficient, δ_V, as a function of temperature and carbon content from the volumetric transformation coefficient for equilibrium transformations:

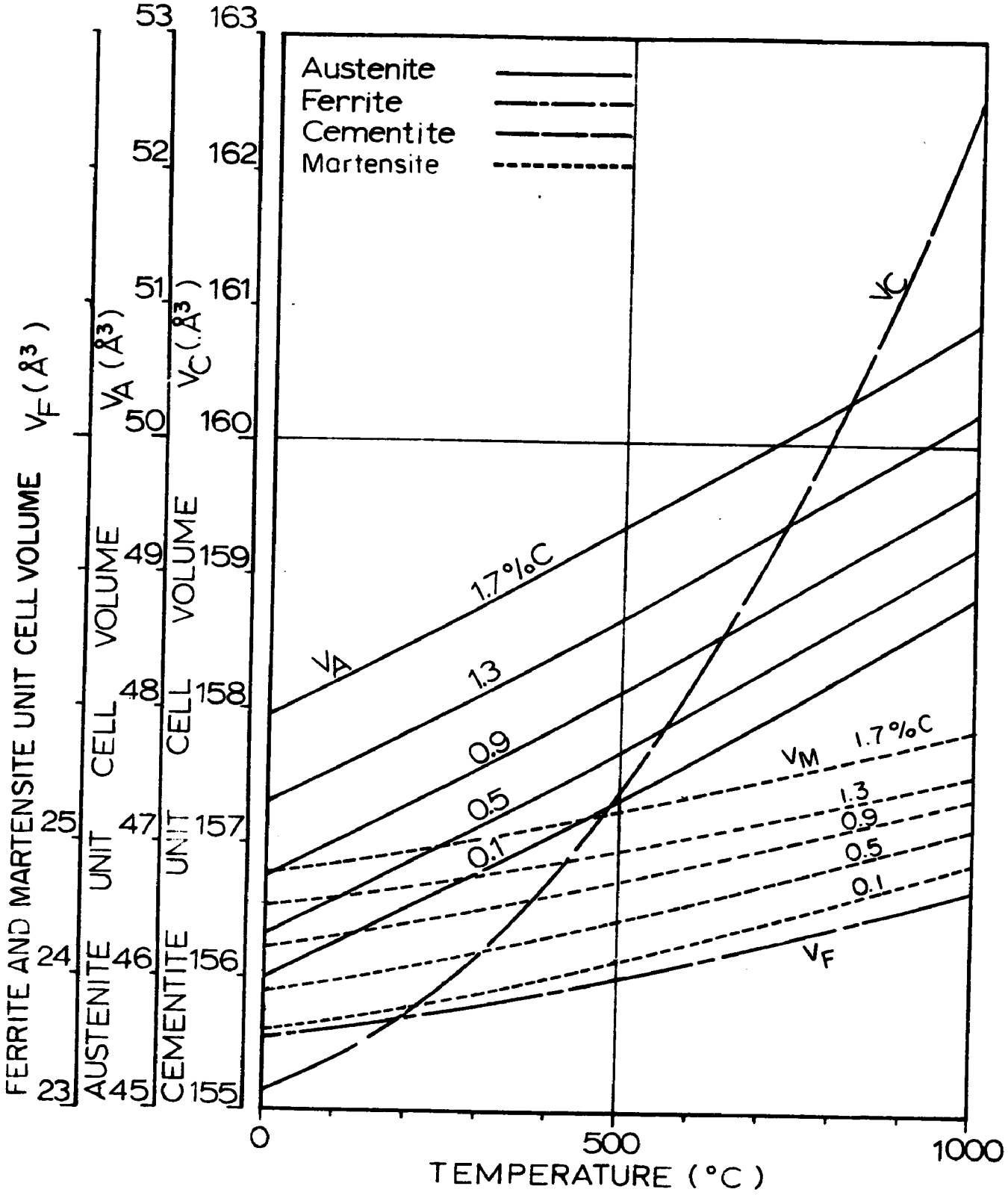


Fig. 34. Volume of unit cells of austenite, ferrite and cementite calculated from (33) and of martensite unit cell volume calculated from Roberts (13)

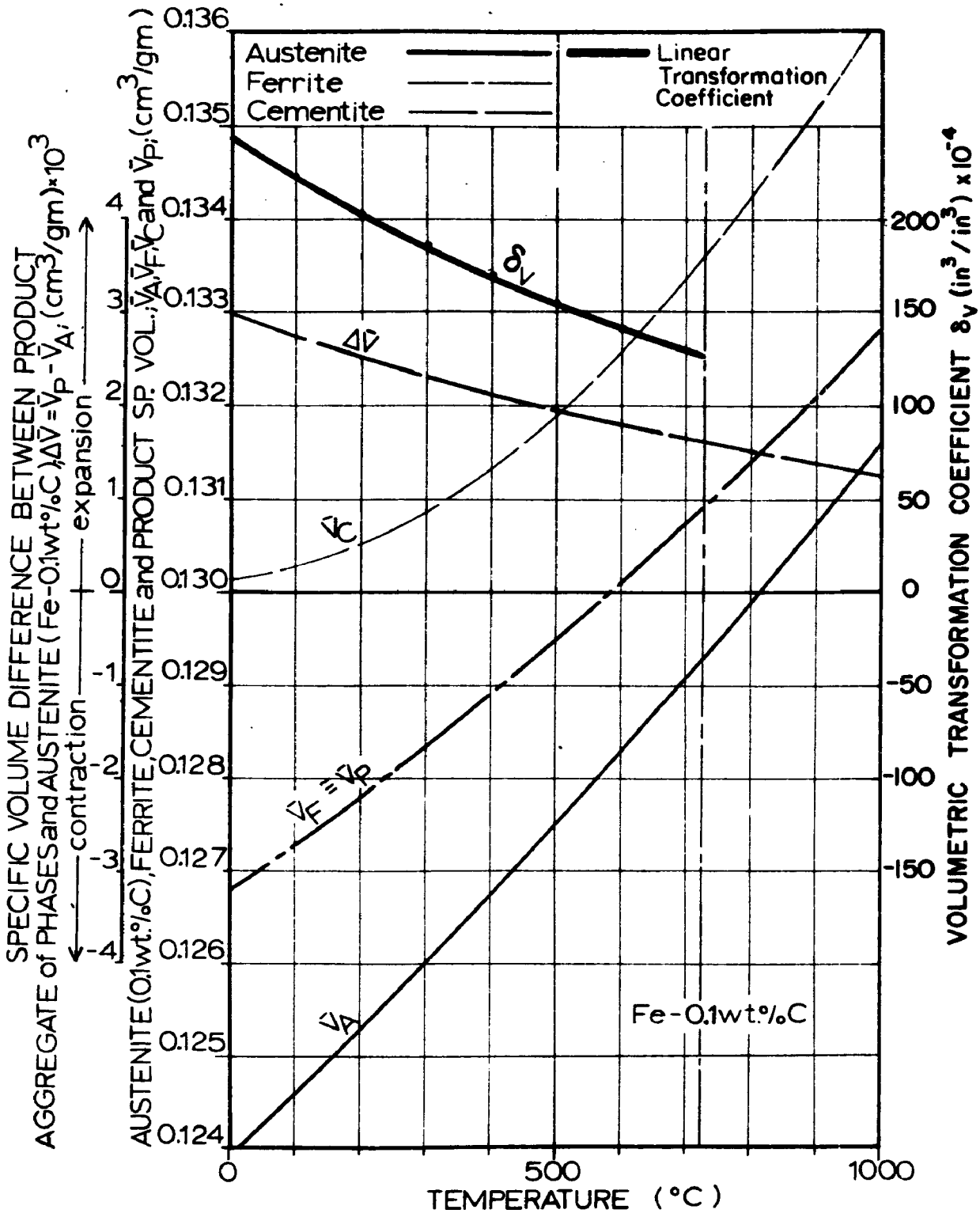


Fig. 35-A. Summary of calculation procedure for δ_V (isothermal) for 0.1% C as f(T)

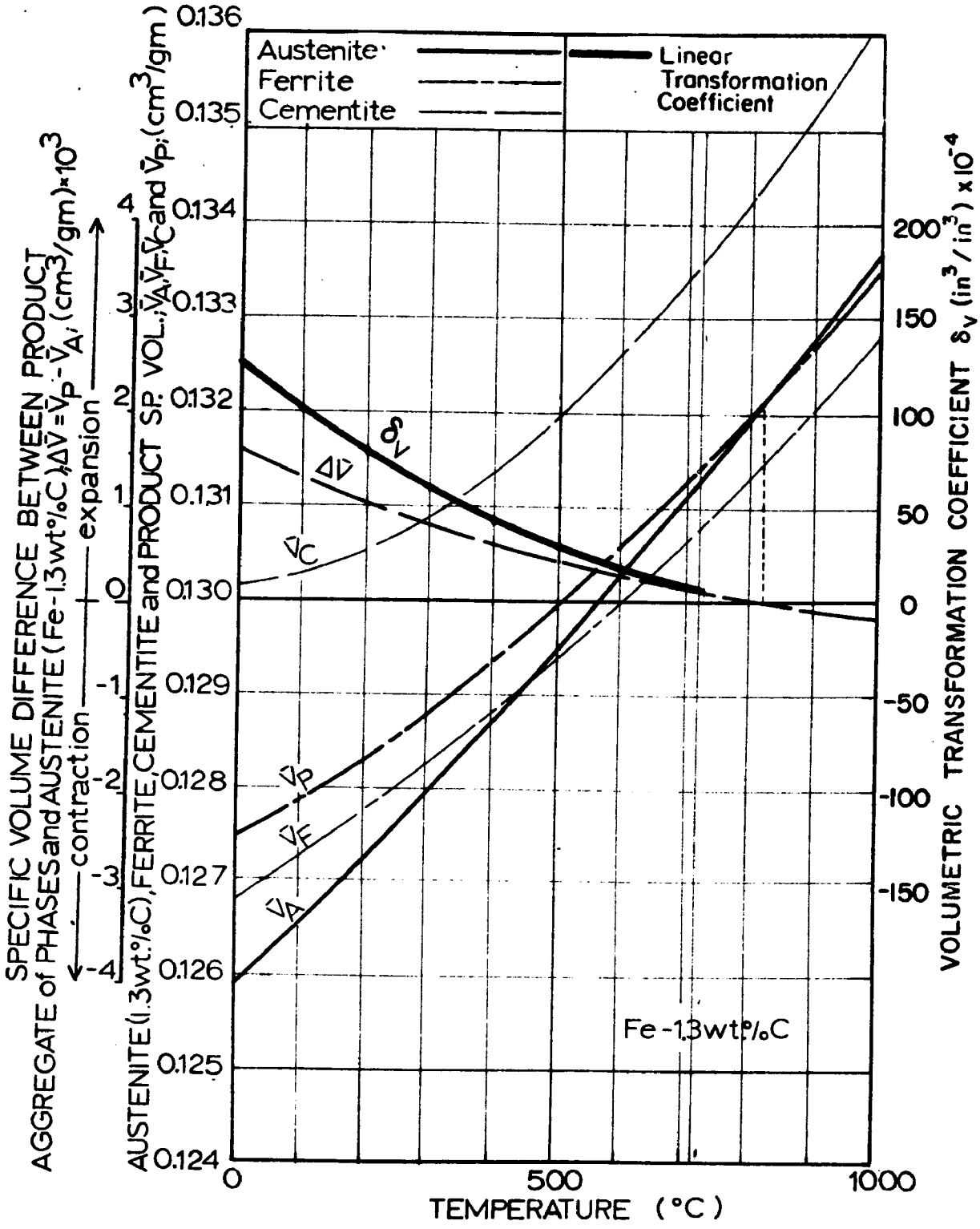


Fig. 35-B. Summary of calculation procedure for δ_V (isothermal) for 1.3% C as f(T)

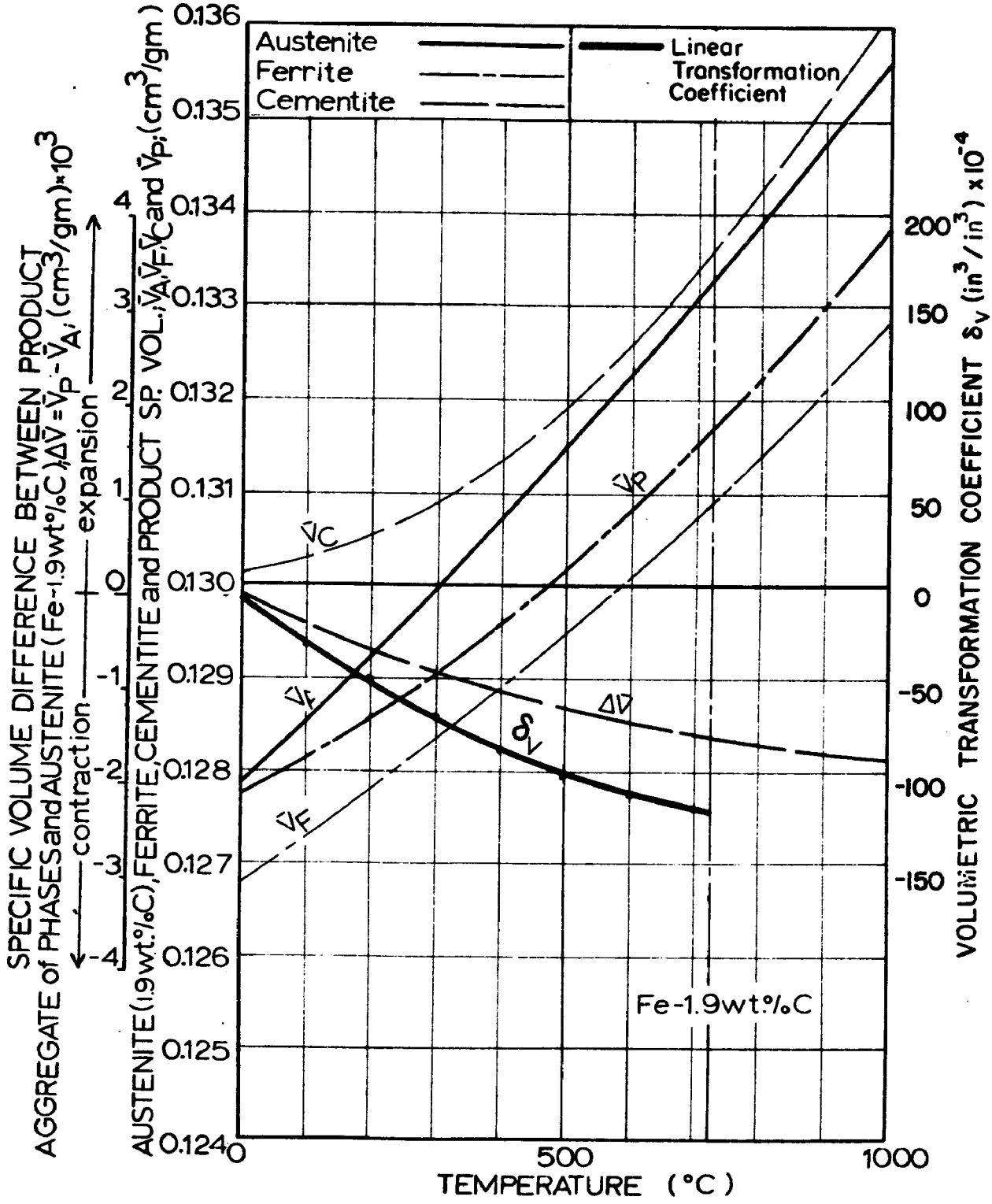


Fig. 35-C. Summary of calculation procedure for δ_V (isothermal) for 1.9% C as f(T)

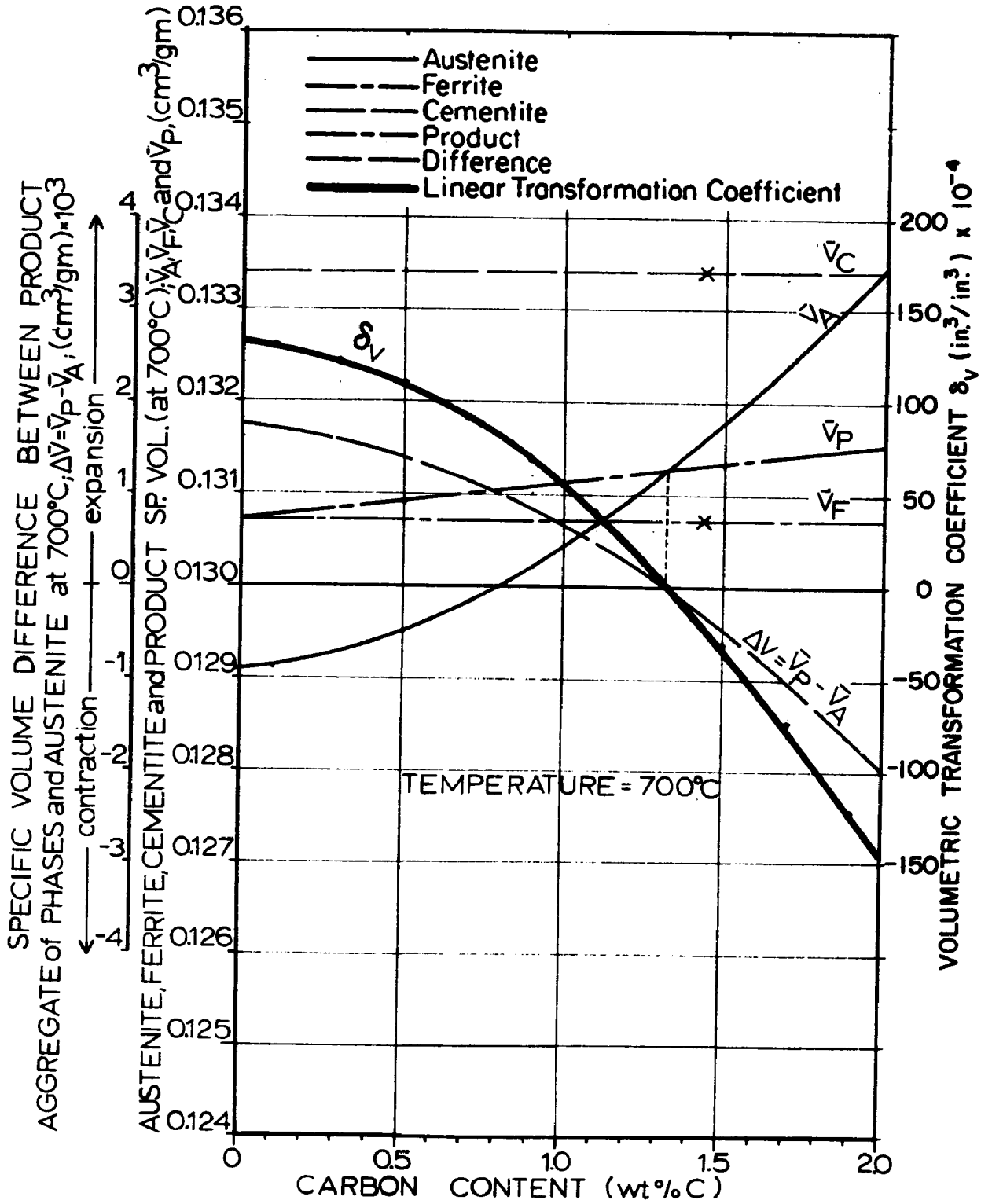


Fig. 36-A. Summary of calculation procedure for δ_V (isothermal) for 700°C as f(% C)

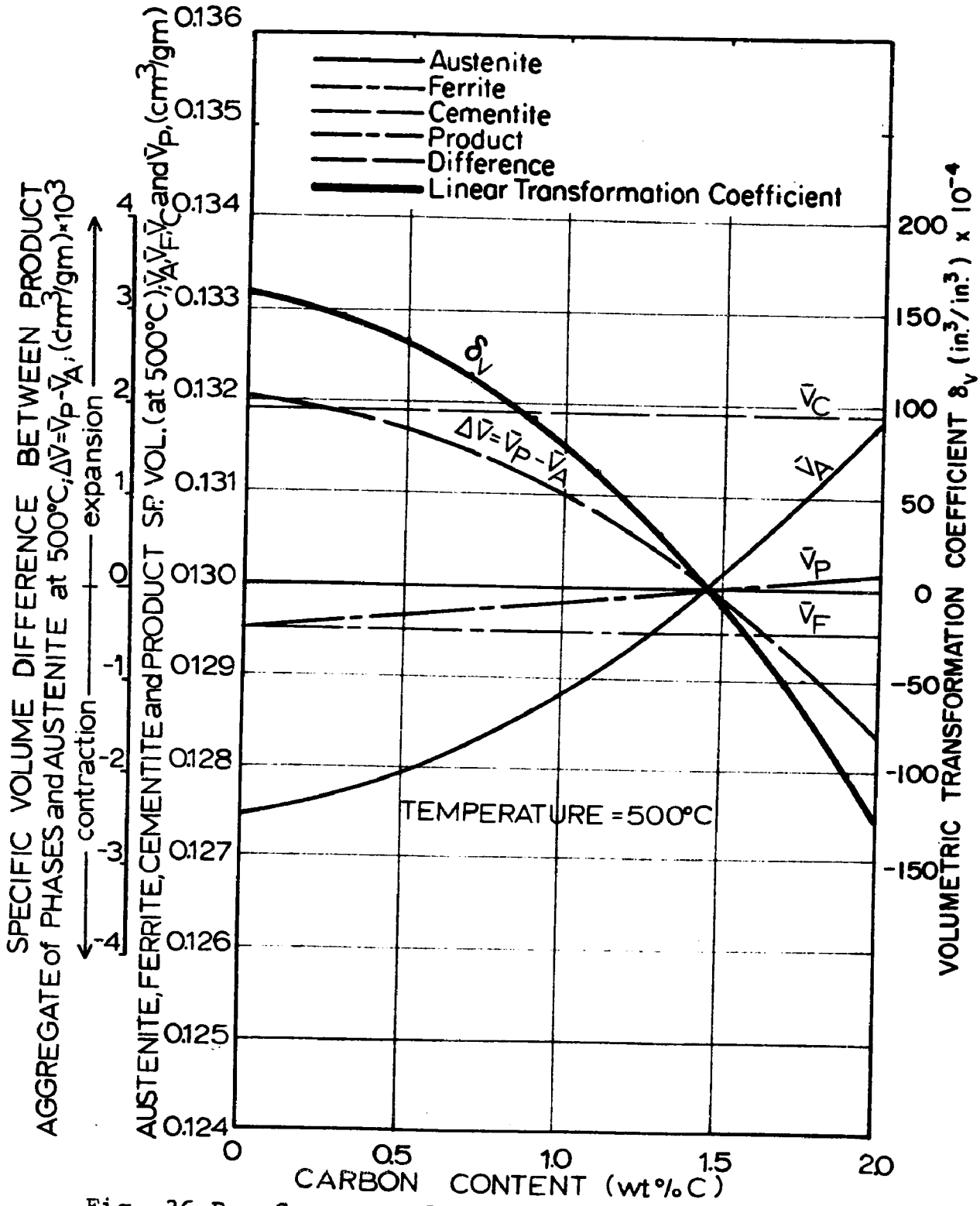


Fig. 36-B. Summary of calculation procedure for δ_V (isothermal) for 500°C as f(% C)

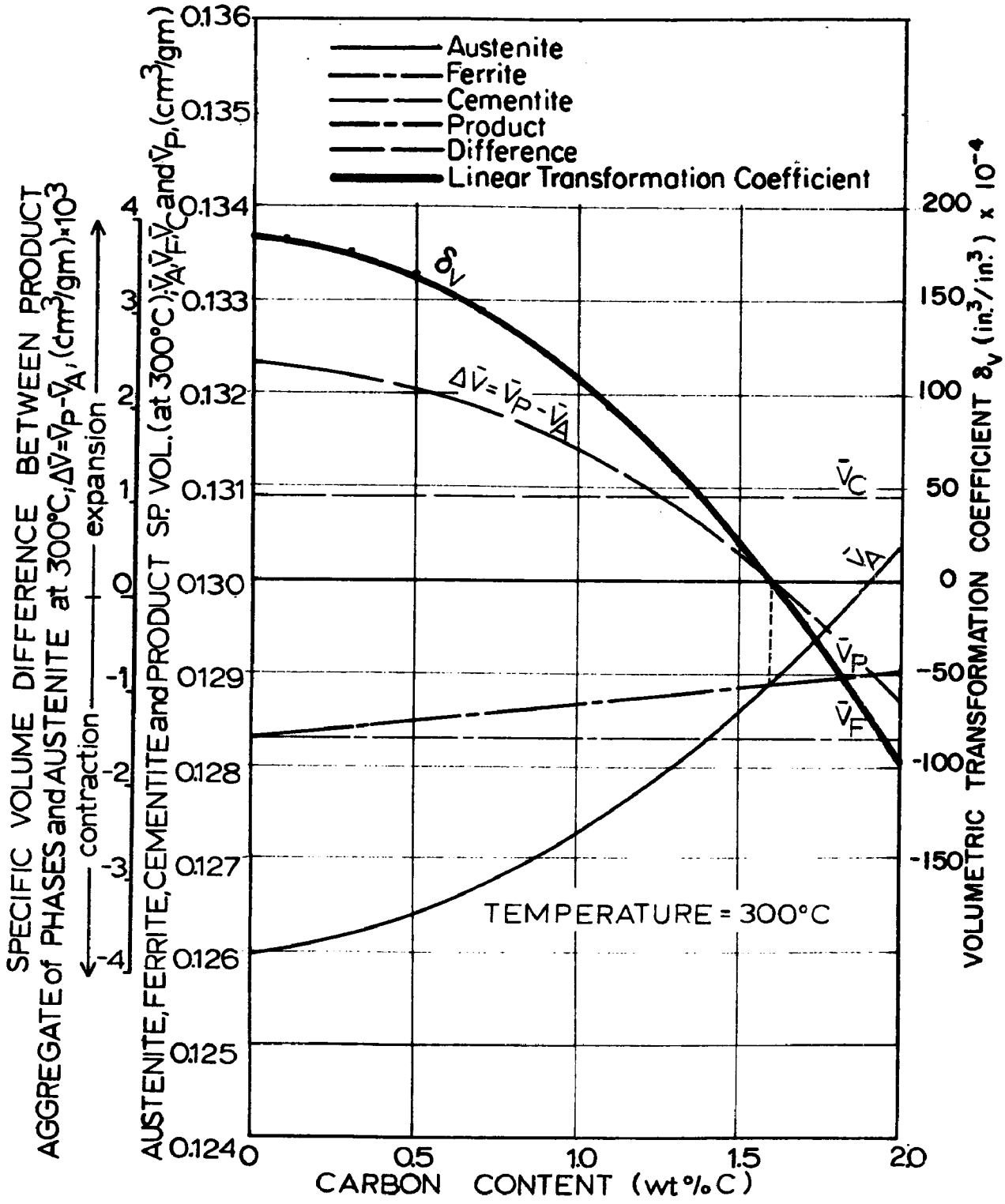


Fig. 36-C. Summary of calculation procedure for δ_V (isothermal) for 300°C as f(% C)

$$\delta_V = (245.1 - 21.27\ C - 54.4\ C^2 - 2.1101\ T\ 10^{-1} + \\ + 6.97\ T^2\ 10^{-5})\ 10^{-4} \qquad (16)$$

Figures 17-A and B show the values of δ_V predicted from this calculation.

Figures 34, 35 and 36 are a summary of the calculation procedure. Figure 34 shows how the unit cell volumes of austenite, ferrite and cementite vary with the temperature. Both ferrite and austenite are almost linear while the curvature for cementite is quite pronounced.

A summary of the calculation procedure as a function of the temperature is shown in Fig. 35-A for a 0.1 wt % C and Fig. 35-C for a 1.9 wt % C. This summary graph shows first the specific volumes of all phases (austenite, ferrite and cementite) and the specific volume of the product as obtained from

$$\overline{V}_P = f_F^W\ \overline{V}_F + f_C^W\ \overline{V}_C \qquad (17)$$

Then the difference between the specific volume of austenite and the aggregate of product phases is shown as obtained from

$$\Delta\overline{V} = \overline{V}_P - \overline{V}_A \qquad (18)$$

Finally the transformation coefficient is calculated by

$$\delta_V = \frac{\Delta\overline{V}}{\overline{V}_A} \qquad (19)$$

Figure 36 is the same summary as a function of the carbon content for three temperatures.

4) Sample Calculation

To illustrate the calculation procedure, and to check the reported results, this sample calculation was performed for three carbon contents and three temperatures each. An electronic calculator was used for the computation. Lattice parameters were calculated by means of equations (13), (14) and (15) and the following table is a summary of their values for each carbon content and temperature, Table 12.

Table 12. Lattice parameters of austenite, ferrite and cementite for sample calculation

%C	T°C	a_A	a_F	a_C	b_C	c_C
0.30	100	3.5940	2.8691	4.5271	5.0554	6.7467
0.30	400	3.6151	2.8815	4.5396	5.0979	6.7710
0.30	700	3.6373	2.8946	4.5576	5.1269	6.8096
1.10	100	3.6166	2.8691	4.5271	5.0884	6.7467
1.10	400	3.6377	2.8815	4.5396	5.0973	6.7710
1.10	700	3.6598	2.8946	4.5576	5.1269	6.8096
1.90	100	3.6494	2.8691	4.5271	5.0884	6.7467
1.90	400	3.6705	2.8815	4.5396	5.0979	6.7710
1.90	700	3.6926	2.8946	4.5576	5.1269	6.8096

In order to calculate the specific volume ratios by means of equations (11) and (12), it is necessary to

calculate first the unit cell volume ratios V_F/V_A and V_C/V_A and $(1 + C^F/Fe^F)$, $(1 + C^A/Fe^A)$ and the constant $(3 + AW_C/AW_{Fe})$.

Table 13. Unit cell volumes and unit cell volume ratios (sample calculation)

%C	T C	V_A	V_F	V_C	V_C/V_F	V_F/V_A	V_C/V_A
0.30	100	46.4231	23.6177	155.4149	6.5804	0.5087	3.3478
0.30	400	47.2455	23.9252	156.6974	6.5495	0.5064	3.3167
0.30	700	48.1213	24.2530	159.1156	6.5607	0.5040	3.3066
1.10	100	47.3043	23.6177	155.4149	6.5805	0.4992	3.2854
1.10	400	48.1372	23.9252	156.6974	6.5495	0.4970	3.2552
1.10	700	49.0199	24.2530	159.1156	6.5607	0.4948	3.2459
1.90	100	48.6032	23.6177	155.4149	6.5804	0.4859	3.1976
1.90	400	49.4511	23.9252	156.6974	6.5495	0.4838	3.1687
1.90	700	50.3497	24.2530	159.1156	6.5607	0.4817	3.1602

Since the carbon solubility of ferrite (equilibrium) is only a function of temperature, the factor $(1 + C^F/Fe^F)$ is not a function of the carbon content, Table 14.

Table 14. Calculation of $(1 + C^F/Fe^F)$

T C	%C	$(1 + C^F/Fe^F)$
100	0.00035	1.00000
400	0.00238	1.00002
700	0.01624	1.00016
725	0.01906	

Since the carbon solubility of austenite does not depend on temperature but on the carbon content of the alloy, the factor $(1 + C^A/Fe^A)$ is only dependent on the carbon content of the alloy, Table 15.

Table 15. Calculation of $(1 + C^A/Fe^A)$

%C	%Fe	$(1 + C^A/Fe^A)$
0.30	99.70	1.00301
1.10	98.90	1.01112
1.90	98.10	1.01937

The coefficient $(1 + AW_X/AW_{Fe}) = 3.2151$.

At this point the specific volume ratios can be computed for each carbon content and temperature of transformation, Tables 16 and 17.

Table 16. Calculation of $\overline{V}_C/\overline{V}_A$

%C	T C	$(1+C^A/Fe^A)$	V_C/V_A	ρ_C/ρ_A
0.30	100	1.00301	3.34779	1.0444
0.30	400	1.00301	3.31666	1.0347
0.30	700	1.00301	3.30655	1.0316
1.10	100	1.01112	3.28542	1.0333
1.10	400	1.01112	3.25523	1.0238
1.10	700	1.01112	3.24594	1.0208
1.90	100	1.01937	3.19763	1.0138
1.90	400	1.01937	3.16874	1.0047
1.90	700	1.01937	3.16021	1.0020

Table 17. Calculation of $\bar{V}_F/\bar{V}_A$

%C	T C	$(1+C^A/Fe^A)$	$(1+C^F/Fe^F)$	V_F/V_A	ρ_F/ρ_A
0.30	100	1.00301	1.00000	0.50875	1.0206
0.30	400	1.00301	1.00002	0.50640	1.0158
0.30	700	1.00301	1.00016	0.50399	1.0109
1.10	100	1.01112	1.00000	0.49927	1.0096
1.10	400	1.01112	1.00002	0.49702	1.0051
1.10	700	1.01112	1.00016	0.49476	1.0004
1.90	100	1.01937	1.00000	0.48593	0.9907
1.90	400	1.01937	1.00002	0.48382	0.9864
1.90	700	1.01937	1.00016	0.48169	0.9819

Ferrite and cementite weight fractions have been calculated from equation (7), Table 18.

Table 18. Calculation of f_F^W and f_C^W

%C	T °C	f_F^W	f_C^W
0.30	100	0.95514	0.04486
0.30	400	0.95543	0.04457
0.30	700	0.95742	0.04258
1.10	100	0.83537	0.16463
1.10	400	0.83563	0.16437
1.10	700	0.83737	0.16263
1.90	100	0.71561	0.28439
1.90	400	0.71582	0.28418
1.90	700	0.71731	0.28269

Finally the volume change per unit volume due to the equilibrium transformation of austenite to ferrite and cementite can be computed from equation (6), Table 19.

Table 19. Calculation of δ_V

%C	T °C	$f_F^w(\frac{\bar{V}_F}{\bar{V}_A})$	$f_C^w(\frac{\bar{V}_C}{\bar{V}_A})$	δ_V
0.30	100	0.99755	0.04685	0.02167
0.30	400	0.97053	0.04612	0.01664
0.30	700	0.96786	0.04393	0.01178
1.10	100	0.84339	0.17011	0.01350
1.10	400	0.83989	0.16828	0.00817
1.10	700	0.83771	0.16601	0.00372
1.90	100	0.70896	0.28832	-0.00273
1.90	400	0.70609	0.28552	-0.00840
1.90	700	0.70433	0.26326	-0.01242

B) MARTENSITE TRANSFORMATION

This calculation is performed in two steps. First, δ_V is computed as a function of C and T disregarding the fact that the range of temperatures of transformations is fixed. Therefore δ_V is calculated for all possible temperatures.

Second, from the knowledge of Ms and Mf, and from the calculations performed in (1), a single line can be drawn to describe δ_V at Mf.

1) Basic Computation

In this case the initial phase specific volume is also the austenite specific volume and the final is the martensite specific volume.

$$\bar{V}_i = \bar{V}_A \qquad \bar{V}_f = \bar{V}_M \tag{20}$$

Therefore from equation (2),

$$\delta_V = \frac{\bar{V}_M - \bar{V}_A}{\bar{V}_A} = \frac{\bar{V}_M}{\bar{V}_A} - 1 \tag{21}$$

The specific volumes of austenite and martensite can be calculated from equation (3),

$$\bar{V}_A = \frac{AN \cdot V_A}{n_{Fe}^A \cdot AW_{Fe} + n_C^A \cdot AW_C}$$

$$\bar{V}_M = \frac{AN \cdot V_M}{n_{Fe}^M \cdot AW_{Fe} + n_C^M \cdot AW_C} \tag{22}$$

AN = Avogadro's Number

V_A = Austenite Unit Cell Volume = a_A^3

a_A = Austenite Unit Cell in (cm)

V_M = Martensite Unit Cell Volume = $a_M^2 \cdot c_M$

a_M and c_M = Martensite Unit Cell Lattice Parameters in (cm)

AW_{Fe} = Atomic Weight of Iron

AW_C = Atomic Weight of Carbon

n_{Fe}^A = Number of Iron Atoms per Unit Cell of Austenite = 4

n_{Fe}^M = Number of Iron Atoms per Unit Cell of Martensite = 2

$n_C^A = (C^A/Fe^A) \cdot (AW_{Fe}/AW_C) \cdot n_{Fe}^A$

$n_C^M = (C^M/Fe^M) \cdot (AW_{Fe}/AW_C) \cdot n_{Fe}^M$

C^A = Weight Percent of Carbon dissolved in Austenite

Fe^A = Weight Percent of Iron in Austenite

C^M = Weight Percent of Carbon in Austenite

Fe^M = Weight Percent of Iron in Martensite.

Assuming complete carbon solution in austenite, C^A = C the carbon weight percent of the Fe-C alloy. Assuming complete transformation of austenite to martensite, $C^M = C^A$ if no aging happens during transformation. Therefore the specific volumes of austenite and martensite can be rewritten as,

$$\bar{V}_A = \frac{AN \cdot a_A^3}{4.AW_{Fe} \cdot \left[1 + \left(\frac{C^A}{Fe^A}\right)\right]} \qquad (23)$$

$$\bar{V}_M = \frac{AN \cdot a_M^2 \cdot c_M}{2 \cdot AW_{Fe} + \left(\frac{C^M}{Fe^M}\right) \cdot \left(\frac{AW_{Fe}}{AW_C}\right) \cdot 2 \cdot AW_C}$$

$$\bar{V}_M = \frac{AN \cdot a_M^2 \cdot c_M}{2 \cdot AW_{Fe} \cdot \left[1 + \left(\frac{C^M}{Fe^M}\right)\right]}$$

or since $C^M = C^A$ and therefore $Fe^M = Fe^A$,

$$\bar{V}_M = \frac{AN \cdot a_M^2 \cdot c_M}{2 \cdot AW_{Fe} \cdot \left[1 + \left(\frac{C^A}{Fe^A}\right)\right]} \qquad (24)$$

Therefore the specific volume ratio of martensite to austenite can be given by,

$$\frac{\overline{V}_M}{\overline{V}_A} = \frac{\dfrac{AN \cdot a_M^2 \cdot c_M}{2 \cdot AW_{Fe} \cdot \left[1 + \dfrac{C^A}{Fe^A}\right]}}{\dfrac{AN \cdot a_A^3}{4 \cdot AW_{Fe} \cdot \left[1 + \dfrac{C^A}{Fe^A}\right]}}$$

$$\frac{\overline{V}_M}{\overline{V}_A} = 2 \cdot \frac{a_M^2 \cdot c_M}{a^3} \qquad (25)$$

Therefore the volume change during martensite transformation at a given temperature can be given by,

$$\delta_V = 2 \cdot \frac{a_M^2 \cdot c_M}{a_M^3} - 1 \qquad (26)$$

2) Assumptions

For the development of this equation the following assumptions have been made:

Assumption 1: C^A = C or that 100% solution of carbon in austenite occurred during austenitization.

Assumption 2: C^M = C or that during transformation there were no carbon atoms rejected out of the tetragonal martensite unit cell (no tempering effect).

Assumption 3: The volume coefficient of thermal expansion of martensite has been considered the same as the one for ferrite.

Assumption 4: Austenite decomposition goes to 100% completion.

3) Results

The transformation volume change for martensite reaction has been performed by means of equation (26). Figure 18-B illustrates the dependence of the martensite transformation coefficient on temperature and Fig. 18-A its dependence on the carbon content of the Fe-C alloy. In both figures, lines showing the start of the martensite transformation and different percentages of completion have been included. The temperatures at which martensite starts transforming, Ms, have been calculated for each carbon content from the Bain and Paxton (85) equation for low alloy steels,

$$Ms(C) = 561 - 474\ (\%C) - 33\ (\%Mn) - 17\ (\%Ni) - 17\ (\%Cr) - 21\ (\%Mo) \qquad (27)$$

The line defining the different percentages of transformation has been calculated from the Koistinen and Marburger (86) equation (empirically determined) that defines the volume fraction of retained austenite, $f_A^V = 1 - f$, in terms of the number of degrees C of undercooling below Ms,

$$f_A^V = 1 - f = \exp[\alpha(Ms - T_q)] \qquad (28)$$

where $\alpha = -0.011$ is the empirical parameter, T_q is the quenching temperature and f is the volume fraction of martensite formed at this temperature. According to Magee (88) this parameter is given by,

$$\alpha = \overline{V} \cdot \frac{\partial \Delta G_v^{\gamma-\alpha'}}{dT} \qquad (29)$$

where $\overline{V}$ is the average volume of newly formed martensite plates and $\Delta G_v^{\gamma-\alpha'}$ is the driving free energy favoring the formation of martensite. Brook et al. (89) have found that the slope

$$m = - \frac{df}{dT} \qquad (30)$$

a parameter equivalent to α, differed among iron alloys from 0.008 to 0.013 and that much of this variation could be directly correlated with the known values of $\frac{\partial \Delta G_v^{\gamma-\alpha'}}{dT}$ for each alloy.

For the present calculation, $\alpha = -0.011$ from Kcistinen and Marburger, has been adopted because it fits experimental data for pure Fe-C alloys. The lattice parameter equation for austenite used in this calculation is equation (13) used before for part A.

The unit cell volume of martensite has been computed by means of

$$V_M = V_M^{RT} + (V_F - V_F^{RT}) \tag{31}$$

where

V_F = unit cell volume of ferrite at a temperature T

V_F^{RT} = unit cell volume of ferrite at room temperature

V_M^{RT} = unit cell volume of martensite at room temperature.

V_F and V_F^{RT} are computed from ferrite lattice as in part A. $\overline{V}_M^{RT}$ can be computed from Roberts (13) summary equations:

$$\begin{aligned} a_M(\mathring{A}) &= 2.867 - 0.013 \text{ (wt \% C)} \\ c_M(\mathring{A}) &= 2.867 + 0.116 \text{ (wt \% C)} \end{aligned} \tag{32}$$

$$\overline{V}_M^{RT} = a_M \cdot c_M \tag{33}$$

Therefore equation (31) gives the unit cell volume of martensite assuming that the volume coefficient of expansion of martensite is the same as ferrite.

BIBLIOGRAPHY

1. Chevenard, P., (1917), Revue de Metal., 14, p. 610.

2. R.A. Flinn, E. Cook and J.A. Fellows, "A Quantitative Study of Austenite Transformation," Trans. ASM, (March 1943), p. 41-70.

3. A.L. Christensen, E.C. Nelson and C.E. Jackson, "A High Speed Dilatometer and the Transformational Behavior of Six Steels in Cooling,"

4. L.A. Willey and W.L. Fink, "An Interferometer Type Dilatometer and Some Typical Results,"

5. O. Werner, "Uber ein neues Dilatometer und seine Anwendung in der Metallkunde," Zeitschrift fur Metallkunde, v. 47, n. 1, (Jan. 1956), p. 28-36.

6. V.E. Mikryukov, "Device for Measuring the Thermal Expansion of Solids in the 20-1000°C Interval," Instr. and Experim. Techn. n. 3, (May-June 1962), p. 581-3.

7. R. Bowles and B. Sugarman, "An Automatic Recording Dilatometer," Journal Sci. Instrum., (1963), v. 40, p. 117-19.

8. J. Barford, "An Automatic Recording Differential Dilatometer," Journal Sci. Instrum., (1963), v. 40, p. 444-5.

9. E.J. Fasiska and H. Wagenblast, "Dilation of Alpha Iron by Carbon," Trans. AIME, (Nov. 1967), v. 239, p. 1818-20.

10. V.E. Bottom, "Fabry-Perot Dilatometer," The Review of Sci. Instrum., v. 35, n. 3, p. 374-6.

11. H. Stuart and N. Ridley, "Thermal Expansion Coefficient of Cementite and Other Phases," Jour. of the Iron and Steel Inst., (July 1966), p. 711-7.

12. F. Lazlo and H. Nolle, Journal Mech. Phys. Solids, (1958/59), v. 7, p. 193-208.

13. C.S. Roberts, "Effect of C on the Volume Fractions and Lattice Parameters of Retained Austenite and Martensite," J. of Metals, (Feb. 1953), p. 203-4.

14. V.M. Yershov and N.L. Olson, "Change in the Linear Expansion Coefficient of Austenite on Transformation to Martensite," Phys. Met. Metallog., (1968), v. 25, n. 5, p. 118.

15. H. Lipson and N.J. Petch, JISI, (1940), v. 142, p. 95-103.

16. W. Hume-Rothery et al., JISI, (1941), v. 145, p. 143-51.

17. E.M. Belikov and A.A. Savinskaya, Phys. Met. Metallogr., (1962), v. 14, n. 2, p. 299-301.

18. E.C. Bain and W.S.N. Warnig, "Austenite Decomposition and Length Changes in Steel," Am. Soc. for Steel Treat., (Jan. 1928), p. 69-25.

19. S.A. Kulin, M. Cohen and B.L. Averbach, Trans. Am. Inst. Min. Engrs. (1952), v. 194, p. 661-8.

20. E.S. Davenport and E.C. Bain, "Transformation of Austenite at Constant Subcritical Temperatures," Trans. AIME, (1930), v. 90, p. 117-132.

21. R.F. Hehemann,"The Bainite Transformation," Phase Transformations-Seminar Book-ASM-October 12-13, 1968, p. 397-432.

22. Z.S. Basinski, W. Hume-Rothery, and A.L. Sutton, Proc. Roy. Soc. London, A229 (1955), p. 459-467.

23. H. Esser and G. Müller, Archiv für das Eisenhüttenwesen, 7, (1933), p. 265.

24. W. Schmidt, Ergebn. tech. Röntgenk. 3, (1933), p. 195.

25. F.C. Nix and D. McNair, Phys. Rev. 60, (1941), p. 597.

26. J.B. Austin and R.H.H. Pearce, Trans. ASM, v. 22, (1934), p. 447.

27. M.E. Straumanis and D.C. Kim, Z. Metallkde., Bd. 60, (1969), H4, p. 273.

28. W. Souders and P. Hidnert, Sci. Pap. U.S. Bureau Stand. 17, (1922), p. 611.

29. M.L. Hill and E.W. Johnson, Trans. AIME, v. 221, (1961), p. 622; v. 215, (1959), p. 717.

30. W. Sounders and P. Hidnert, Sci. Pap. U.S. Bureau Stand., v. 21, (1926/27), p. 524.

31. N. Ridley and H. Stuart, Metal Science Journal, v. 4, (1970), p. 219.

32. N. Ridley, H. Stuart and L. Zwell, Trans. Met. Soc. AIME, (1969), v. 245, p. 1834.

33. N. Ridley, personal communication.

34. H. Stuart and N. Ridley, Journal of the Iron and Steel Institute,(December 1970), p. 1087.

35. V.M. Goldschmidt, Z. Phys. Chem., v. 133, (1928), p. 397.

36. H.J. Goldschmidt, "Advances in X-ray Analysis," v. V, (1962), p. 191: New York (Plenum Press).

37. A. Taylor and H. Sinclair, Proc. Roy. Soc., v. 57, (1945), p. 126.

38. J.S. Nelson and D.P. Riley, Proc. Roy. Soc., v. 57, (1945), p. 160.

39. M.V. Cohen, Rev. Sci. Inst., v. 6,(1935), p. 68-74.

40. W.D. Hoff et al., Rev. Sci. Inst., v. 42, (1965), p. 171.

41. K.H. Jack, Proc. Roy. Soc., A195, (1948), p. 56-61.

42. W. Hume-Rothery and P.W. Reynolds, Proc. Roy. Soc., [A], 167, (1938), p. 25.

43. Z.S. Basinski, W. Hume-Rothery and A.L. Sutton, Proc. Roy. Soc., [A], 229, (1955), p. 429.

44. G. Hagg, Journal of the Iron and Steel Institute, v. 130, (1934), p. 439.

45. E. Ohman, Journal of the Iron and Steel Institute, v. 123, (1931), p. 445.

46. K. Honda and Z. Nishiyama, Sci. Rpts. Tohoku Imp. Univ. Ser. 1, (1932), v. 21, p. 299; Trans. ASST (1932), 20, p. 464.

47. N. Seljakov, G. Kurdjumov and N. Goodtzov, Ztsch. Physik, (1927), v. 45, p. 384.

48. G. Kurdjumov and E. Kaminsky, Ztsch. Physik (1929), v. 53, p. 696.

49. H. Lipson and A.M.B. Parker, Journal of the Iron and Steel Institute, (1944), v. 149, p. 123.

50. J. Mazur, Nature (1950), v. 166, p. 828.

51. M.P. Arbusov, DAN, SSSR (1950, v. 74, p. 1085.

52. S.G. Fletcher, The Tempering of Plain Carbon Steels, Sc.D. Thesis, Massachusetts Institute of Technology, 1943.

53. C.S. Roberts, B.L. Averbach and M. Cohen, Trans. ASM, (1953), v. 45.

54. H. Esser and W. Bungardt, Archiv. Eisen. (1934), v. 7, p. 585.

55. B.L. Averbach, L.S. Castleman and M. Cohen, Trans. ASM, (1950), v. 42, p. 112.

56. C.L. Magee and R.G. Davies, Acta Met., v. 20, (August 1972), p. 1031.

57. A.H. Smith and F.C. Thompson, Journal of the Iron and Steel Institute, (1952), v. 171, p. 38.

58. S. Sato, Sci. Rep. Tohoku Univ. (a), v. 14, p. 513.

59. B.S. Lement, "Distortion in Tool Steels," Published by Am. Soc. for Met., Metals Park, Ohio.

60. S.G. Fletcher and M. Cohen, (Part I), Trans. ASM, v. 34, (1945), p. 216.

61. S.G. Fletcher and M. Cohen,(Part II), Trans. ASM, v. 40, (1948), p. 703.

62. S.G. Fletcher and M. Cohen, (Part III), Trans. ASM, v. 40, (1948), p. 728.

63. H. Esser and G. Müller, Archiv. für das Eisenhüttenwesen, 7, (1933), p. 267-68.

64. R.I. Entin, Decomposition of Austenite by Diffusional Processes, Met. Soc. of AIME. Interscience Publishers, New York, (1962), p. 304.

65. A. Hultgren, Trans. ASM, v. 39, (1947), p. 915.

66. A. Hultgren, Kgl Svenska Vetenskapsakad Handl, v. 4, (1953), p. 3.

67. A. Hultgren, Ternkontorets Ann. v. 135, (1951), p. 403.

68. W. Koch and H.J. Wiester, Stabil und Eisen, v. 69, (1949), p. 73.

69. R.I. Entin, reference 64, p. 295.

70. F.E. Bowman, Trans. ASM, v. 36, (1946), p. 61.

71. H.I. Aaronson and H.A. Domian, Trans. AIME. v. 236, (1966), p. 781.

72. H. Lange and K. Mathieu, Mitt Kaiser-Wilhelm Inst Eisenforsch, v. 20, (1938), p. 125.

73. T. Lyman and A.R. Troiano, Trans. ASM, v. 37, (1946), p. 402.

74. T. Lyman and A.R. Troiano, Trans. AIME, v. 162, (1945), p. 196.

75. S. Steinberg and V. Zyuzin, Rev. Met., v. 31, (1934), p. 554.

76. F. Wever and K. Mathieu, Mitt Kaiser-Wilhelm Inst Eisenforsch, v. 22, (1940), p. 2.

77. E.P. Klier and T. Lyman, Trans. AIME, v. 158, (1944), p. 394.

78. A. Gulyaev, Metallurg, v. 15, (1940), p. 43.

79. S. Steinberg and V. Zyuzin, Arch Eisenhuttenw, v. 7, (1934), p. 537.

80. P. Gordon, M. Cohen and R.S. Rose, Trans. ASM, v. 31, (1943), p. 161.

81. A.R. Troiano, Trans. ASM, v. 41, (1949), p. 1093.

82. L.M. Pevzner, G.M. Rovenski and T.D. Kubyschkina, Dokl Akad Nauk SSSR, v. 85, (1952), p. 811.

83. N.P. Allen, L.B. Pfeil and W.T. Griffiths, Second Report, Alloys Steels, Research Committee, Iron and Steel Institute, (1939), p. 369.

84. P. Vasudevan, L.W. Graham and H.J. Axon, J. Iron Steel Inst., v. 191, (1959), p. 56.

85. Stanley, J.K., Met. Trans., v. 185, (1949), p. 752.

86. Bain, E.C. and H. Paxton, "Alloying Elements in Steels," 2d ed., 3d rev. printing, Chap. 7, ASM, Metals Park, Ohio, 1966.

87. Koistinen D.P. and R.E. Marburger, Acta Met., v. 7, (1959), p. 59.

88. Magee, C.L., same as ref.21, p. 115.

89. Brook, R., A.R. Entwisle and E.F. Ibrahim, J. Iron and Steel Inst., v. 195, (1960), p. 292.